REFERENCES

Abu-Thabit, N.Y., Ali, S.A., and Javaid Zaidi, S.M. (2010) New highly phosphonated polysulfone membranes for PEM fuel cells. Journal of Membrane Science, 360(12), 26-33.

Ahmad, H., Kamarudin, S.K., Hasran, U.A., and Daud, W.R.W. (2010) Overview of hybrid membranes for direct-methanol fuel-cell applications. International Journal of Hydrogen Energy, 35(5), 2160-2175.

Ahmad, M.I., Zaidi, S.M.J., and Rahman, S.U. (2006) Proton conductivity and characterization of novel composite membranes for medium-temperature fuel cells. Desalination, 193(1–3), 387-397.

Auimviriyavat, J., Changkhamchom, S., and Sirivat, A. (2011) Development of poly(ether ether ketone) (PEEK) with inorganic filler for direct methanol fuel cells (DMFCs). Industrial & Engineering Chemistry Research, 50(22), 12527-12533.

Byun, S.C., Jeong, Y.J., Park, J.W., Kim, S.D., Ha, H.Y., and Kim, W.J. (2006) Effect of solvent and crystal size on the selectivity of ZSM-5/Nafion composite membranes fabricated by solution-casting method. Solid State Ionics, 177(37–38), 3233-3243.

Carrette, L., Friedrich, K.A., and Stimming, U. (2001) Fuel Cells – Fundamentals and Applications. Fuel Cells, 1(1), 5-39.

Chen, S.-L., Bocarsly, A. B., and Benziger, J. (2005) Nafion-layered sulfonated polysulfone fuel cell membranes. Journal of Power Sources, 152(0), 27-33.

Chen, S., Yin, Y., Kita, H., and Okamoto, K.-I. (2007) Synthesis and properties of sulfonated polyimides from homologous sulfonated diamines bearing bis(aminophenoxyphenyl)sulfone. Journal of Polymer Science Part A: Polymer Chemistry, 45(13), 2797-2811.

Chien, H.-C., Tsai, L.-D., Huang, C.-P., Kang, C.-Y., Lin, J.-N., and Chang, F.-C. (2013) Sulfonated graphene oxide/Nafion composite membranes for high-performance direct methanol fuel cells. International Journal of Hydrogen Energy, 38(31), 13792-13801.

Choi, J., Patel, R., Han, J., and Min, B. (2010) Proton conducting composite membranes comprising sulfonated Poly(1,4-phenylene sulfide) and zeolite for fuel cell. Ionics, 16(5), 403-408.

Choi, B. G., Huh, Y. S., Park, Y. C., Jung, D. H., Hong, W. H., and Park, H. (2012) Enhanced transport properties in polymer electrolyte composite membranes with graphene oxide sheets. Carbon, 50(15), 5395-5402.

Croce, F., Hassoun, J., Tizzani, C., and Scrosati, B. (2006) Nanoporous composite, low cost, protonic membranes for direct methanol fuel cells. Electrochemistry Communications, 8(7), 1125-1131.

DeLuca, N.W. and Elabd, Y.A. (2006) Polymer electrolyte membranes for the direct methanol fuel cell: A review. Journal of Polymer Science Part B: Polymer Physics, 44(16), 2201-2225.

Devrim, Y., Erkan, S., Baç, N., and Eroğlu, I. (2009) Preparation and characterization of sulfonated polysulfone/titanium dioxide composite membranes for proton exchange membrane fuel cells. International Journal of Hydrogen Energy, 34(8), 3467-3475.

Duangkaew, P. and Wootthikanokkhan, J. (2008) Methanol permeability and proton conductivity of direct methanol fuel cell membranes based on sulfonated poly(vinyl alcohol)–layered silicate nanocomposites. Journal of Applied Polymer Science, 109(1), 452-458.

Fu, Y.Z. and Manthiram, A. (2006) Synthesis and characterization of sulfonated polysulfone membranes for direct methanol fuel cells. Journal of Power Sources, 157(1), 222-225.

Furtado Filho, A.A.M. and Gomes, A.S. (2011) Sulfonated bisphenol-A-polysulfone based composite PEMs containing tungstophosphoric acid and modified by electron beam irradiation. International Journal of Hydrogen Energy 37(7), 6228-6235.

Gao, Y., Robertson, G. P., Guiver, M. D., Jian, X., Mikhailenko, S. D., Wang K., and Kaliaguine S. (2005) Sulfonation of poly(phthalazinones) with fuming sulfuric acid mixtures for proton exchange membrane materials. Journal of Membrane Science, 227(1-2), 39-50.

Ghassemi, H. and McGrath, J.E. (2004) Synthesis and properties of new sulfonated poly(p-phenylene) derivatives for proton exchange membranes. Polymer, 45, 5847-54.

Han, W., Kwan, S.M., and Yeung, K.L. (2012) Zeolite applications in fuel cells: Water management and proton conductivity. Chemical Engineering Journal, 187, 367-371.

He, Y., Tong, C., Geng, L., Liu, L., and Lü, C. (2014) Enhanced performance of the sulfonated polyimide proton exchange membranes by graphene oxide: Size effect of graphene oxide. Journal of Membrane Science, 458, 36-46.

Heo, Y., Im, H., and Kim, J. (2013) The effect of sulfonated graphene oxide on Sulfonated Poly (Ether Ether Ketone) membrane for direct methanol fuel cells. Journal of Membrane Science, 425-426, 11-22.

Herrero, M., Martos, A.M., Varez, A., Galván, J.C., and Levenfeld, B. (2014) Synthesis and characterization of polysulfone/layered double hydroxides nanocomposite membranes for fuel cell application. International Journal of Hydrogen Energy, 39(8), 4016-4022.

Jaafar, J., Ismail, A.F., Matsuura, T., and Nagai, K. (2011) Performance of SPEEK based polymer–nanoclay inorganic membrane for DMFC. Journal of Membrane Science, 382(1-2), 202-211.

Junaidi, M.U.M., Leo, C.P., Ahmad, A.L., Kamal, S.N.M., and Chew, T.L. (2014) Carbon dioxide separation using asymmetric polysulfone mixed matrix membranes incorporated with SAPO-34 zeolite. Fuel Processing Technology, 118, 125-132.

Jung, H.Y. and Park, J.K. (2007) Blend membranes based on sulfonated poly(ether ether ketone) and poly(vinylidene fluoride) for high performance direct methanol fuel cell. Electrochimica Acta, 52(26), 7464-7468.

Kamarudin, S. K., Achmad, F., and Daud W.R.W. (2009) Overview on the application of direct methanol fuel cell (DMFC) for portable electronic devices. International Journal of Hydrogen Energy, 34(16), 6902-6916.

Karlsson, L.E. and Jannasch P. (2004) Polysulfone ionomers for proton-conducting fuel cell membranes: sulfoalkylated polysulfones. Journal of Membrane Science, 230(1–2), 61-70.

Karlsson, L. and Jannasch, P. (2005) Polysulfone ionomers for proton-conducting fuel cell membranes - 2. Sulfophenylated polysulfones and polyphenylsulfones. Electrochimica acta, 50(9), 1939-1946.

Karthikeyan, C.S., Nunes, S.P., Prado, L.A.S.A., Ponce, M.L., Silva, H., Ruffmann, B., and Schulte, K. (2005) Polymer nanocomposite membranes for DMFC application. Journal of Membrane Science, 254(1-2), 139-146.

Kim, D.H. and Kim, S.C. (2008) Transport properties of polymer blend membranes of sulfonated and nonsulfonated polysulfones for direct methanol fuel cell application. Macromolecular Research, 199, 457-466.

Kobayashi, T., Rikukawa, M., Sanui, K., and Ogata, N. (1998) Proton-conducting polymers derived from poly(ether-etherketone) and poly(4-phenoxybenzoyl-1, 4-phenylene). Solid, 106, 219-225.

Li, W., Fu, Y.Z., Manthiram, A., and Guiver, M.D. (2009) Blend Membranes Consisting of Sulfonated Poly(ether ether ketone) and Polysulfone Bearing 4-Nitrobenzimidazole for Direct Methanol Fuel Cells. Journal of The Electrochemical Society, 156(2), B258.

Libby, B. (2001) Improving selectivity in methanol fuel cell membranes: A study of a polymer-zeolite composite membrane. Ph.D. Dissertation, University of Minnesota, Minnesota, U.S.A.

Libby, B., Smyrl, W.H., and Cussler, E.L. (2003) Polymer-zeolite composite membranes for direct methanol fuel cells. AIChE Journal, 49(4), 991-1001.

Lin, C.K., Kuo, J.F., and Chen, C.Y. (2009) Preparation of nitrated sulfonated poly(ether ether ketone) membranes for reducing methanol permeability in direct methanol fuel cell applications. Journal of Power Sources, 187(2), 341-347.

Liu, F., Ma, B.R., Zhou, D., Xiang, Y.H., and Xue, L.X. (2014) Breaking through tradeoff of Polysulfone ultrafiltration membranes by zeolite 4A. Microporous and Mesoporous Materials, 186, 113-120.

Lufrano, F., Baglio, V., Staiti, P., Arico, A.S., and Antonucci, V. (2006) Development and characterization of sulfonated polysulfone membranes for direct methanol fuel cells. Desalination, 199(1-3), 283-285.

Lufrano, F., Baglio, V., Staiti, P., Arico, A.S., and Antonucci, V. (2008) Polymer electrolytes based on sulfonated polysulfone for direct methanol fuel cells. Journal of Power Sources, 179(1), 34-41.

Lufrano, F., Baglio, V., Di Blasi, O., Staiti, P., Arico, A.S., and Antonucci, V. (2012) Solid polymer electrolyte based on sulfonated polysulfone membranes and acidic silica for direct methanol fuel cells. Solid State Ionics, 216, 90-94.

Macksasitorn, S., Changkhamchom, S., Sirivat, A., and Siemanond, K. (2012) Sulfonated poly(ether ether ketone) and sulfonated poly(1,4-phenylene ether ether sulfone) membranes for vanadium redox flow batteries. High Performance Polymers, 24(7), 603-608.

Maiti, J., Kakati, N., Lee, S.H., Jee, S.H., and Yoon, Y.S. (2011) PVA nano composite membrane for DMFC application. Solid State Ionics, 201(1), 21-26.

McKeen, J.C., Yan, Y.S., and Davis, M.E. (2008) Proton Conductivity in Sulfonic Acid-Functionalized Zeolite Beta: Effect of Hydroxyl Group. Chemistry of Materials, 20(12), 3791-3793.

Miyatake, K., Yasuda, T., Hirai, M., Nanasawa, M., and Watanabe, M. (2007) Synthesis and properties of a polyimide containing pendant sulfophenoxypropoxy groups. Journal of Polymer Science Part A: Polymer Chemistry, 45(1), 157-163.

Nicotera, I., Simari, C., Coppola, L., Zygouri, P., Gournis, D., Brutti, S., and Baglio, V. (2011) Sulfonated graphene oxide platelets in nafion nanocomposite membrane: advantages for application in direct methanol fuel cells. The Journal of Physical Chemistry C, 118(42), 24357-24368.

Nonjola, P.T., Mathe, M.K., and Modibedi, R.M. (2013) Chemical modification of polysulfone: Composite anionic exchange membrane with TiO_2 nano-particles. International Journal of Hydrogen Energy, 38(12), 5115-5121.

Park, H.S., Kim, Y.J., Hong, W.H., and Lee, H.K. (2006) Physical and electrochemical properties of Nafion/polypyrrole composite membrane for DMFC. Journal of Membrane Science, 272(1-2), 28-36.

Qiao, J., Hamaya, T., and Okada, T. (2005) New highly proton-conducting membrane poly(vinylpyrrolidone) (PVP) modified poly(vinyl alcohol)/2-acrylamido-2-methyl-1- propanesulfonic acid (PVA–PAMPS) for low temperature direct methanol fuel cells (DMFCs). Polymer, 46, 10809-10816.

Saxena, P. and Gaur, M.S. (2009) Electrical conduction mechanism of polyvinylidenefluoride (PVDF) – polysulfone (PSF) blend film. Journal of Electrostatics, 67(6), 844-849.

Sen, D., Ghosh, A.K., Mazumder, S., Bindal, R.C., and Tewari, P.K. (2014) Novel polysulfone–spray-dried silica composite membrane for water purification: Preparation, characterization and performance evaluation. Separation and Purification Technology, 123, 79-86.

Shim, S.H., Kim, K.T., Lee, J.U., and Jo, W.H. (2012) Facile method to functionalize graphene oxide and its application to poly(ethylene terephthalate)/graphene composite. ACS Applied Material Interfaces, 4(8), 4184-4191.

Tricoli, V. and Nannetti, F. (2003) Zeolite–Nafion composites as ion conducting membrane materials. Electrochimica Acta, 48(18), 2625-2633.

Tseng, C.-Y., Ye, Y.-S., Cheng, M.-Y., Kao, K.-Y., Shen, W.-C., Rick, J., and Hwang, B.-J. (2011) Sulfonated polyimide proton exchange membranes with graphene oxide show improved proton conductivity, methanol crossover impedance, and mechanical properties. Advanced Energy Materials, 1(6), 1220-1224.

Unnikrishnan, L., Madamana, P., Mohanty, S., and Nayak, S.K. (2012) Polysulfone/C30B nanocomposite membranes for fuel cell Applications: Effect of various sulfonating agents. Polymer-Plastics Technology and Engineering, 51(6), 568-577.

Vernersson, T., Lafitte, B., Lindbergh, G., and Jannasch, P. (2006) A Sulfophenylated Polysulfone as the DMFC Electrolyte Membrane – an Evaluation of Methanol Permeability and Cell Performance. Fuel Cells, 6(5), 340-346.

Wang, F., Hickner, M., Qing, J., Harrison, W., Mecham, J., Zawodzinski, T.A. and McGrath, J.E. (2001) Synthesis of highly sulfonated poly(arylene ether sulfone) random (statistical) copolymers via direct polymerization, Macromolecules, 175, 387-395.

Wang, J., Zheng, X., Wu, H., Zheng, B., Jiang, Z., Hao, X., and Wang, B. (2008) Effect of zeolites on chitosan/zeolite hybrid membranes for direct methanol fuel cell. Journal of Power Sources, 178(1), 9-19.

Wootthikanokkhan, J. and Seeponkai, N. (2006) Methanol permeability and properties of DMFC membranes based on sulfonated PEEK/PVDF blends. Journal of Applied Polymer Science, 102(6), 5941-5947.

Xu, T., Hou, W., Shen, X., Wu, H., Li, X., Wang, J., and Jiang, Z. (2011) Sulfonated titania submicrospheres-doped sulfonated poly(ether ether ketone) hybrid membranes with enhanced proton conductivity and reduced methanol permeability. Journal of Power Sources, 196(11), 4934-4942.

Xue, S. and Yin, G. (2006) Methanol permeability in sulfonated poly(etheretherketone) membranes: A comparison with Nafion membranes. European Polymer Journal, 42(4), 776-785.

Yang, C.C., Lee, Y.J., and Yang, J.M. (2009) Direct methanol fuel cell (DMFC) based on PVA/MMT composite polymer membranes. Journal of Power Sources, 188(1), 30-37.

Yang, C.C., Chien, W.C., and Li, Y.J. (2010) Direct methanol fuel cell based on poly(vinyl alcohol)/titanium oxide nanotubes/poly(styrene sulfonic acid) (PVA/nt-TiO2/PSSA) composite polymer membrane. Journal of Power Sources, 195(11), 3407-3415.

Yildirim, M.H., Curòs, A.R., Motuzas, J., Julbe, A., Stamatialis, D.F., and Wessling M. (2009) Nafion®/H-ZSM-5 composite membranes with superior performance for direct methanol fuel cells. Journal of Membrane Science, 338(1–2), 75-83.

Zarrin, H., Higgins, D., Jun, Y., Chen, Z., and Fowler, M. (2011) Functionalized graphene oxide nanocomposite membrane for low humidity and high temperature proton exchange membrane fuel cells. The Journal of Physical Chemistry C, 115(42), 20774-20781.

Zhu, Y., and Manthiram, A. (2011) Synthesis and characterization of polysulfone-containing sulfonated side chains for direct methanol fuel cells. Journal of Power Sources, 196(18), 7481-7487.

Zhang, Z., Desilets, F., Felice, V., Mecheri, B., Licoccia, S., and Tavares, A.C. (2011) On the proton conductivity of Nafion–Faujasite composite membranes for low temperature direct methanol fuel cells. Journal of Power Sources, 196(22), 9176–9187.

Zhang, L., Shi, T., Wu, S., and Zhou, H. (2013) Sulfonated graphene oxide: the new and effective material for synthesis of polystyrene-based nanocomposites. Colloid and Polymer Science, 291(9), 2061-2068.

APPENDICES

Appendix A Sulfonation Process and Degree of Sulfonation

Sulfonation process is the method for attaching a sulfonic group onto the polymer backbone. 2.0 g of the polysulfone (PSF) was dissolved in 10 mL of dichloromethane (DCM) and vigorously stirred at room temperature until homogeneous. Then the sulfuric acid was added into the polymer solution and stirred continuously for 4 h. The sulfonated polymer was precipitated into methanol ice bath under continuous stirring. The precipitate was filtered and washed by using distilled water until the pH of polymer became neutral. The sulfonated polymer was dried at 100 °C for 24 h.

Degree of sulfonation (DS) is represented by the number of sulfonic acid group per repeating unit of polymer. The DS of sulfonated polymer was determined by titration the sulfonated polymer solution with 0.01 M NaOH using phenolphthalein as an indicator. The DS was calculated by the following Eq (A1):

$$DS(\%) = \frac{(V_{NaOH} \times M_{NaOH})/1000}{\text{Mole of polymer membrane}} \times 100 \quad \text{(A1)}$$

where V_{NaOH} refers to the volume of sodium hydroxide solution, and C_{NaOH} refers to the concentration of sodium hydroxide solution.

Table A1 Sulfonation condition of PSF at 25 °C for 4 h for film casting

Weight of PSF (g)	Mole of PSF	Volume H_2SO_4 (ml)	Mole of H_2SO_4	H_2SO_4 /PSF Mole ratio	DCM Volume (ml)	Volume Fraction	Yield (%)	DS (%)
1.2151	0.0027	20	0.05	17	10	0.64	99.51	12.75
2.0014	0.045	30	0.09	20	10	0.72	96.25	15.65
2.0104	0.045	30	0.18	40	10	0.72	85.36	19.90
2.0163	0.045	30	0.27	60	10	0.72	98.89	61.44
2.0085	0.045	30	0.36	80	10	0.72	109.3	71.55

Appendix B Identification of FT-IR Spectrum of Polysulfone and Sulfonated Polysulfone

The polymers (PSF) and sulfonated polymers (S-PSF) functional groups were determined using the FT-IR spectrometer (Nicolet, Nexus 670). The samples were measured directly in the wave number range of 400-1600 cm^{-1} with a resolution of 4 cm^{-1} and 64 scans using potassium bromide (KBr; dried at 100 °C for 24 h) as a background materials. The composite material composed of sample and KBr was compressed into pellets and inserted in the sample holder (Macksasitorn *et al.*, 2012).

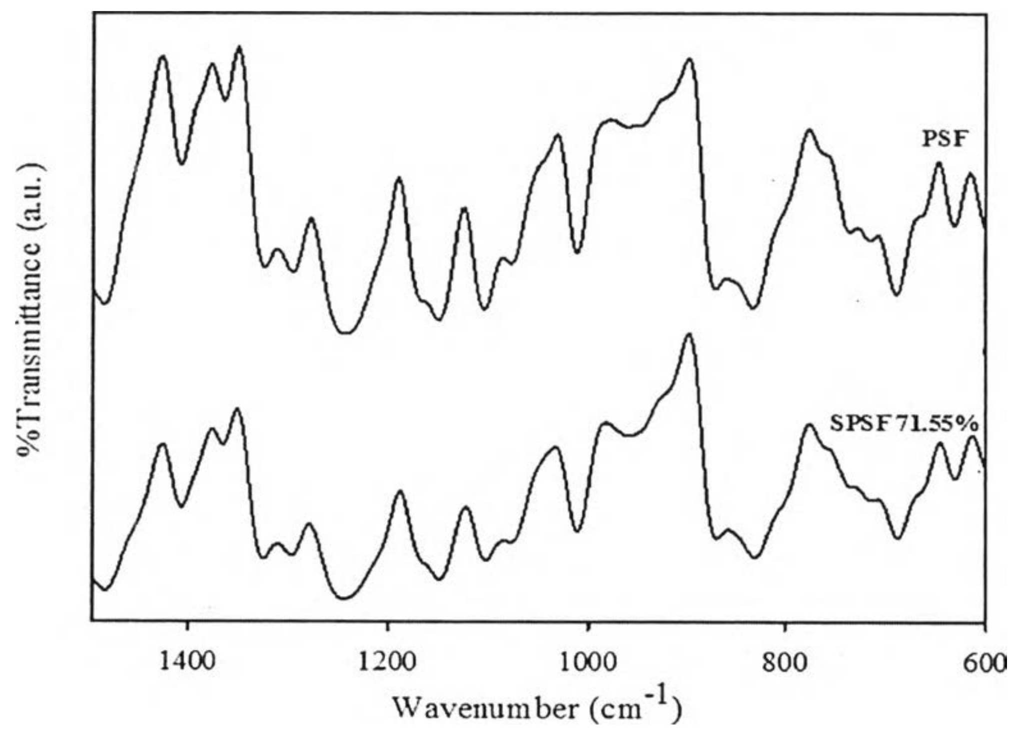

Figure B1 FT-IR spectra of polysulfone (PSF) and sulfonated polysulfone (S-PSF) at 0.72 of degree of sulfonation.

Table B1 The FT-IR absorption spectra of PSF and S-PSF

Wavenumbers (cm^{-1})	Assignments	References
696	S=O stretching of sodium sulfonate groups	Xiao *et al.*, 2002
700	Symmetric S-O stretching	Devrim *et al.*, 2009
706	S-O stretching	Lakshmi *et al.*, 2005
709	S-O stretching	Zaidi *et al.*, 2003
1014	Symmetric stretching of the diphenyl ether unit	Herrero *et al.*, 2014
1024	S=O stretching	Zaidi *et al.*, 2003
1026	S=O stretching	Lakshmi *et al.*, 2005
1028, 1243, 1084	Asymmetric and symmetric O=S=O stretching of $-SO_3H$ groups	Xiao *et al.*, 2002
1029, 1086	Symmetric and asymmetric stretching vibration O=S=O due to sodium $-SO_3H$ group in polymer	Xing *et al.*, 2005
1030, 1098	Symmetric and asymmetric stretching of $-SO_3H$ groups	Wang *et al.*, 2003
1030, 1098	Symmetric and asymmetric stretching of the $-SO_3H$ groups	Devrim *et al.*, 2009
1030	Symmetric stretching of the $-SO_3H$ groups	Herrero *et al.*, 2014
1080	Symmetric O=S=O stretching	Zaidi *et al.*, 2003
1104	Symmetric O=S=O stretching	Karlsson *et al.*, 2004
1107	Para in-plane aromatic C-H bond	Devrim *et al.*, 2009
1150	Symmetric O=S=O stretching	Devrim *et al.*, 2009
1164	Asymmetric O=S=O stretching	Lakshmi *et al.* 2005
1150 - 1350	Asymmetric stretching of the $-SO_3H$ groups	Herrero *et al.*, 2014
1203	Asymmetric O=S=O stretching vibrations	Wang *et al.*, 2003

Table B1 (Cont.) The FT-IR absorption spectra of PSF and S-PSF

Wavenumbers (cm^{-1})	**Assignments**	**References**
1229, 1099, 1021	Asymmetric and symmetric O=S=O stretching vibrations of $-SO_3H$ groups	Wang *et al.*, 2006
1245	Asymmetric O=S=O stretching	Karlsson *et al.*, 2004
1252	Asymmetric O=S=O stretching	Zaidi *et al.*, 2003
1301, 1149	Asymmetric and symmetric O=S=O stretching of sulfone groups	Xiao *et al.*, 2002
1482	Tri-substituted on aromatic phenyl due to sulfonation in phenyl ring	Xing *et al.*, 2005
1490	C-C aromatic	Zaidi *et al.*, 2003
1492, 1470,1414, 1402	1,3,4-trisubstituted aromatic C-C skeletal vibrations	Lakshmi *et al.*, 2005
1501	Di-substituted on aromatic phenyl for non-sulfonated	Xing *et al.*, 2005
3400	O-H stretching of the $-SO_3H$ group	Herrero *et al.*, 2014
3440, 1252, 1080, 1024	Sulfonic acid groups	Zaidi *et al.*, 2003
3450-3430	O-H vibration	Zaidi *et al.*, 2003
1150 - 1350	Asymmetric stretching of the $-SO_3H$ groups	Herrero *et al.*, 2014
1203	Asymmetric O=S=O stretching vibrations	Wang *et al.*, 2003
1229, 1099, 1021	Asymmetric and symmetric O=S=O stretching vibrations of $-SO_3H$ groups	Wang *et al.*, 2006
1245	Asymmetric O=S=O stretching	Karlsson *et al.*, 2004

Appendix C Nuclear Magnetic Resonance (NMR)

The structure of sulfonated PSF was determined by a NMR spectrometer (Bruker Biospin Avance 500 MHz NMR spectrometer) using deuterated dimethyl sulfoxide (DMSO-d_6) as the solvent at room temperature.

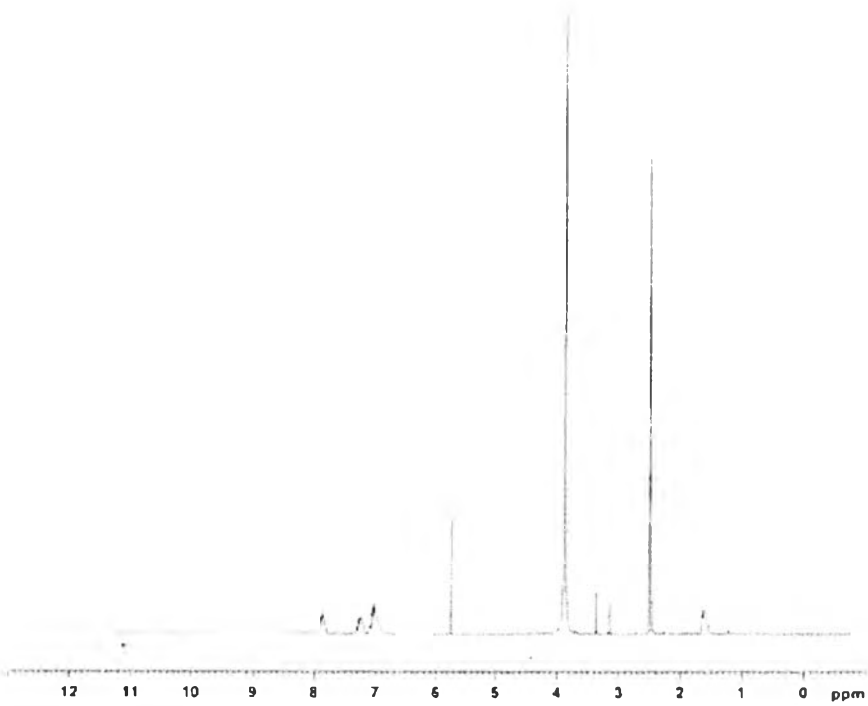

Figure C1 ^{1}H-NMR spectrum for sulfonated Polysulfone (S-PSF).

The proton resonance at 7.72 ppm is assigned to the proton adjacent to the new pendent sulfonic acid on the PSF structure [Devrim *et al.*, 2009].

Table C1 Chemical Shift (ppm) from ^{1}H-NMR spectra for S-PSF

Position	Type of Proton	S-PSF	Literature	
		Chemical Shift (ppm)	Chemical Shift (ppm)	Author, Year
1', 4'	Aromatic-H	6.95	6.9	Devrim, 2009
			6.95	Unnikrishnan, 2012
1, 4	Aromatic-H	7.05	7.1	Devrim, 2009
			7.05	Unnikrishnan, 2012
2, 2'	Aromatic-H	7.25	7.3	Devrim, 2009
			7.25	Unnikrishnan, 2012
2'	New pendent sulfonic acid	7.80	7.72	Devrim, 2009
			7.75	Unnikrishnan, 2012
3, 3'	Aromatic-H	7.87	7.9	Devrim, 2009
			7.85	Unnikrishnan, 2012

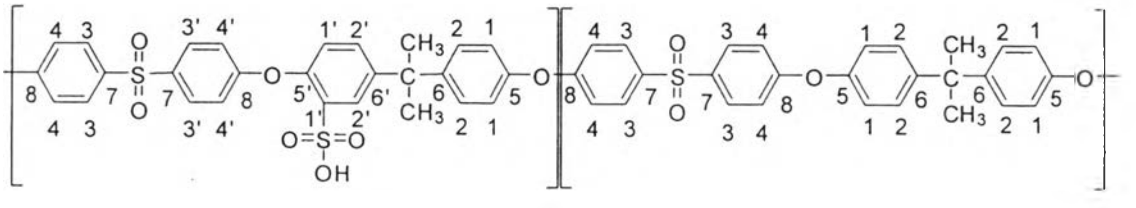

Figure C2 Chemical structure of Sulfonated Polysulfone (S-PSF).

Appendix D Thermogravimetric Analysis

The thermal property of the polymers and sulfonated polysulfone (S-PSF) and S-PSF/Zeolite Y composite membranes were investigated using a Thermo-Gravimetric/Differential Thermal Analyzer (TG/DTA; Perkin Elmer, Pyris Diamond). The samples were inserted into an alumina pan at the weight of 4-10 mg and. The measurements were carried out under nitrogen flow with the temperature range of 30 °C to 700 °C at a heating rate of 10 °C. min^{-1} (Zhang *et al.*, 2011).

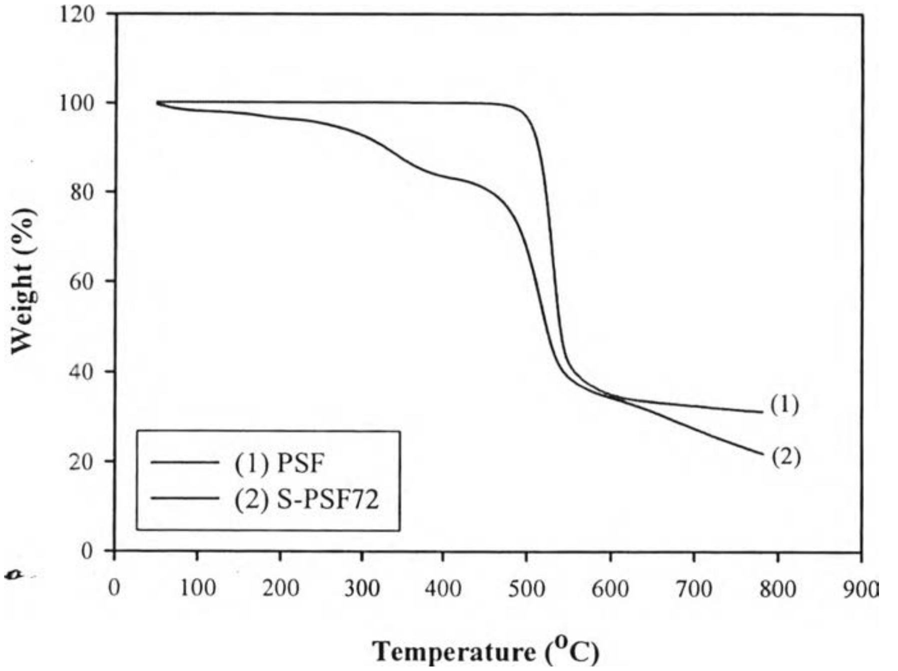

Figure D1 TGA thermograms of polysulfone (PSF) and sulfonated polysulfone (S-PSF) at 0.72 of degrees of sulfonation.

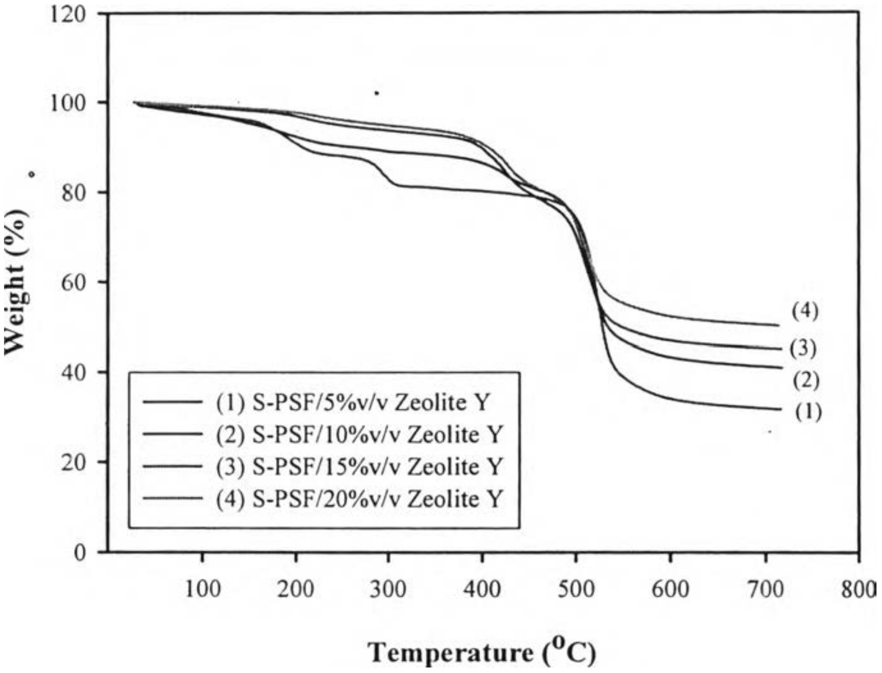

Figure D2 TGA curve for S-PSF/Zeolite Y composite membranes.

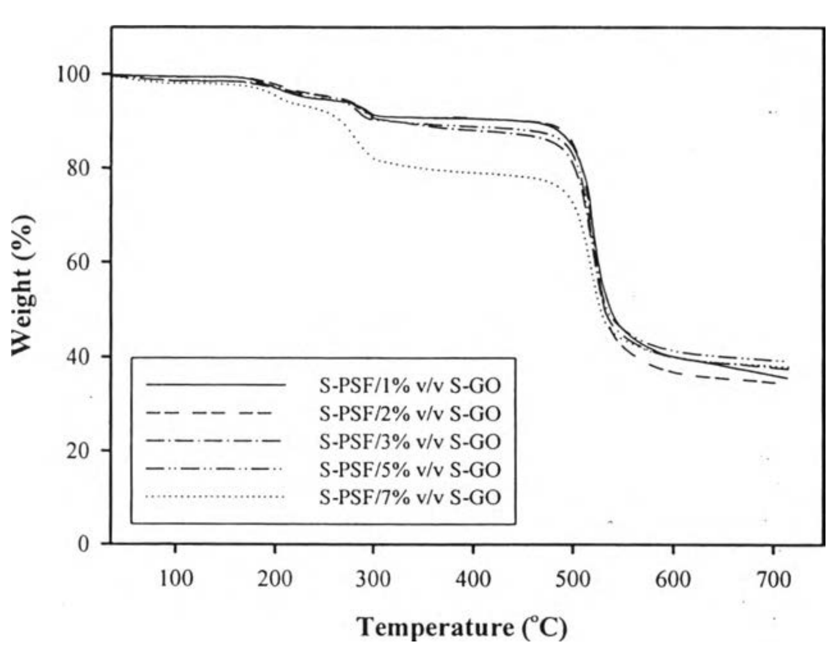

Figure D3 TGA curve for S-PSF/S-GO composite membranes.

Table D1 Thermal stability of S-PSF and S-PSF/Zeolite Y composite membranes

Sample	Temperature (°C)	Degradation
S-PSF (DS = 0.7155)	50 – 180	Loss of water and residual solvent during casting
	180 – 400	Decomposition of sulfonic acid groups
	> 400	Degradation of S-PSF backbone
S-PSF/5% v/v Zeolite Y	50 – 240	Loss of water and residual solvent during casting
	240 – 400	Decomposition of sulfonic acid groups
	> 400	Degradation of S-PSF backbone
S-PSF/10% v/v Zeolite Y	50 – 260	Loss of water and residual solvent during casting
	260 – 430	Decomposition of sulfonic acid groups
	> 430	Degradation of S-PSF backbone
S-PSF/15% v/v Zeolite Y	50 – 300	Loss of water and residual solvent during casting
	300 – 440	Decomposition of sulfonic acid groups
	> 440	Degradation of S-PSF backbone
S-PSF/20% v/v Zeolite Y	50 – 320	Loss of water and residual solvent during casting
	320 – 440	Decomposition of sulfonic acid groups
	> 440	Degradation of S-PSF backbone

Table D2 Thermal stability of S-PSF/S-GO composite membranes

Sample	Temperature (°C)	Degradation
S-PSF/1% v/v S-GO	50 – 220	Loss of water and residual solvent during casting
	220 – 380	Decomposition of sulfonic acid groups
	> 380	Degradation of S-PSF backbone
S-PSF/2% v/v S-GO	50 – 250	Loss of water and residual solvent during casting
	250 – 400	Decomposition of sulfonic acid groups
	> 400	Degradation of S-PSF backbone
S-PSF/3% v/v S-GO	50 – 225	Loss of water and residual solvent during casting
	225 – 410	Decomposition of sulfonic acid groups
	> 410	Degradation of S-PSF backbone
S-PSF/5% v/v S-GO	50 – 220	Loss of water and residual solvent during casting
	220 – 380	Decomposition of sulfonic acid groups
	> 380	Degradation of S-PSF backbone
S-PSF/7% v/v S-GO	50 – 215	Loss of water and residual solvent during casting
	215 – 400	Decomposition of sulfonic acid groups
	> 400	Degradation of S-PSF backbone

Appendix E Proton Conductivity Under Dry State

The impedance data was measured by using an impedance phase analyzer HP 4194 at various frequencies from100 Hz to 2 MHz and at room temperature. The membranes were cut into 5 ×5 cm^2 specimens for the measurement. The proton conductivity was calculated from EQ. E.1:

$$\sigma\ (S/cm) = \frac{d}{R \times A} \quad \text{(E1)}$$

where d is the sample thickness (cm), A is the contact area of the sample ($\pi r^2 = \pi(3.8/2)^2 = 11.34\ cm^2$)., and R can be derived from the low intercept of the high frequency semi-circle on a complex impedance plane with the Re (*Z*) axis.

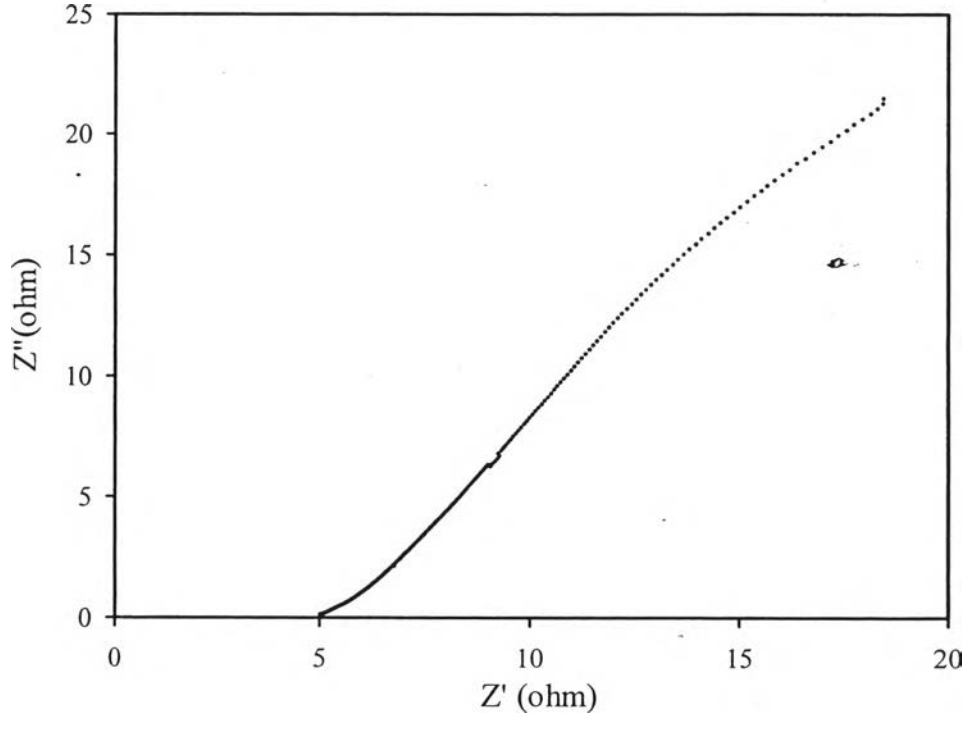

Figure E1 Nyquist plot of the Nafion117 membrane.

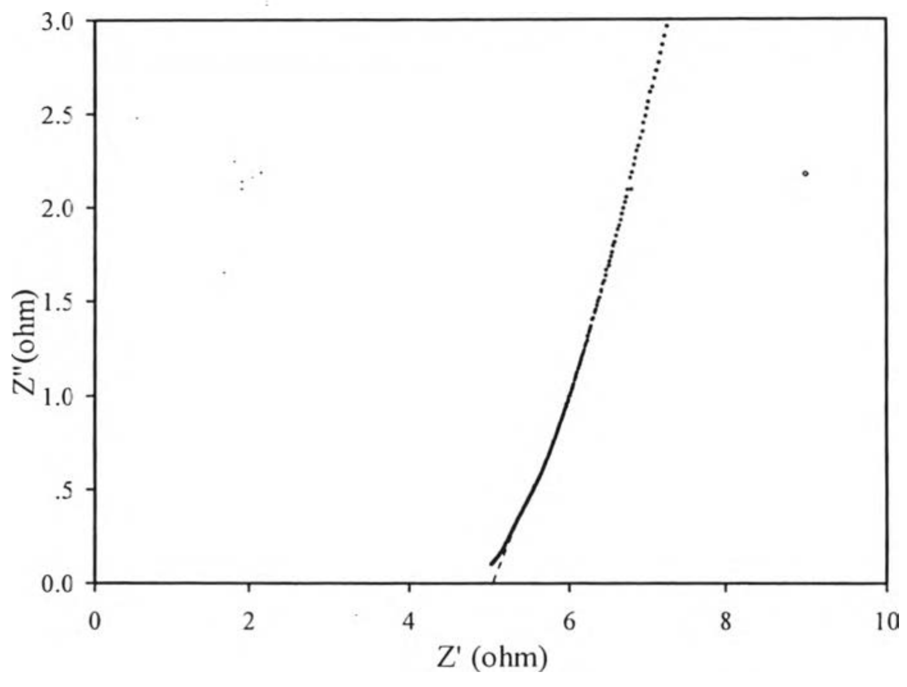

Figure E2 Enlarged Nyquist plot of the Nafion117 membrane (R = 5.00 ohm).

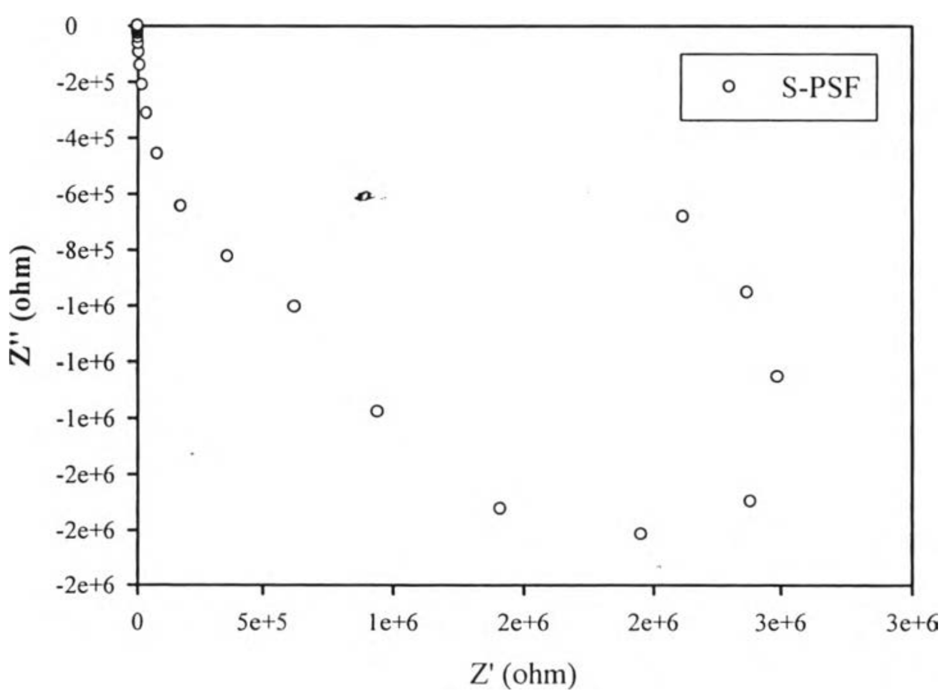

Figure E3 Nyquist plot of the S-PSF with a DS of 0.72 at 27 °C under dry state.

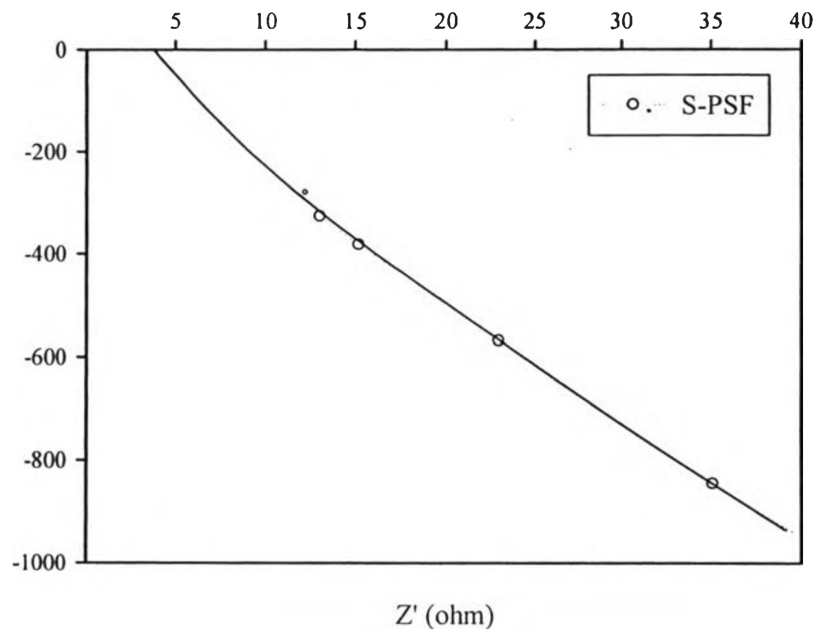

Figure E4 Enlarged Nyquist plot of the S-PSF with a DS of 0.72 at 27 °C under dry state (R = 3.94 ohm).

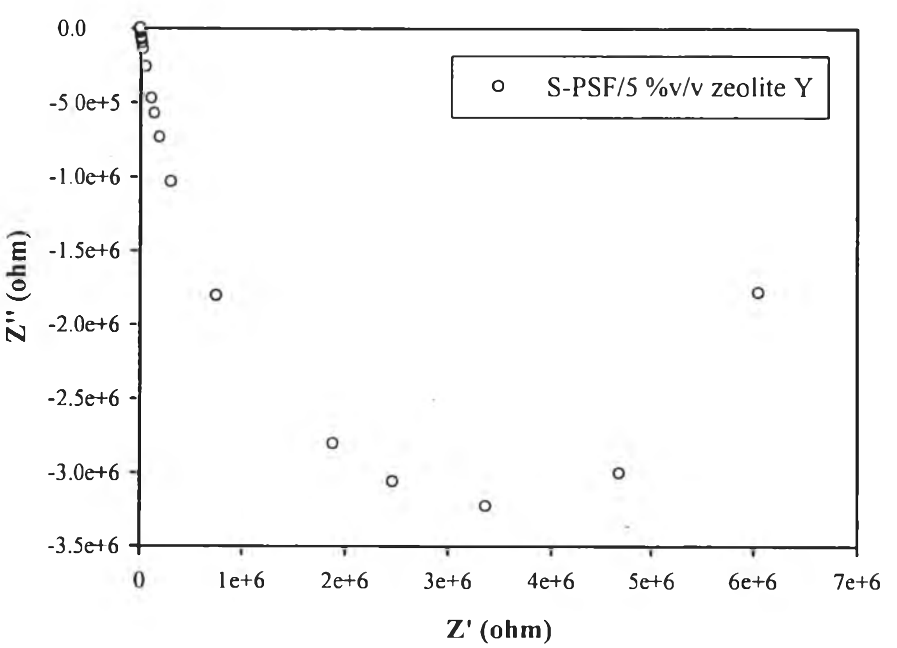

Figure E5 Nyquist plot of the S-PSF with 5% v/v of Zeolite Y at 27 °C under dry state.

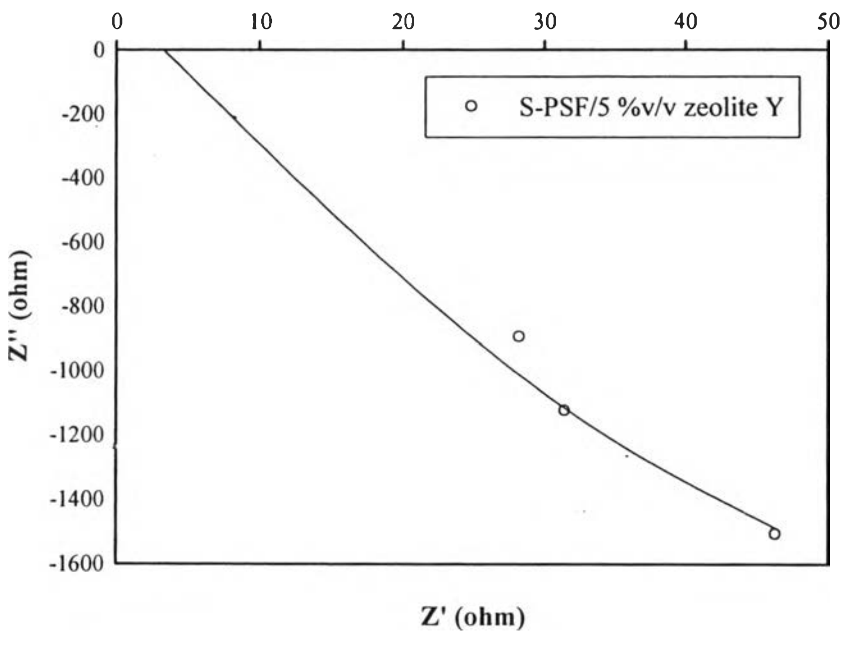

Figure E6 Enlarged Nyquist plot of the S-PSF with 5% v/v of Zeolite Y at 27 °C under dry state (R = 2.89 ohm).

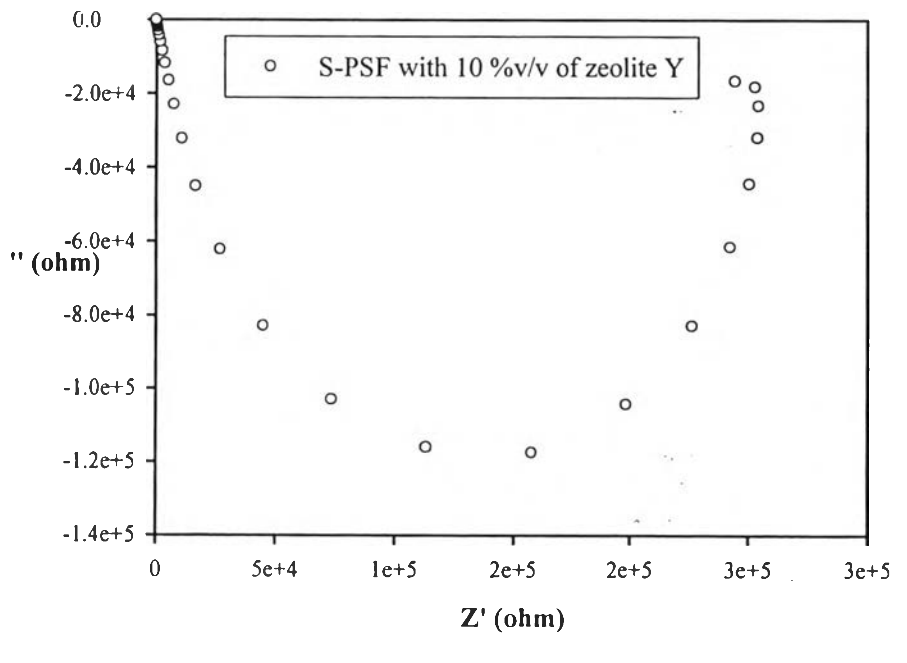

Figure E7 Nyquist plot of the S-PSF with 10% v/v of Zeolite Y at 27 °C under dry state.

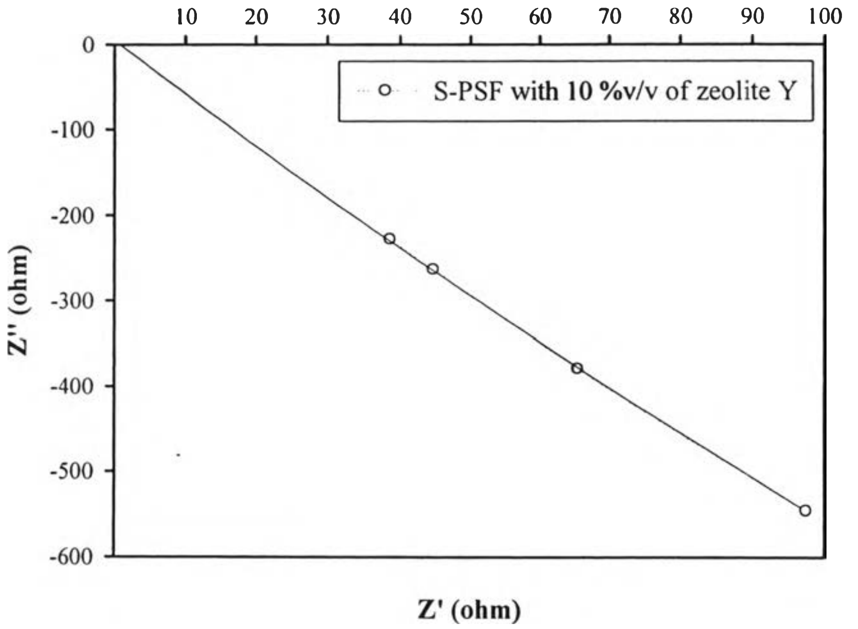

Figure E8 Enlarged Nyquist plot of the S-PSF with 10% v/v of Zeolite Y at 27 °C under dry state (R = 1.05 ohm).

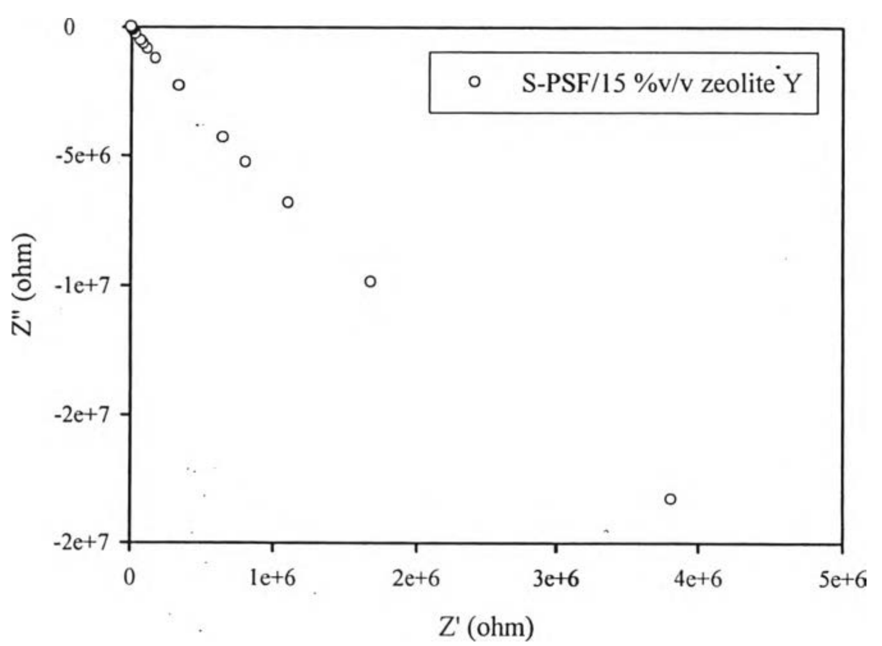

Figure E9 Nyquist plot of the S-PSF with 15% v/v of Zeolite Y at 27 °C under dry state.

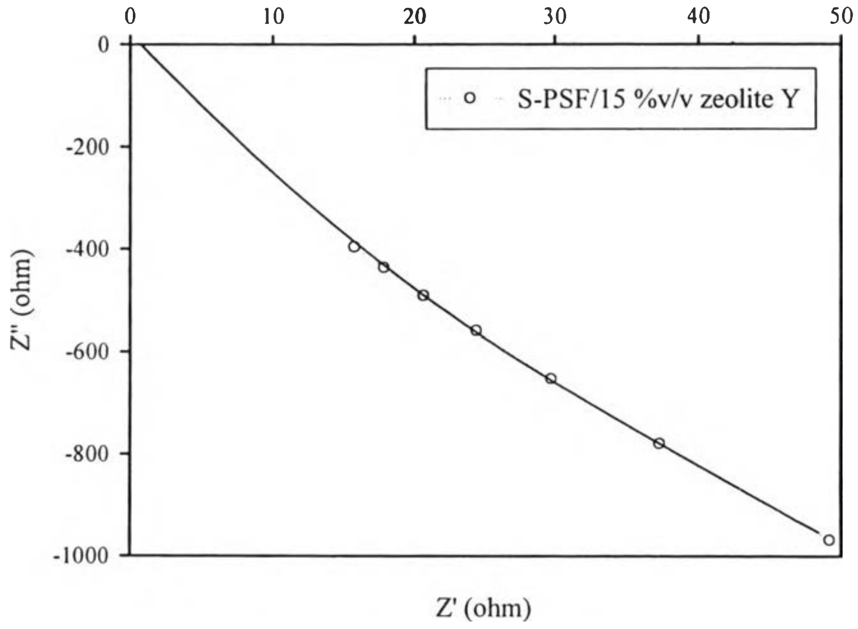

Figure E10 Enlarged Nyquist plot of the S-PSF with 15% v/v of Zeolite Y at 27 °C under dry state (R = 0.96 ohm).

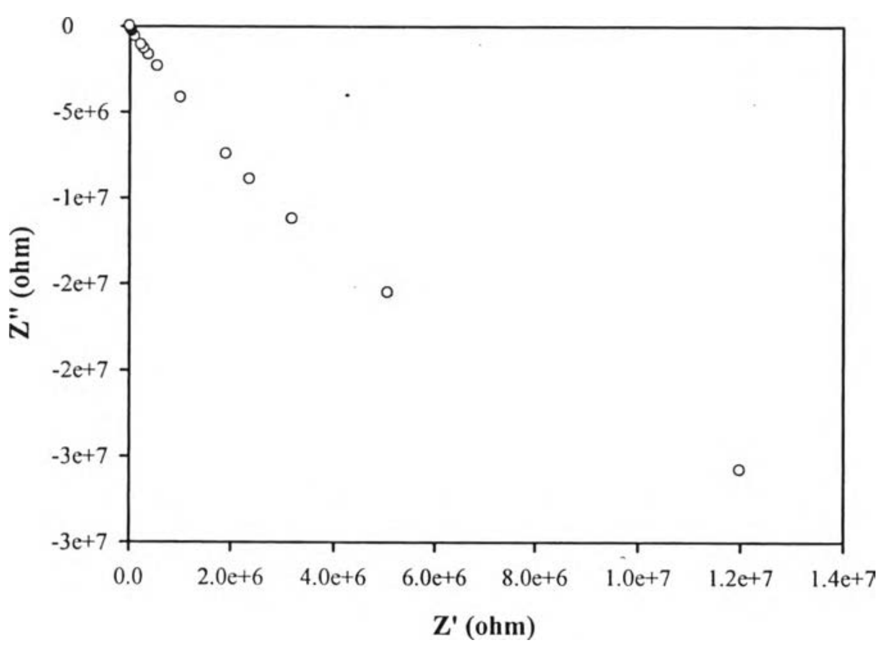

Figure E11 Nyquist plot of the S-PSF with 20% v/v of Zeolite Y at 27 °C under dry state.

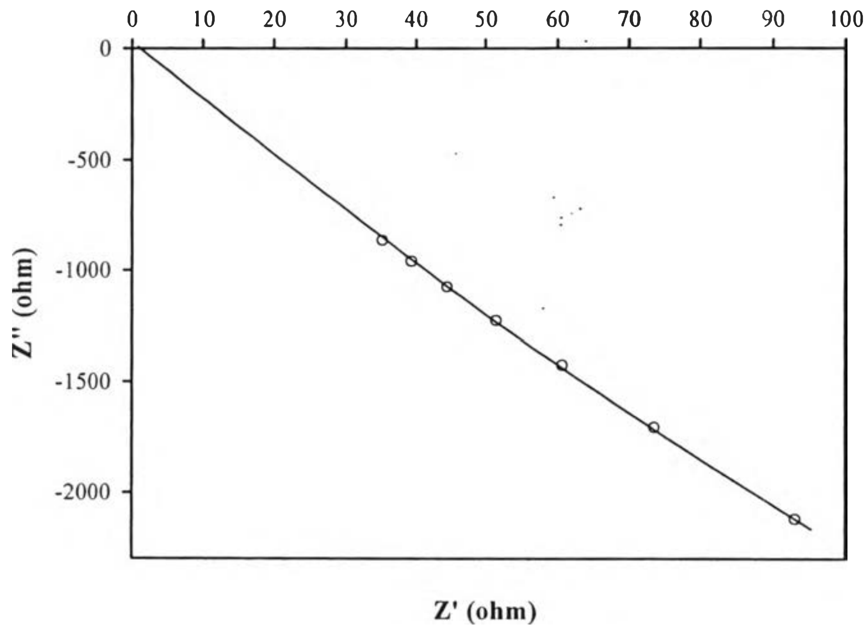

Figure E12 Enlarged Nyquist plot of the S-PSF with 20% v/v of Zeolite Y at 27 °C under dry state (R = 1.41 ohm).

Table E1 Proton conductivity of the S-PSF/Zeolite Y composite membrane with a DS of 0.72 at 27 °C under dry state

Polymer	Thickness (cm)	Contact Area (cm^2)	R (ohm)	Proton Conductivity (S/cm)
S-PSF72	0.0199± 0.0010	11.34	3.94 ± 0.11	4.45×10^{-4} ± 1.28×10^{-5}
S-PSF/Zeolite Y 5 %v/v	0.0245 ± 0.0033	11.34	2.89 ± 0.14	7.47×10^{-4} ± 3.43×10^{-5}
S-PSF/Zeolite Y 10 %v/v	0.0178± 0.0008	11.34	1.05 ± 0.08	1.50×10^{-3} ± 1.19×10^{-4}
S-PSF/Zeolite Y 15 %v/v	0.0193± 0.0009	11.34	0.96 ± 0.07	1.77×10^{-3} ± 1.33×10^{-4}
S-PSF/Zeolite Y 20 %v/v	0.0185± 0.0017	11.34	1.41 ± 0.13	1.16×10^{-3} ± 1.06×10^{-4}
Nafion 117	0.0180	11.34	5.00	2.88×10^{-4}

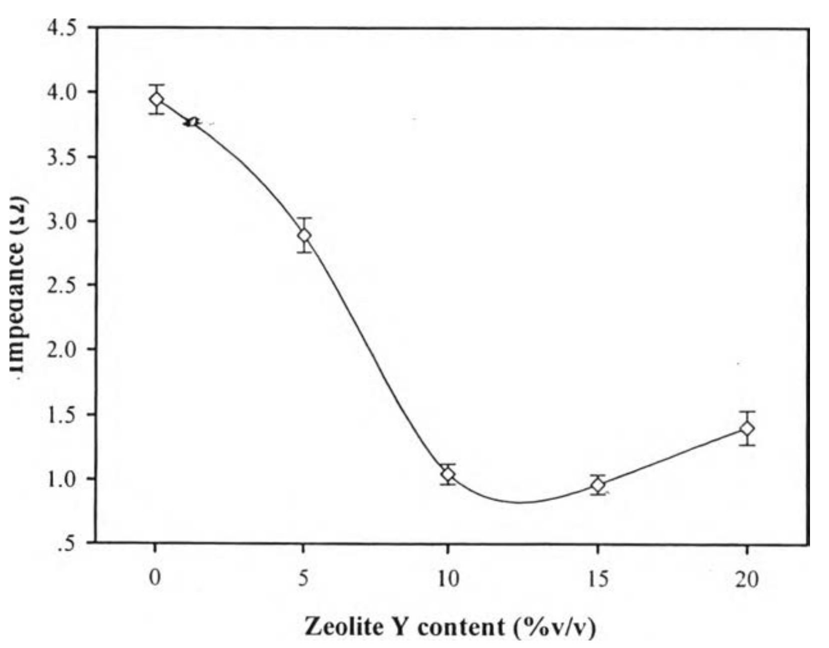

Figure E13 Impedance of the S-PSF/Zeolite Y composite membrane with a DS of 0.72 at 27 °C under dry state.

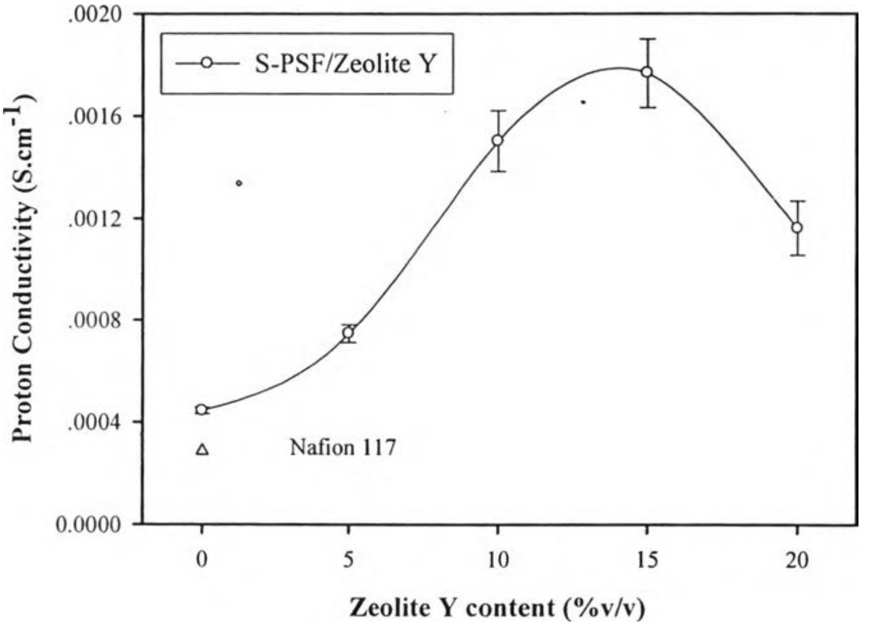

Figure E14 Proton conductivity of the S-PSF/Zeolite Y composite membrane with a DS of 0.72 at 27 °C under dry state.

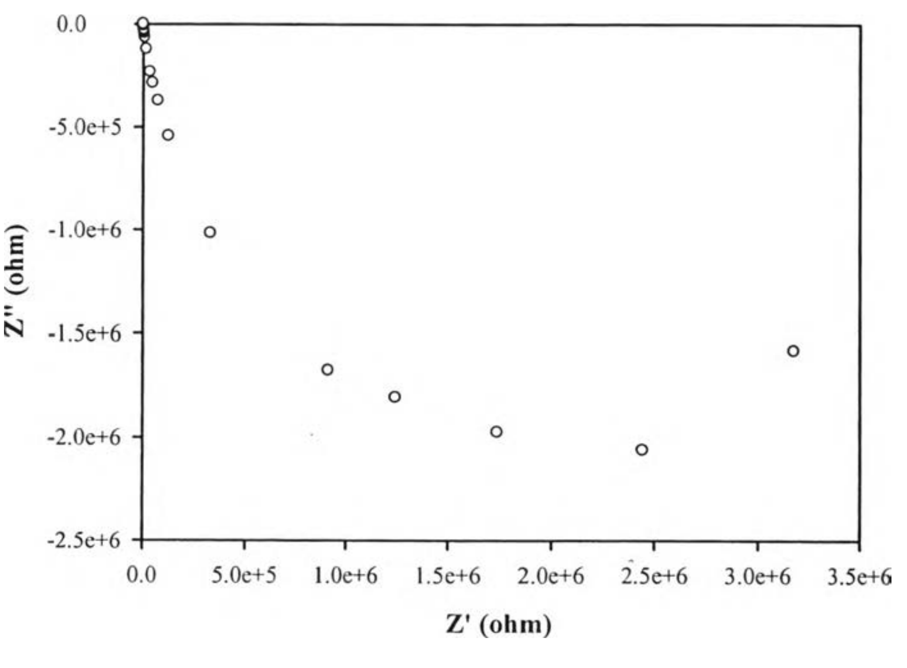

Figure E15 Nyquist plot of the S-PSF with 1% v/v of S-GO at 27 °C under dry state.

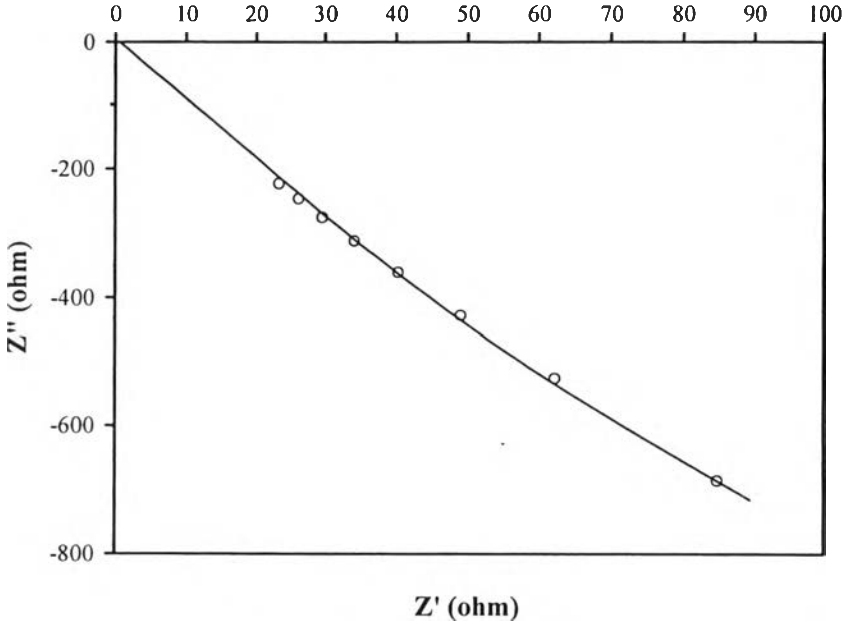

Figure E16 Enlarged Nyquist plot of the S-PSF with 1% v/v of S-GO at 27 °C under dry state (R = 1.18 ohm).

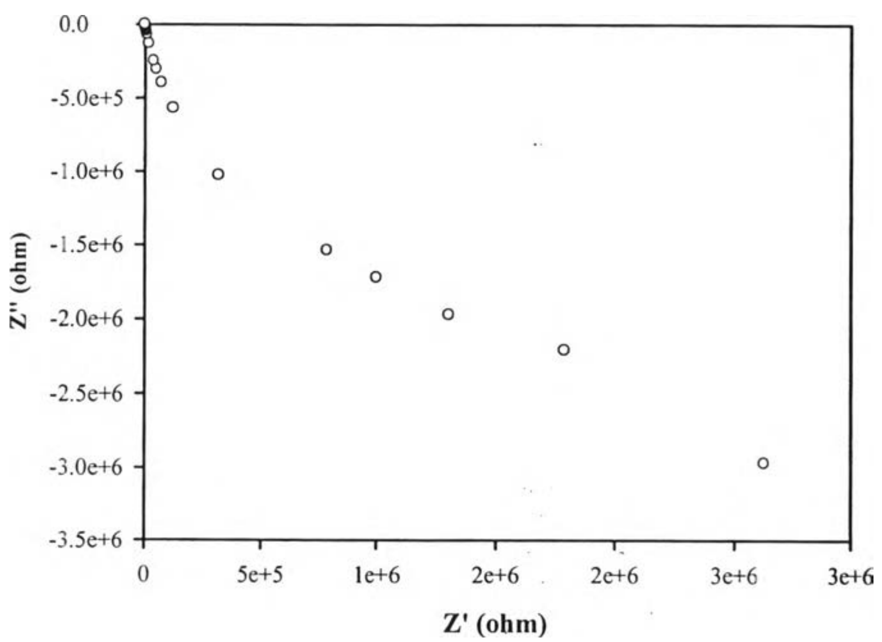

Figure E17 Nyquist plot of the S-PSF with 2% v/v of S-GO at 27 °C under dry state.

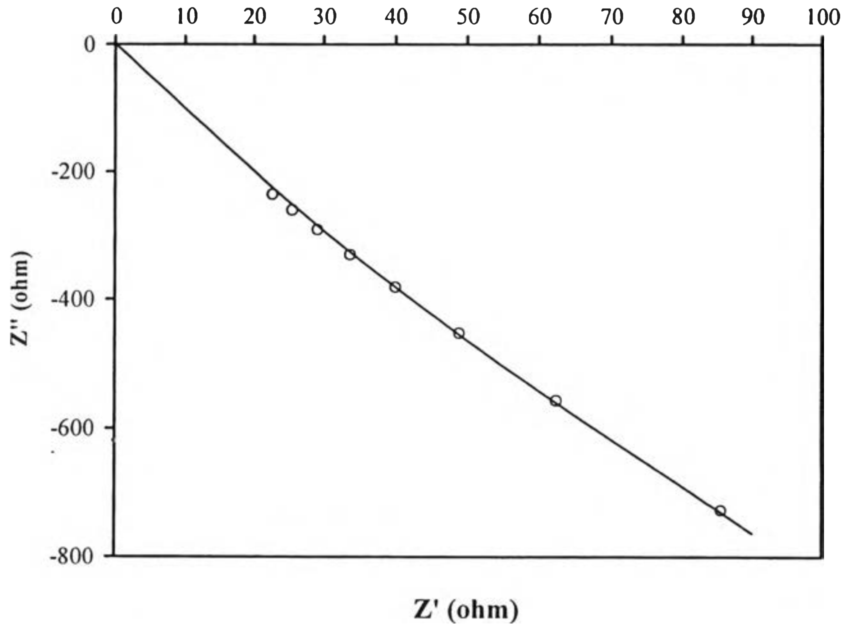

Figure E18 Enlarged Nyquist plot of the S-PSF with 2% v/v of S-GO at 27 °C under dry state (R = 0.68 ohm).

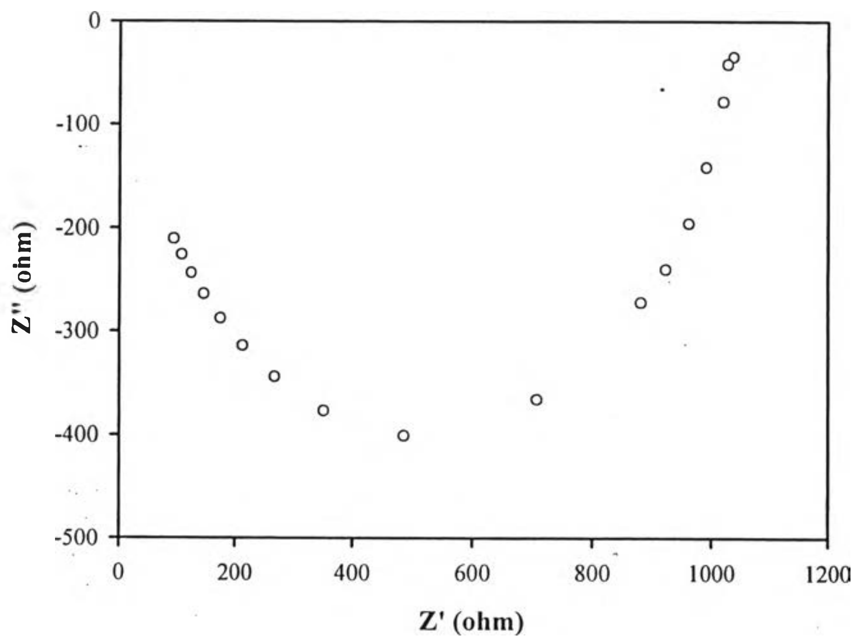

Figure E19 Nyquist plot of the S-PSF with 3% v/v of S-GO at 27 °C under dry state.

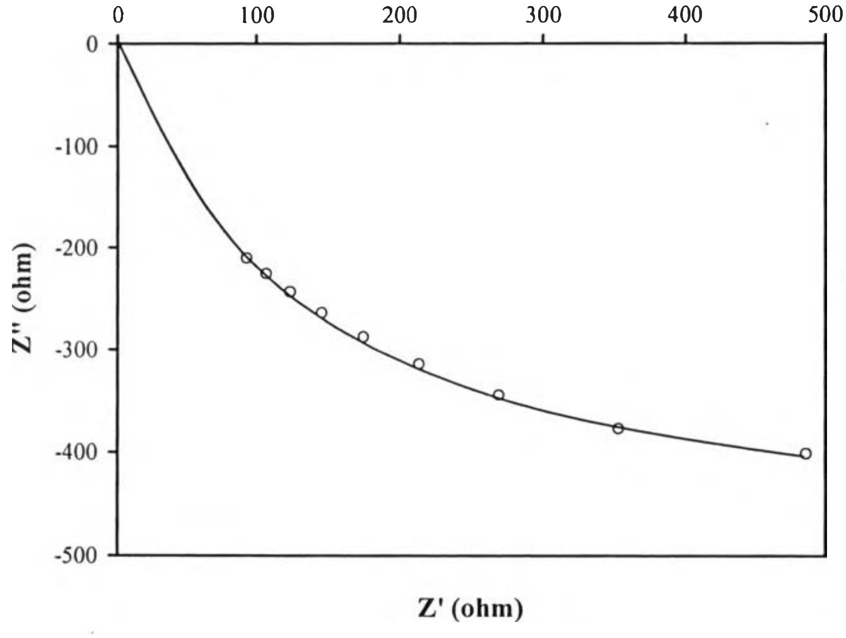

Figure E20 Enlarged Nyquist plot of the S-PSF with 3% v/v of S-GO at 27 °C under dry state (R = 0.57 ohm).

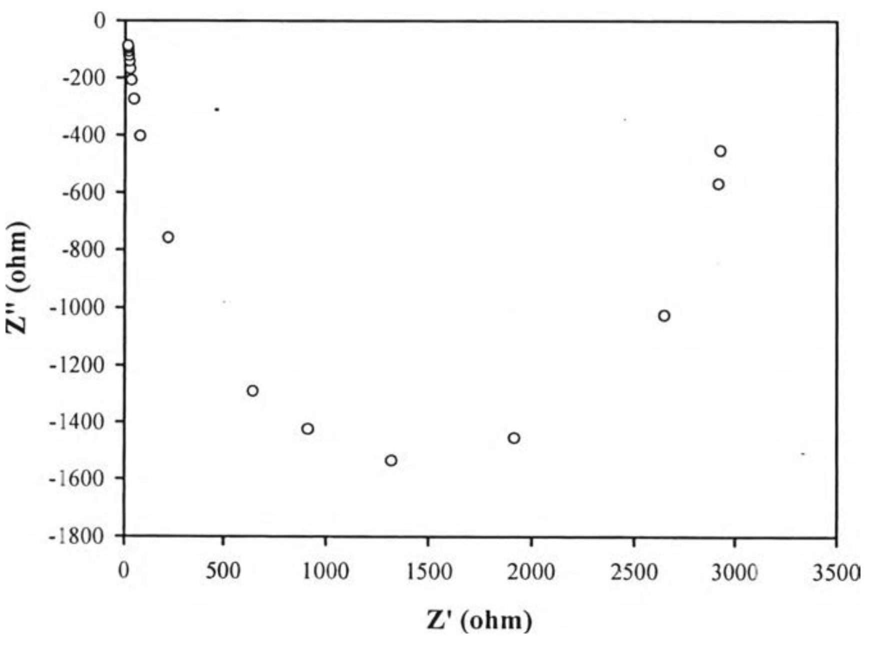

Figure E21 Nyquist plot of the S-PSF with 5% v/v of S-GO at 27 °C under dry state.

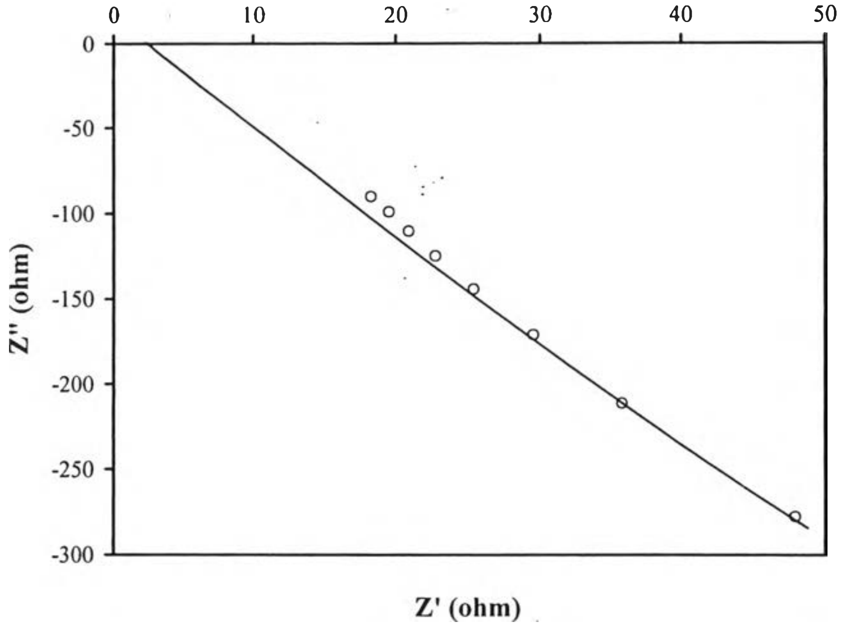

Figure E22 Enlarged Nyquist plot of the S-PSF with 5% v/v of S-GO at 27 °C under dry state (R = 1.18 ohm).

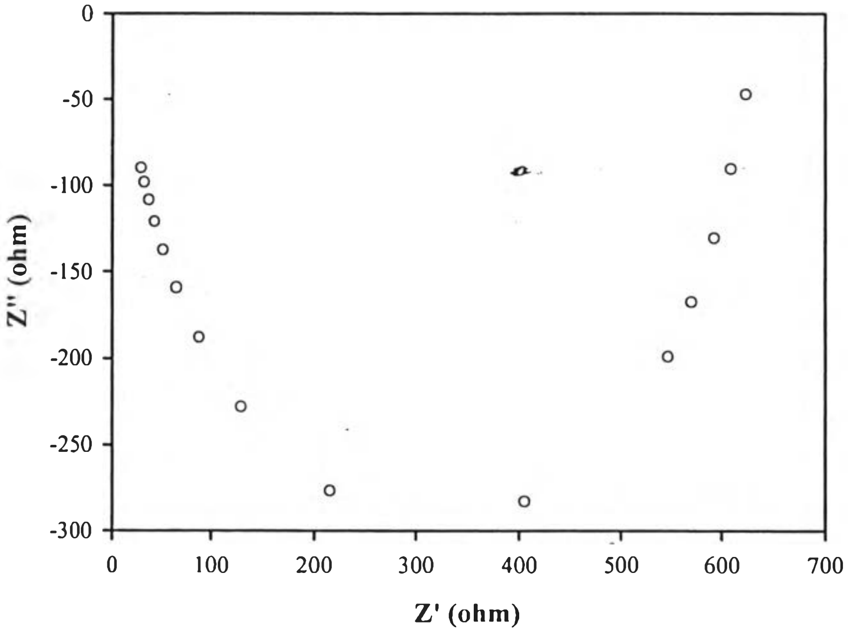

Figure E23 Nyquist plot of the S-PSF with 7% v/v of S-GO at 27 °C under dry state.

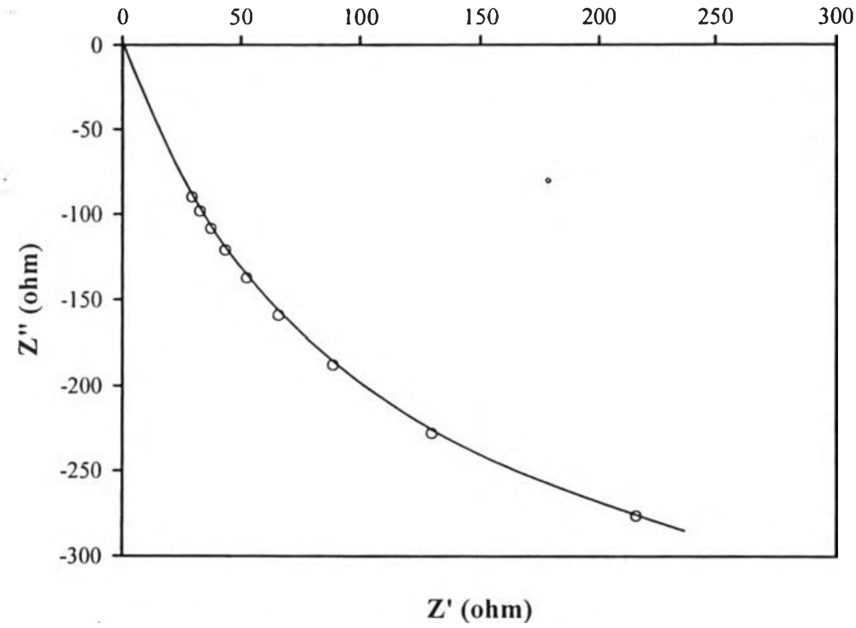

Figure E24 Enlarged Nyquist plot of the S-PSF with 7% v/v of S-GO at 27 °C under dry state (R = 1.31 ohm).

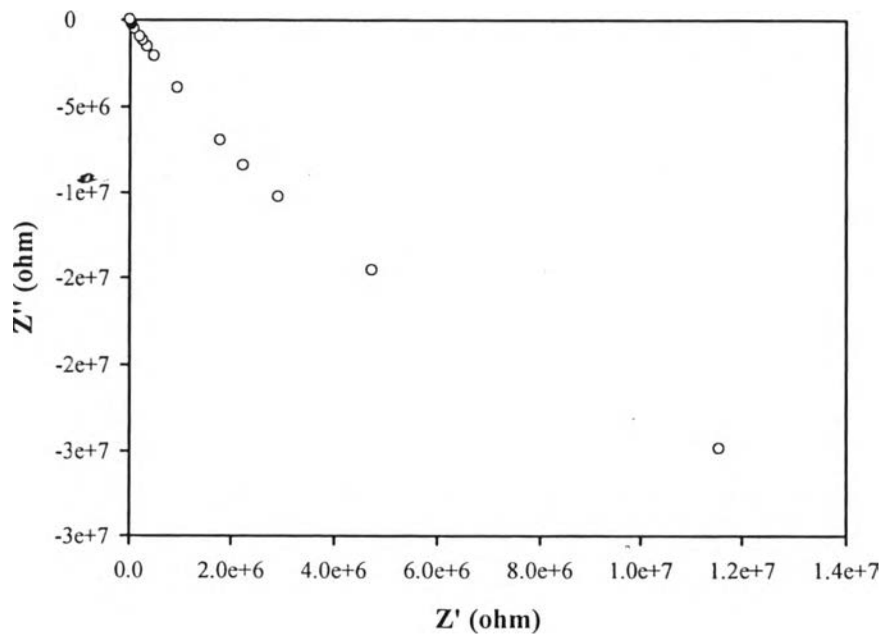

Figure E25 Nyquist plot of the pristine S-GO at 27 °C under dry state.

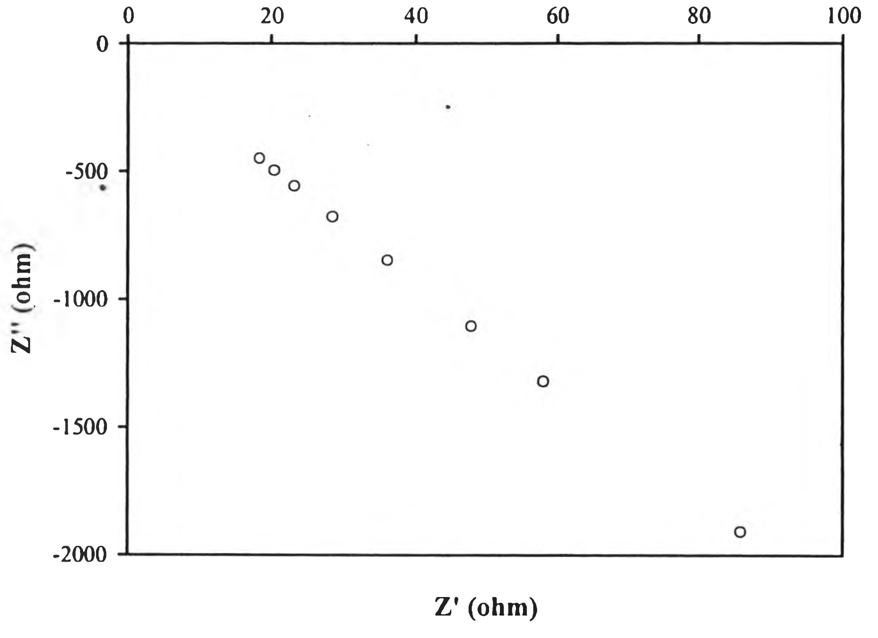

Figure E26 Enlarged Nyquist plot of the pristine S-GO at 27 °C under dry state.

Table E2 Proton conductivity of the S-PSF/S-GO composite membrane with a DS of 0.72 at 27 °C under dry state

Polymer	**Thickness (cm)**	**Contact Area (cm^2)**	**R (ohm)**	**Proton Conductivity (S/cm)**
Nafion 117	0.0180	11.34	5.00	2.88×10^{-4}
S-PSF72	0.0199± 0.0010	11.34	3.94 ± 0.11	4.45×10^{-4} ± 1.28×10^{-5}
S-GO	0.0306 ± 0.0005	11.34	0.27 ± 0.04	1.00×10^{-2} ± 1.46×10^{-3}
S-PSF/1S-GO	0.0187 ± 0.0011	11.34	1.18 ± 0.13	1.40×10^{-3} ± 1.57×10^{-4}
S-PSF/2S-GO	0.0191 ± 0.0006	11.34	0.68 ± 0.14	2.57×10^{-3} ± 5.23×10^{-4}
S-PSF/3S-GO	0.0192 ± 0.0010	11.34	0.57 ± 0.03	3.01×10^{-3} ± 1.90×10^{-4}
S-PSF/5S-GO	0.0188 ± 0.0059	11.34	1.18 ± 0.13	1.41×10^{-3} ± 1.57×10^{-4}
S-PSF/7S-GO	0.0180 ± 0.0078	11.34	1.31 ± 0.19	1.23×10^{-3} ± 1.75×10^{-4}

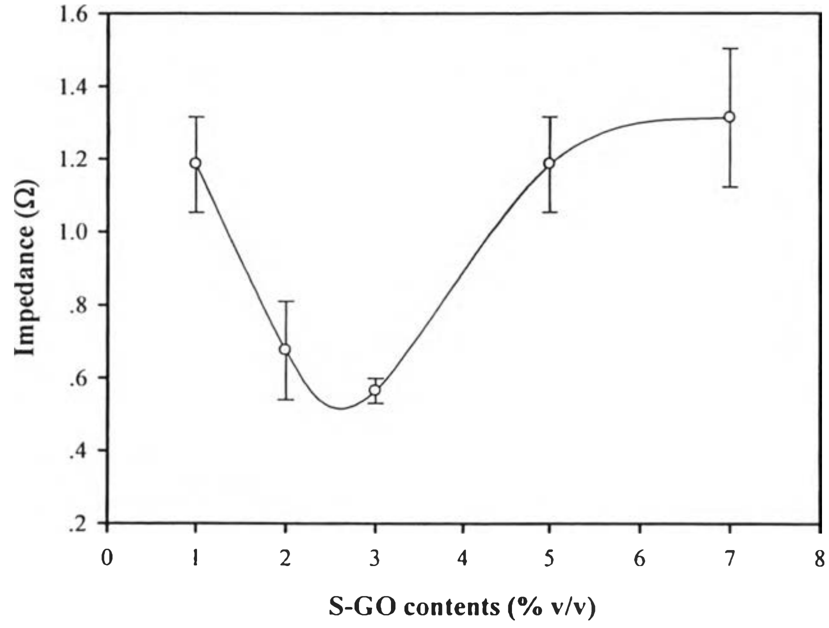

Figure E27 Impedance of the S-PSF/S-GO composite membrane with a DS of 0.72 at 27 °C under dry state.

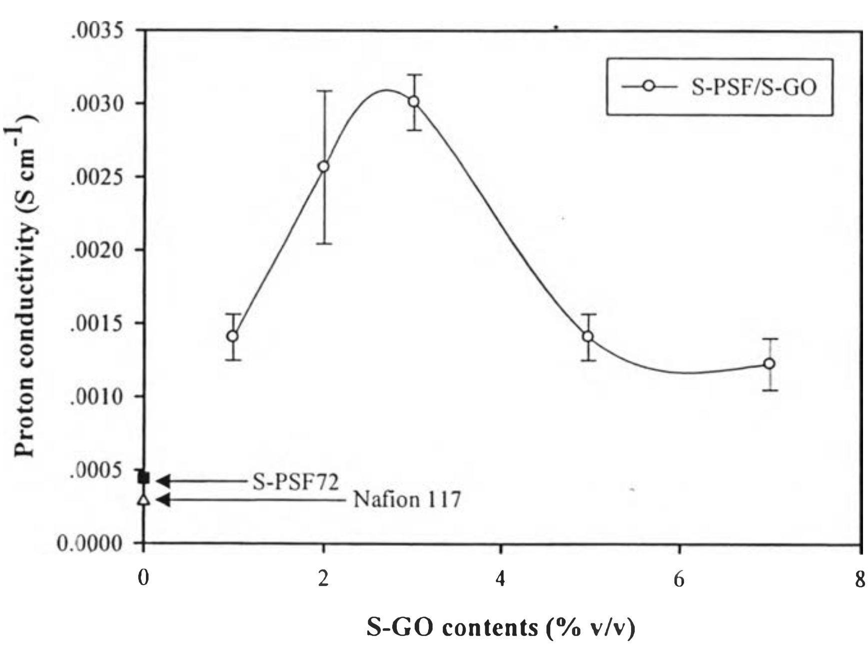

Figure E28 Proton conductivity of the S-PSF/S-GO composite membrane with a DS of 0.72 at 27 °C under dry state.

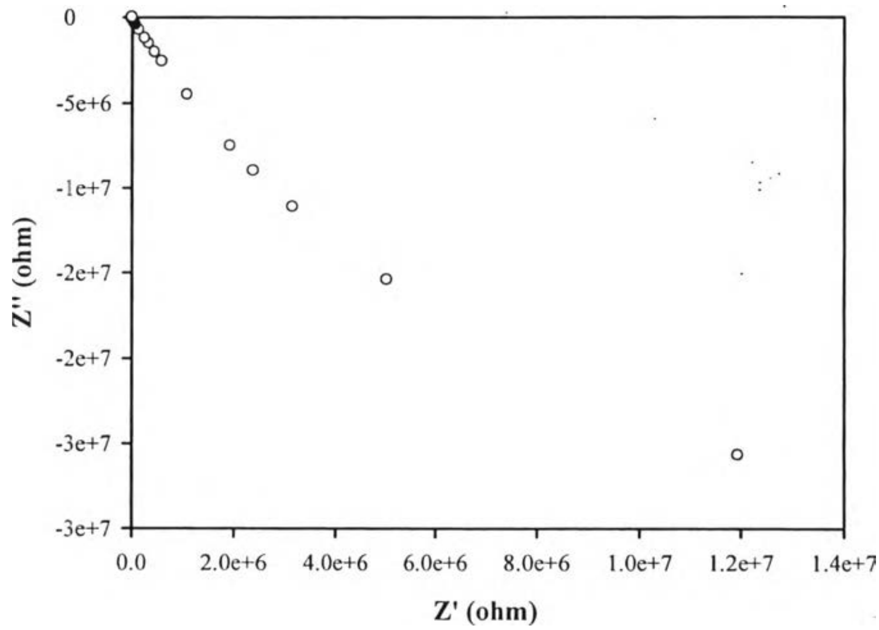

Figure E29 Nyquist plot of the S-PSF with 3% v/v of S-GO and 12% v/v of zeolite Y at 27 °C under dry state.

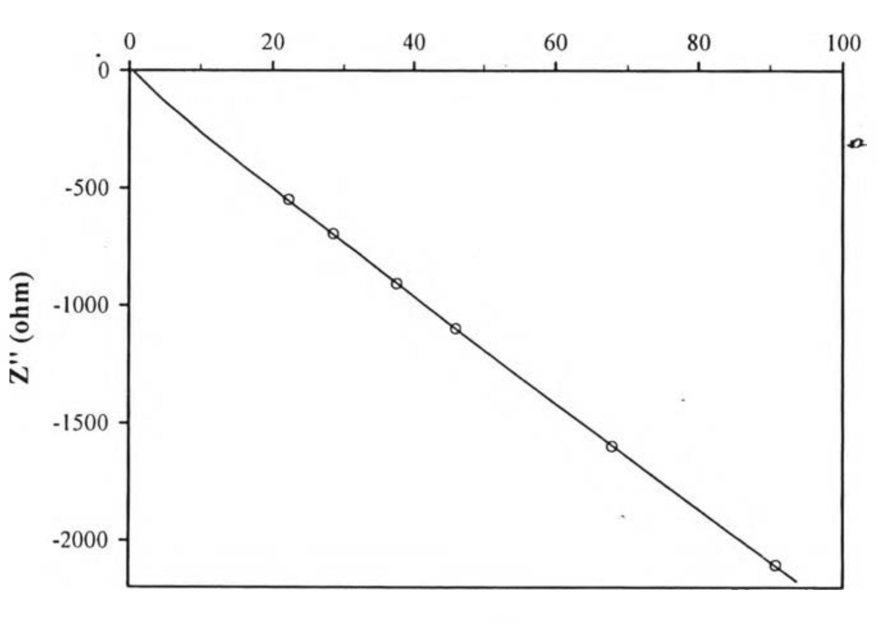

Figure E30 Enlarged Nyquist plot of the S-PSF with 3% v/v of S-GO and 12% v/v of zeolite Y at 27 °C under dry state (R = 0.61 ohm).

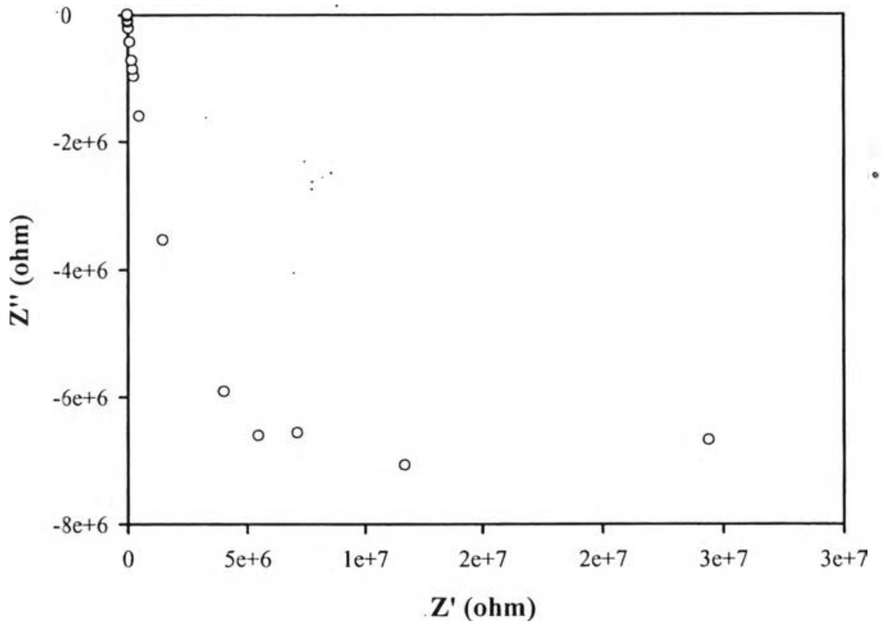

Figure E31 Nyquist plot of the S-PSF with 3% v/v of S-GO and 15% v/v of zeolite Y at 27 °C under dry state.

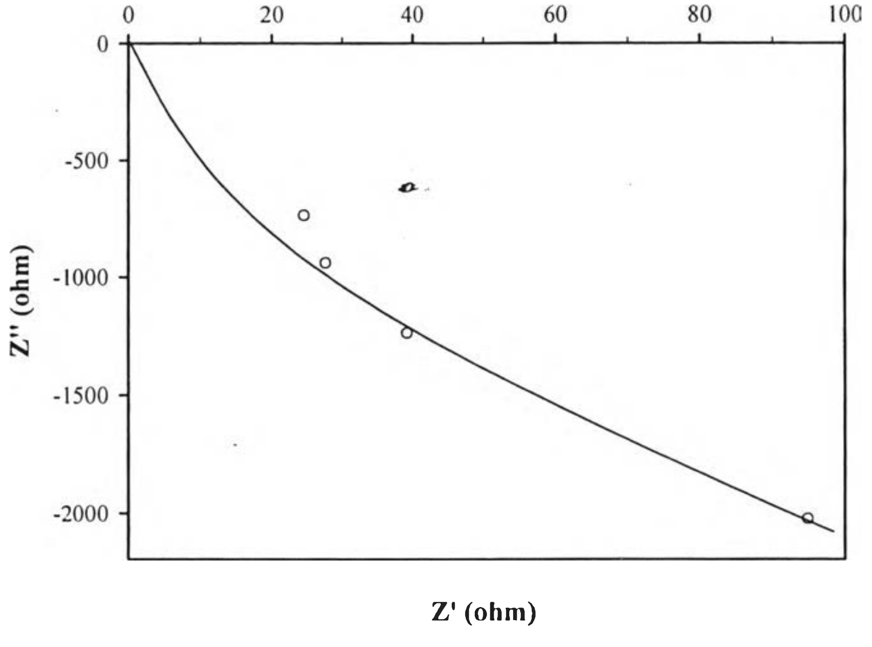

Figure E32 Enlarged Nyquist plot of the S-PSF with 3% v/v of S-GO and 15% v/v of zeolite Y at 27 °C under dry state (R = 0.77 ohm).

Table E3 Proton conductivity of the hybrid membranes with a DS of 0.72 at 27 °C under dry state

Polymer	Thickness (cm)	Contact Area (cm^2)	R (ohm)	Proton Conductivity (S/cm)
Nafion 117	0.0180	11.34	5.00	2.88×10^{-4}
S-PSF72	0.0199± 0.0010	11.34	3.94 ± 0.11	4.45×10^{-4} ± 1.28×10^{-5}
S-PSF/15Y	0.0193± 0.0009	11.34	0.96 ± 0.07	1.77×10^{-3} ± 1.33×10^{-4}
S-PSF/3S-GO	0.0192 ± 0.0010	11.34	0.57 ± 0.03	3.01×10^{-3} ± 1.90×10^{-4}
S-PSF/3S-GO/12Y	0.0182± 0.0010	11.34	0.61 ± 0.04	2.63×10^{-3} ± 1.75×10^{-4}
S-PSF/3S-GO/15Y	0.0188 ± 0.0011	11.34	0.77 ± 0.11	2.18×10^{-3} ± 3.12×10^{-4}

Appendix F Proton Conductivity Under Wet State

The impedance data was measured by using an LCR meter (Agilent E4980A) at various frequencies from 100 Hz to 2 MHz and at room temperature. The membranes were cut into 5 × 5 cm^2 specimens and immersed in distilled water at 27 °C for 24 h before the measurement. The proton conductivity was calculated from Eq. F1:

$$\sigma\ (s/cm) = \frac{d}{R \times A} \qquad \text{(F1)}$$

where d is the sample thickness, A is the contact area of the sample ($\pi r^2 = \pi(3.8/2)^2 = 11.34\ cm^2$), and R can be derived from the low intercept of the high frequency semi-circle on a complex impedance plane with the Re (Z) axis.

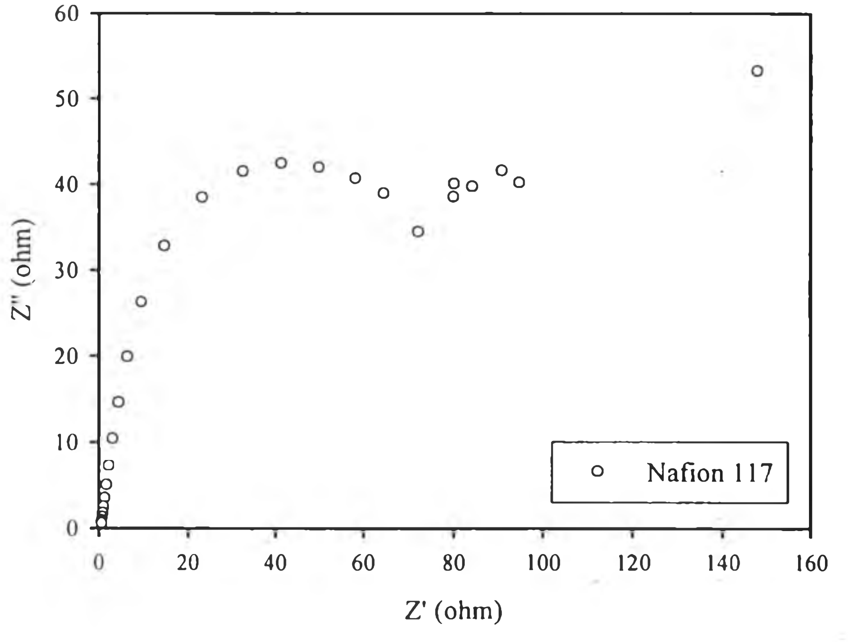

Figure F1 Nyquist plot of the Nafion117 membrane.

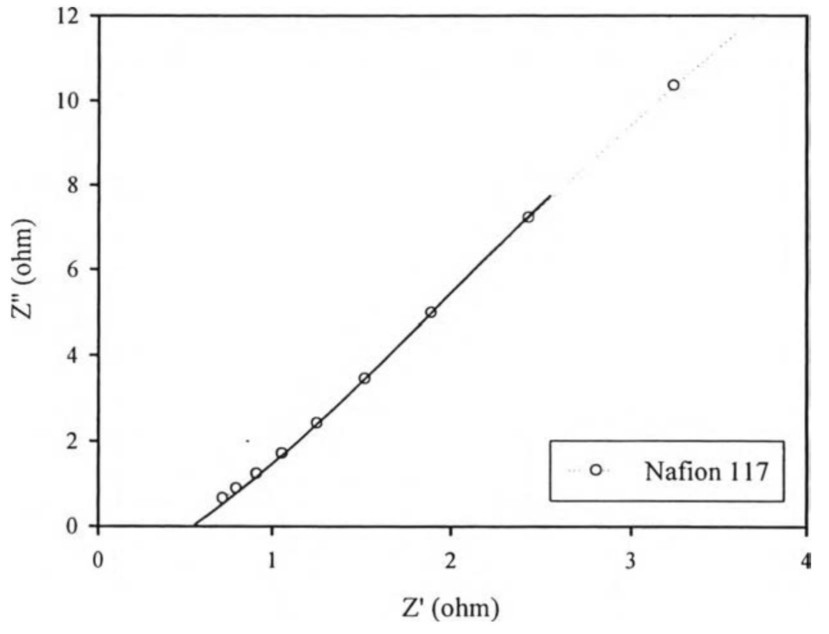

Figure F2 Enlarged Nyquist plot of the Nafion117 membrane (R = 0.18 ohm).

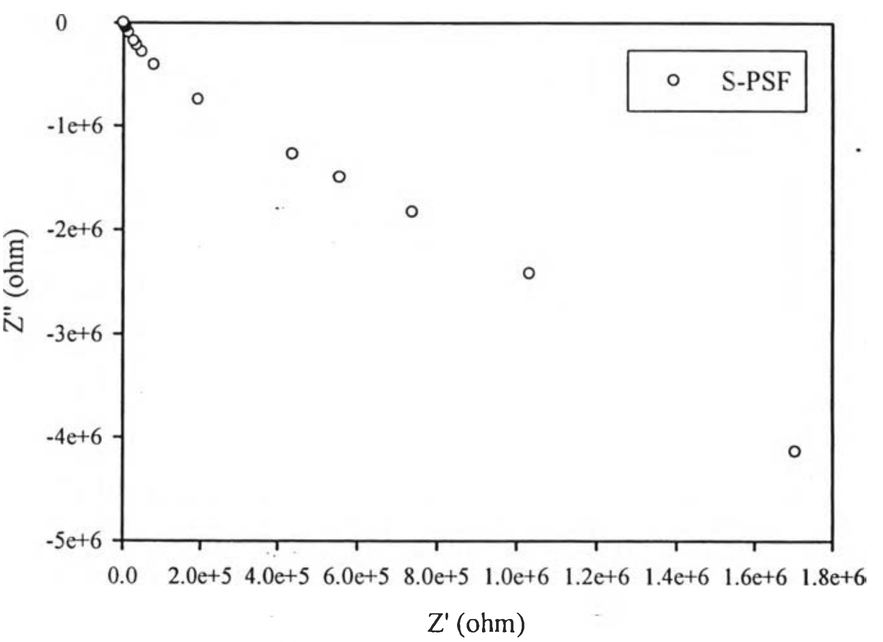

Figure F3 Nyquist plot of the S-PSF with a DS of 0.72 at 27 °C under wet state.

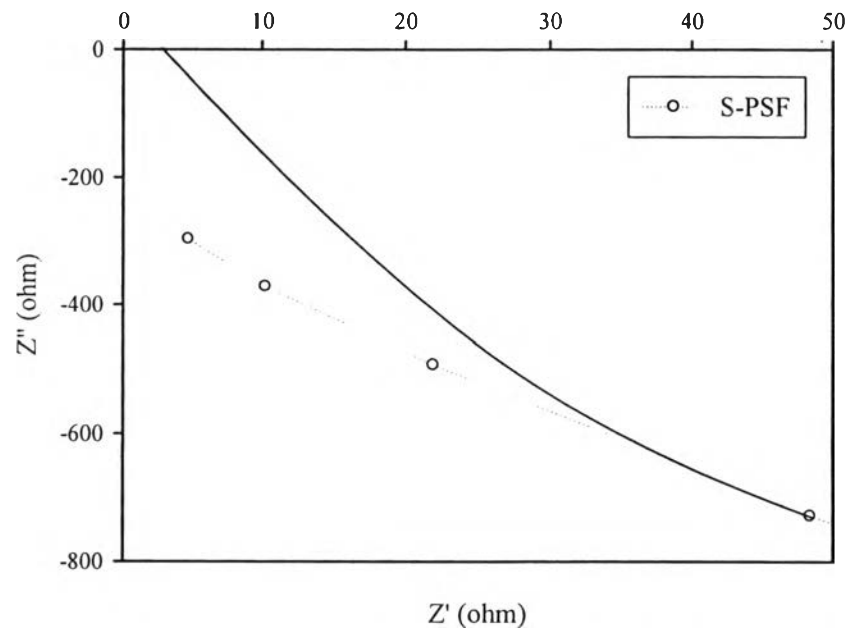

Figure F4 Enlarged Nyquist plot of the S-PSF with a DS of 0.72 at 27 °C under wet state (R = 3.28 ohm).

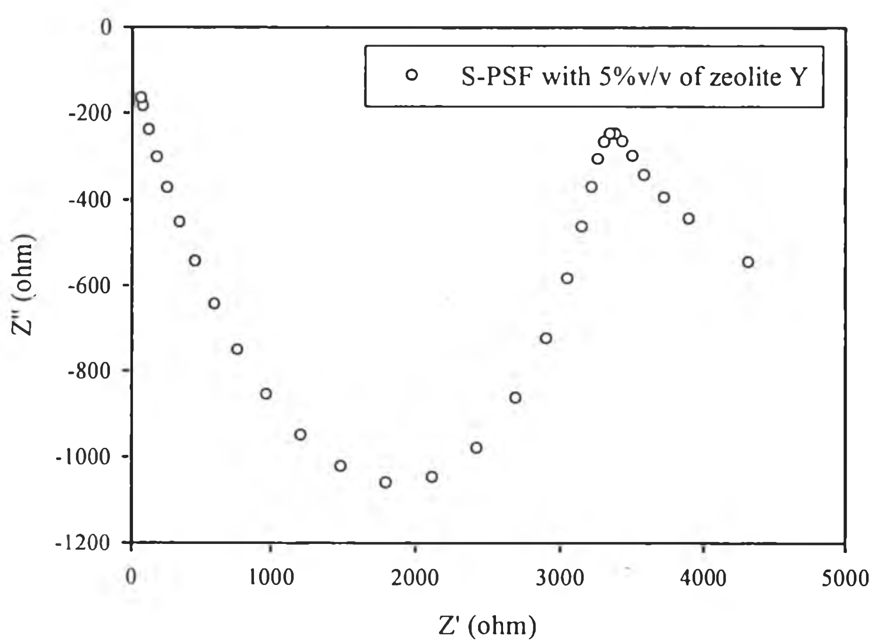

Figure F5 Nyquist plot of the S-PSF with 5% v/v of Zeolite Y at 27 °C under wet state.

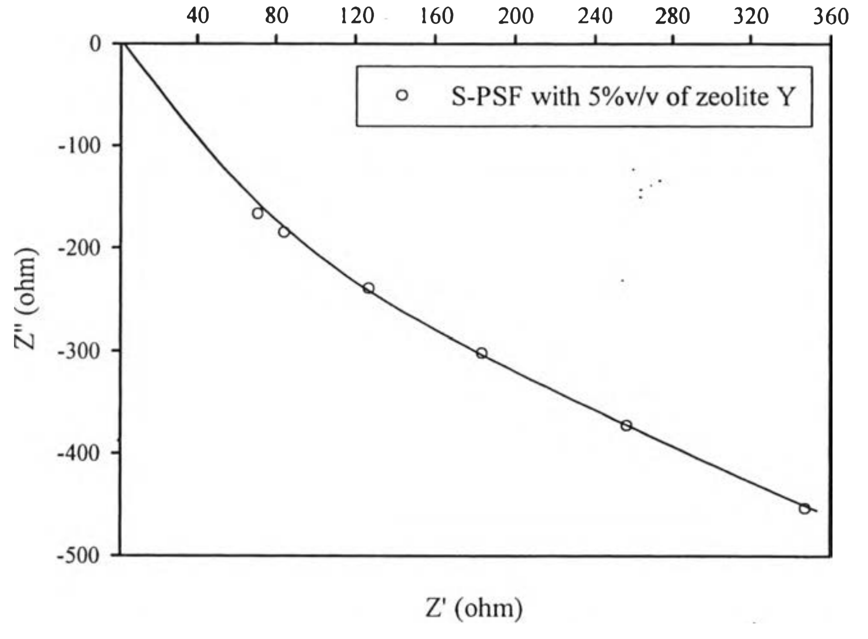

Figure F6 Enlarged Nyquist plot of the S-PSF with 5% v/v of Zeolite Y at 27 °C under wet state (R = 1.82 ohm).

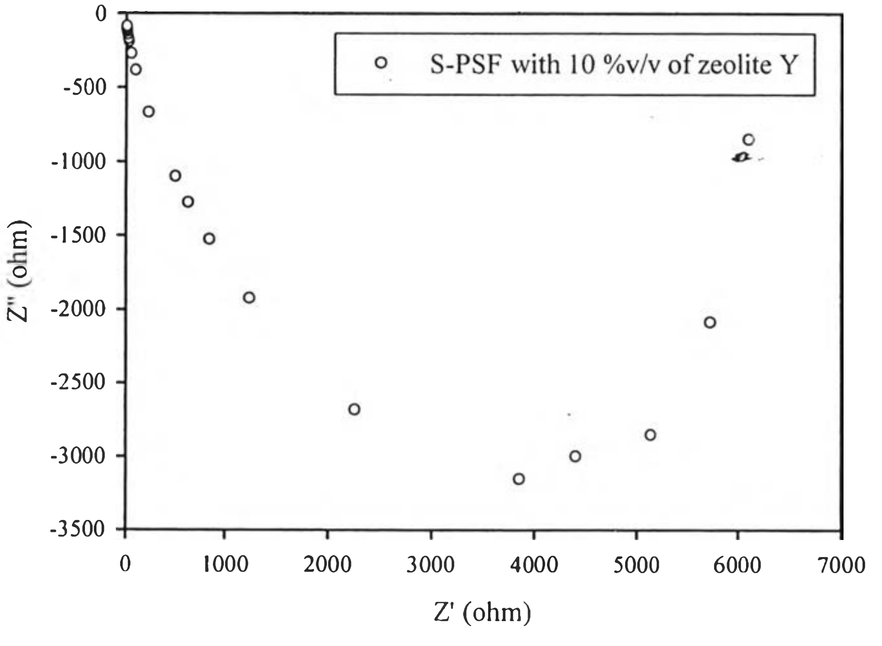

Figure F7 Nyquist plot of the S-PSF with 10% v/v of Zeolite Y at 27 °C under wet state.

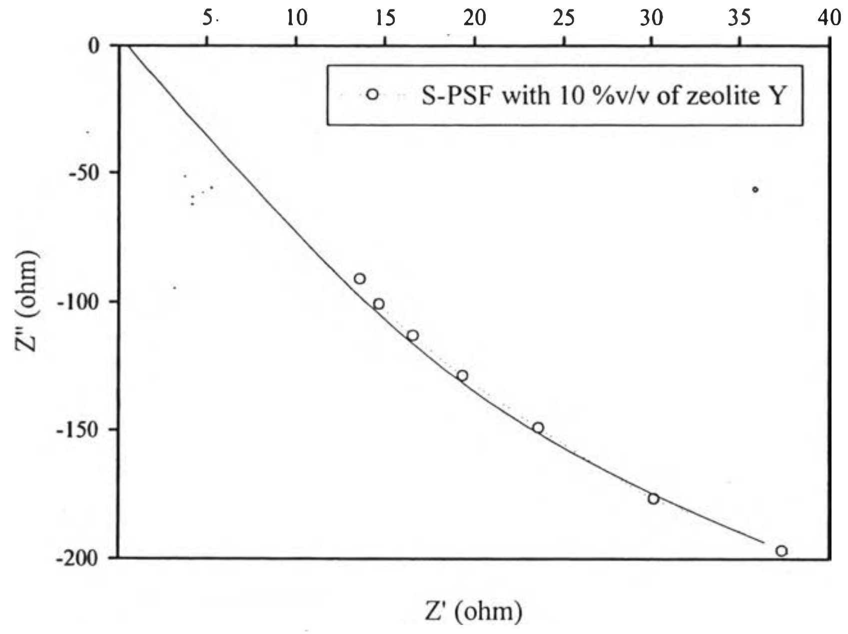

Figure F8 Enlarged Nyquist plot of the S-PSF with 10% v/v of Zeolite Y at 27 °C under wet state (R = 0.85 ohm).

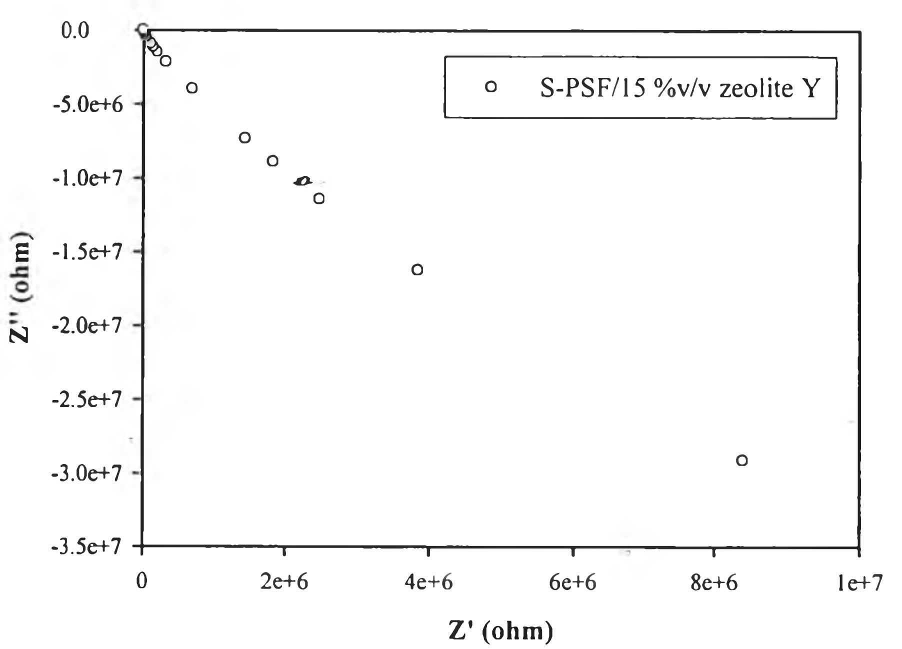

Figure F9 Nyquist plot of the S-PSF with 15% v/v of Zeolite Y at 27 °C under wet state.

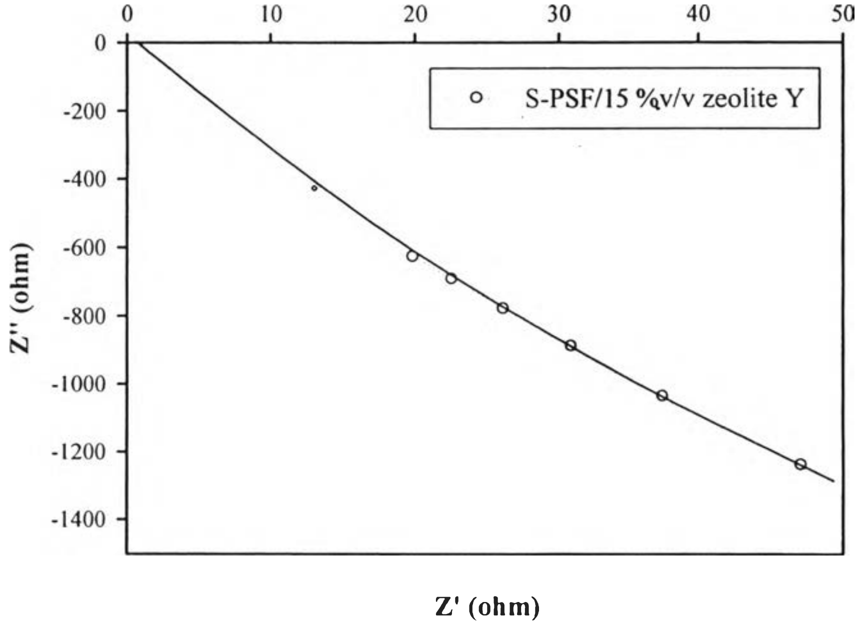

Figure F10 Enlarged Nyquist plot of the S-PSF with 15% v/v of Zeolite Y at 27 °C under wet state (R = 0.70 ohm).

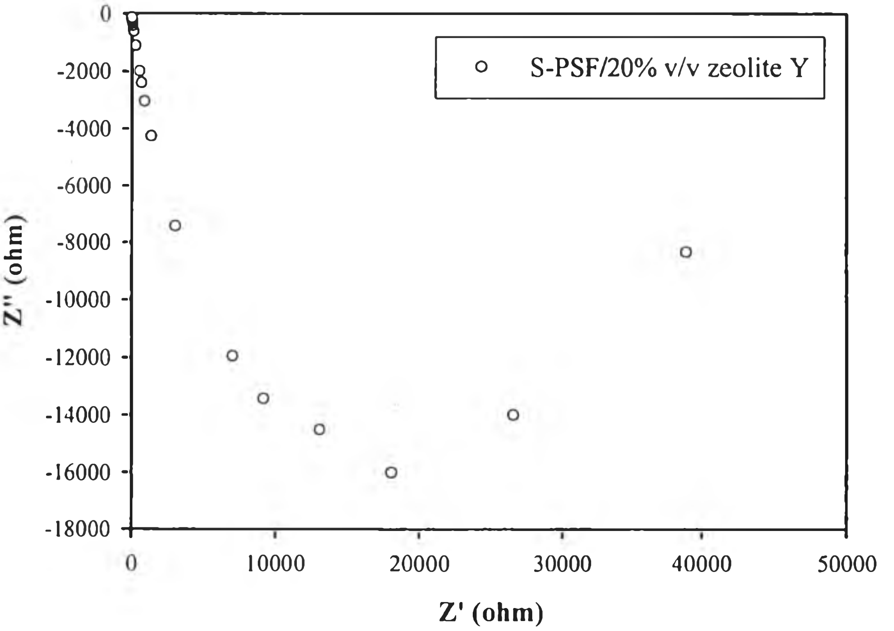

Figure F11 Nyquist plot of the S-PSF with 20% v/v of Zeolite Y at 27 °C under wet state.

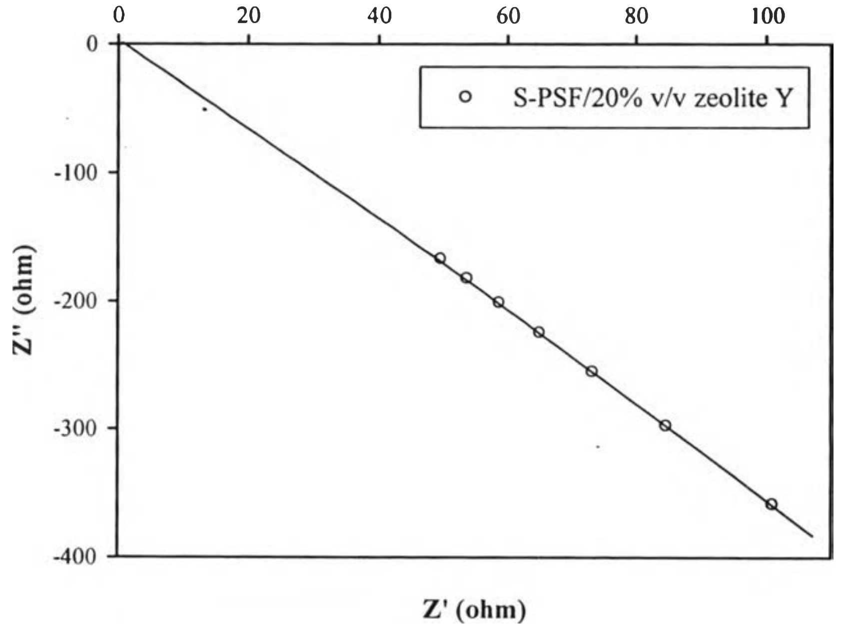

Figure F12 Enlarged Nyquist plot of the S-PSF with 20% v/v of Zeolite Y at 27 °C under wet state (R = 1.11 ohm).

Table F1 Proton conductivity of the S-PSF/Zeolite Y composite membrane at 27 °C under wet state

Polymer	Thickness (cm)	Contact Area (cm^2)	R (ohm)	Proton Conductivity (S/cm)
S-PSF72	0.0202 ± 0.0010	11.34	3.28± 0.25	5.46×10^{-4} ± 4.35×10^{-5}
S-PSF/Zeolite Y 5 %v/v	0.0163 ± 0.0013	11.34	1.82 ± 0.09	7.90×10^{-4} ± 3.79×10^{-5}
S-PSF/Zeolite Y 10 %v/v	0.0168± 0.0021	11.34	0.85 ± 0.06	1.74×10^{-3} ± 1.25×10^{-4}
S-PSF/Zeolite Y 15 %v/v	0.0184± 0.0009	11.34	0.70 ± 0.08	2.33×10^{-3} ± 2.36×10^{-4}
S-PSF/Zeolite Y 20 %v/v	0.0186± 0.0015	11.34	1.11± 0.22	1.52×10^{-3} ± 3.27×10^{-4}
Nafion 117	0.0200	11.34	0.18	3.17×10^{-3}

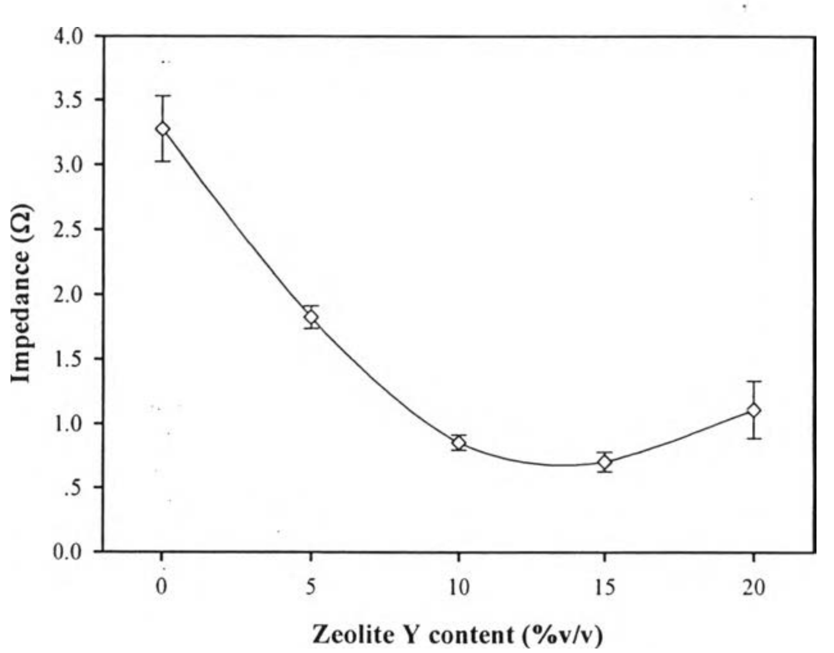

Figure F13 Impedance of the S-PSF/Zeolite Y composite membrane with a DS of 0.72 at 27 °C under wet state.

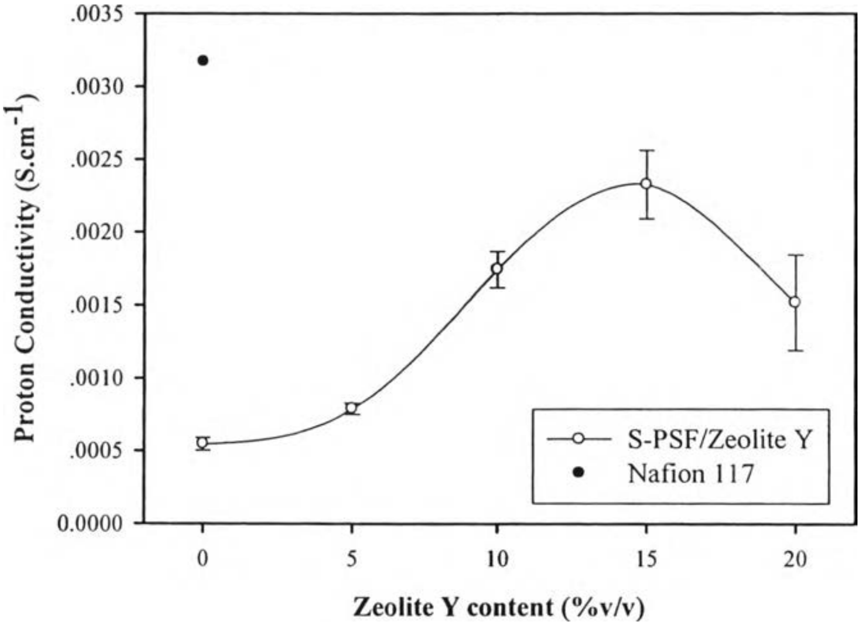

Figure F14 Proton conductivity of the S-PSF/Zeolite Y composite membrane with a DS of 0.72 at 27 °C under wet state.

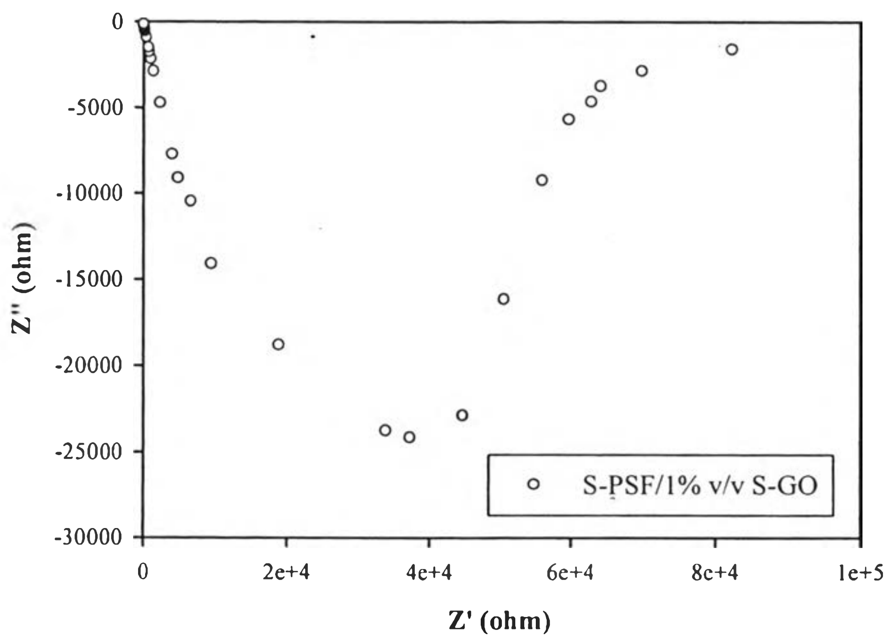

Figure F15 Nyquist plot of the S-PSF with 1% v/v of S-GO at 27 °C under wet state.

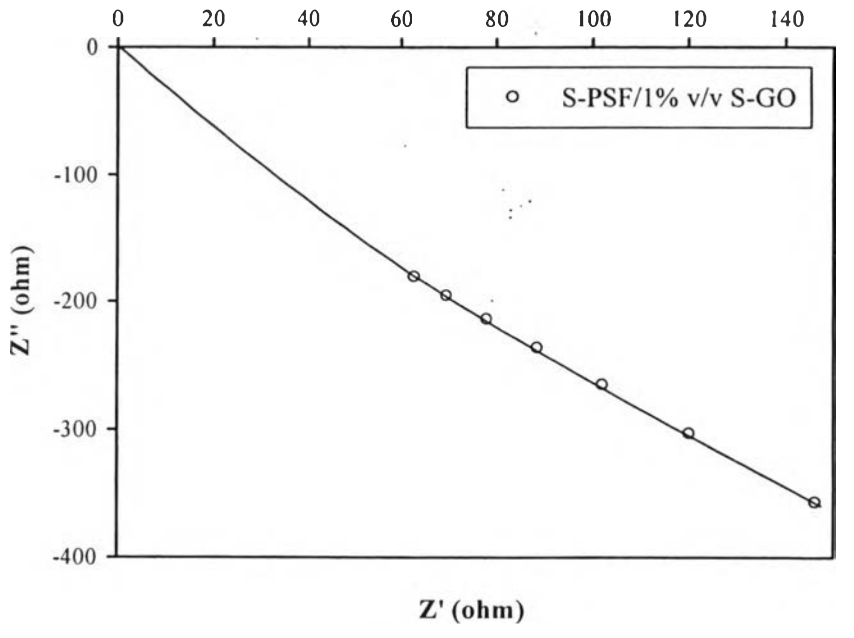

Figure F16 Enlarged Nyquist plot of the S-PSF with 1% v/v of S-GO at 27 °C under wet state (R = 0.98 ohm).

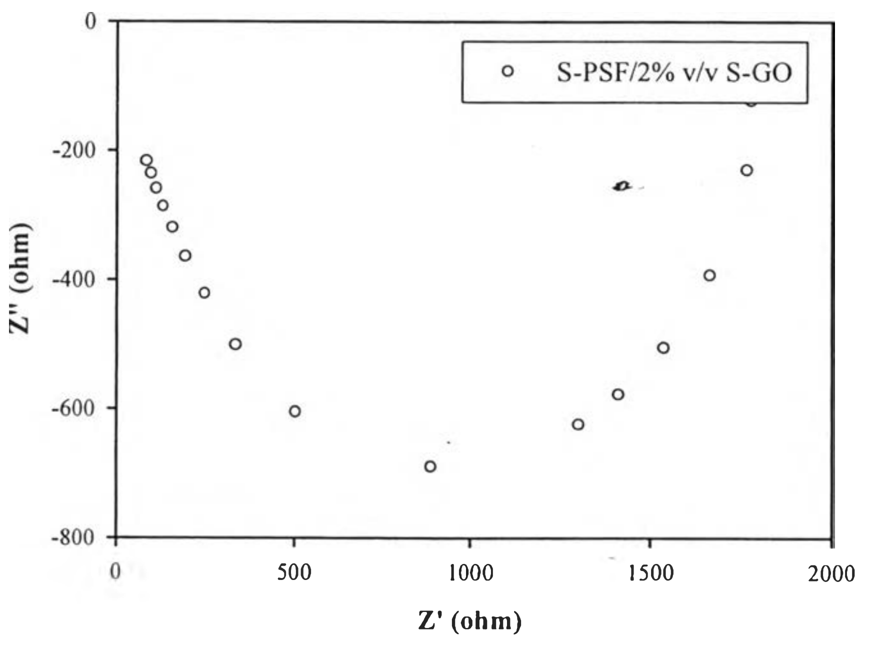

Figure F17 Nyquist plot of the S-PSF with 2% v/v of S-GO at 27 °C under wet state.

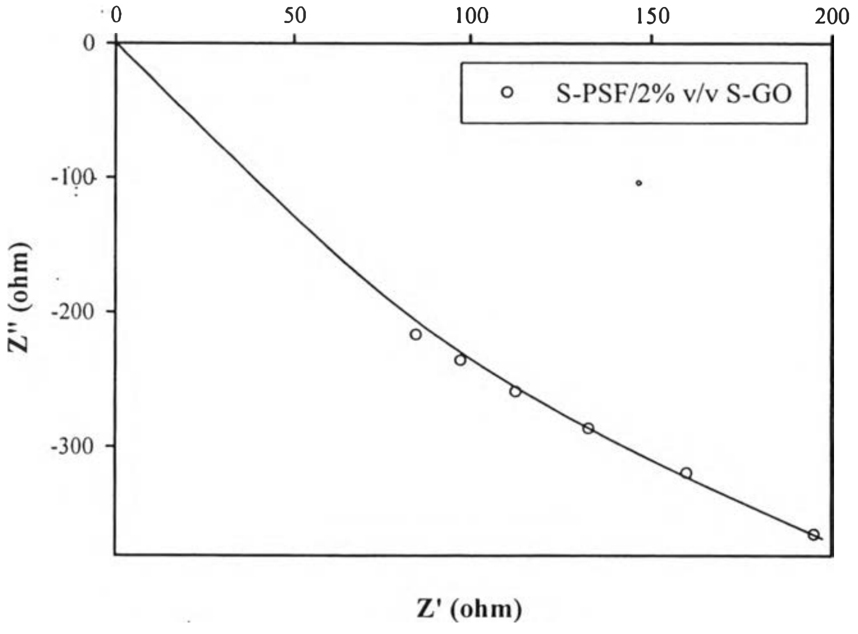

Figure F18 Enlarged Nyquist plot of the S-PSF with 2% v/v of S-GO at 27 °C under wet state (R = 0.59 ohm).

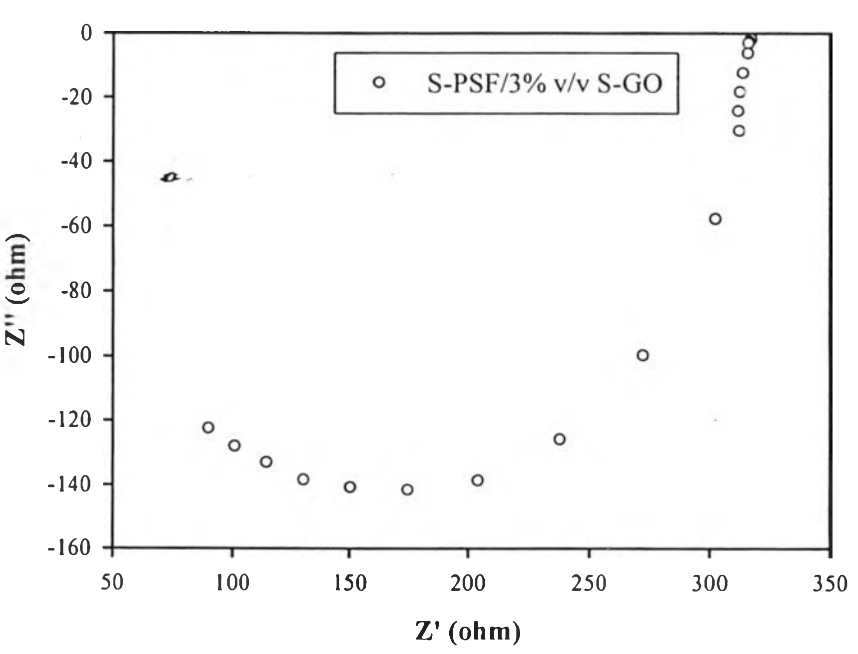

Figure F19 Nyquist plot of the S-PSF with 3% v/v of S-GO at 27 °C under wet state.

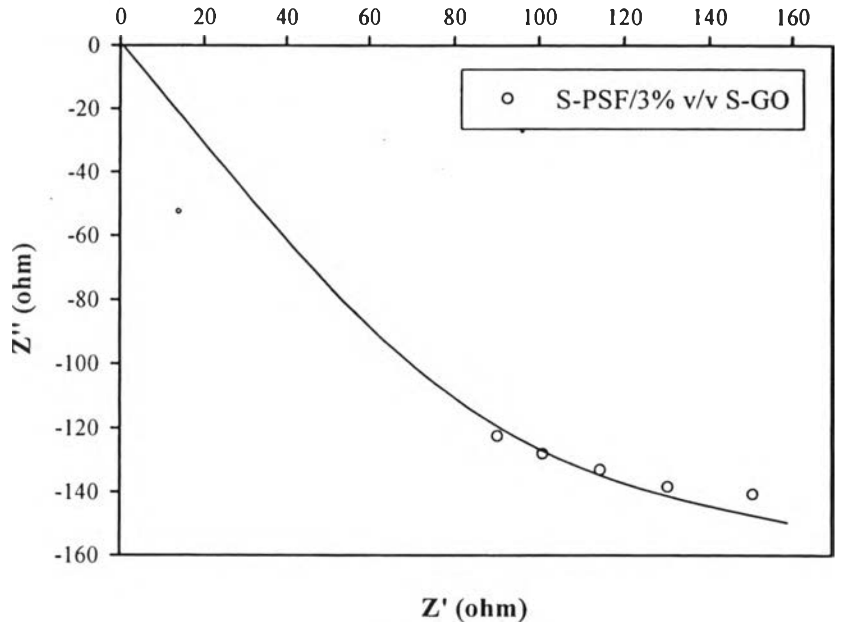

Figure F20 Enlarged Nyquist plot of the S-PSF with 3% v/v of S-GO at 27 °C under wet state (R = 0.40 ohm).

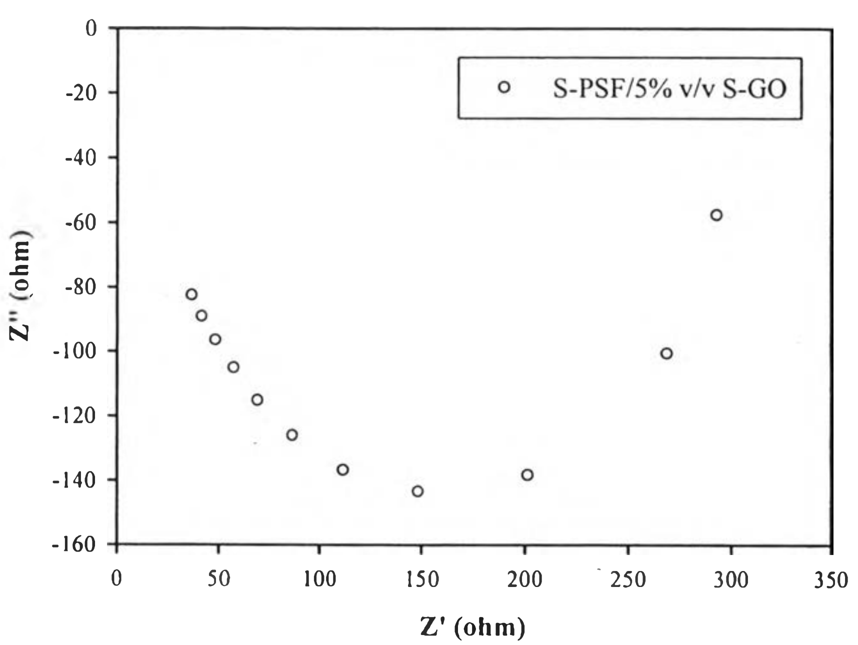

Figure F21 Nyquist plot of the S-PSF with 5% v/v of S-GO at 27 °C under wet state.

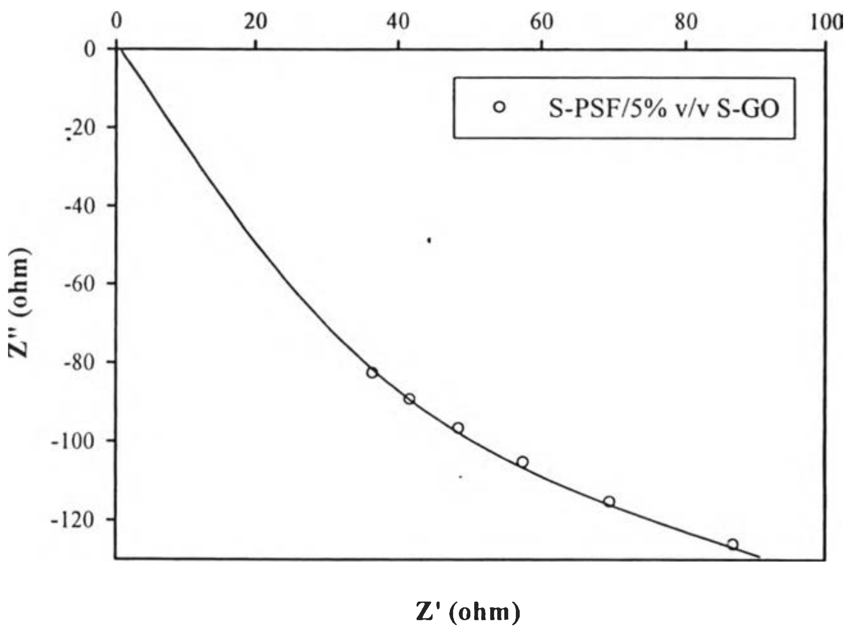

Figure F22 Enlarged Nyquist plot of the S-PSF with 5% v/v of S-GO at 27 °C under wet state (R = 0.83 ohm).

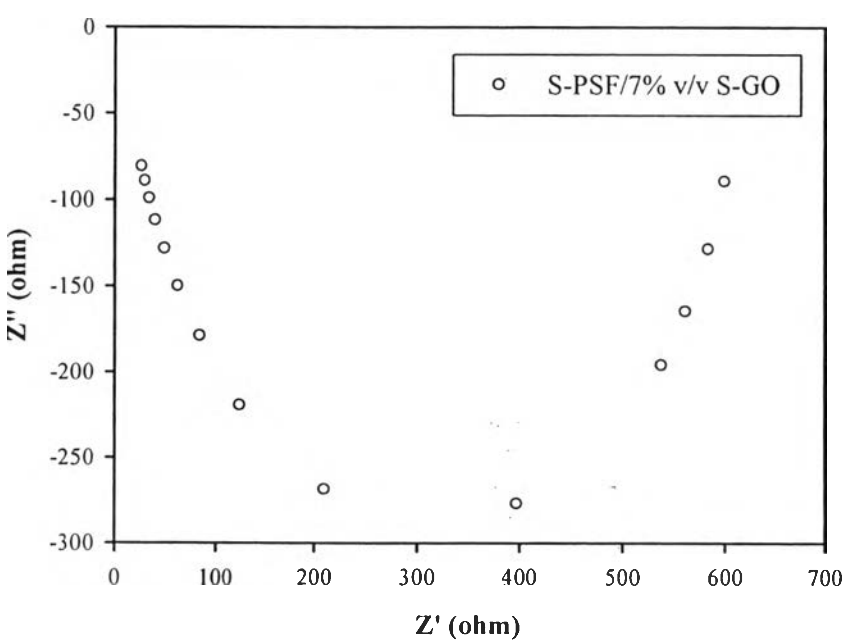

Figure F23 Nyquist plot of the S-PSF with 7% v/v of S-GO at 27 °C under wet state.

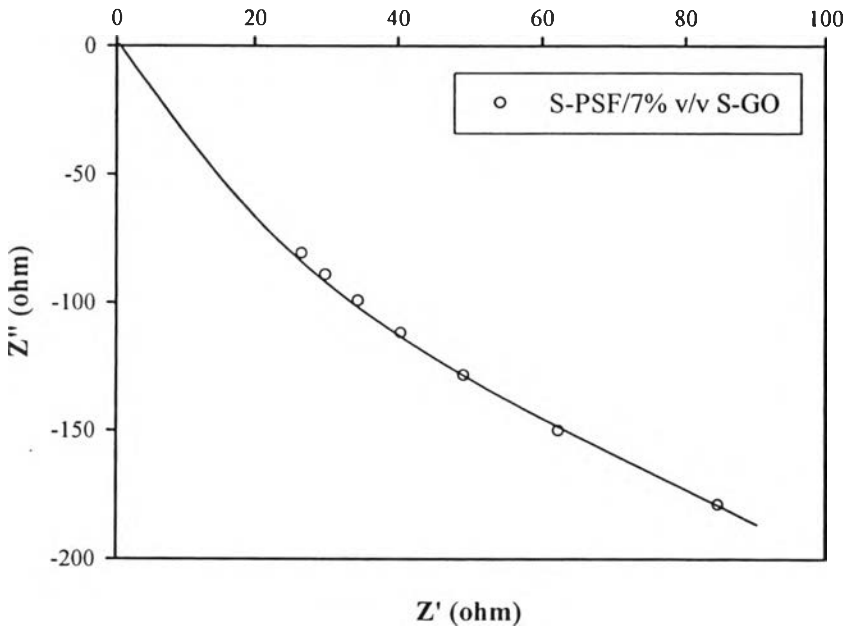

Figure F24 Enlarged Nyquist plot of the S-PSF with 7% v/v of S-GO at 27 °C under wet state (R = 0.94 ohm).

Table F2 Proton conductivity of the S-PSF/S-GO composite membrane with a DS of 0.72 at 27 °C under dry state

Polymer	**Thickness (cm)**	**Contact Area (cm^2)**	**R (ohm)**	**Proton Conductivity (S/cm)**
S-PSF72	0.0202 ± 0.0010	11.34	3.28± 0.25	5.46×10^{-4} ± 4.35×10^{-5}
S-PSF/S-GO 1 %v/v	0.0189 ± 0.0010	11.34	0.98 ± 0.19	1.74×10^{-3} ± 3.56×10^{-4}
S-PSF/S-GO 2 %v/v	0.0192 ± 0.0005	11.34	0.59 ± 0.05	2.92×10^{-3} ± 2.65×10^{-4}
S-PSF/S-GO 3 %v/v	0.0193 ± 0.0006	11.34	0.40 ± 0.04	4.27×10^{-3} ± 4.6×10^{-4}
S-PSF/S-GO 5 %v/v	0.0190 ± 0.0007	11.34	0.83 ± 0.04	2.02×10^{-3} ± 9.9×10^{-5}
S-PSF/S-GO 7 %v/v	0.0185 ± 0.0012	11.34	0.94 ± 0.14	1.76×10^{-3} ± 2.7×10^{-4}
Nafion 117	0.0200	11.34	5.00	3.17×10^{-3}

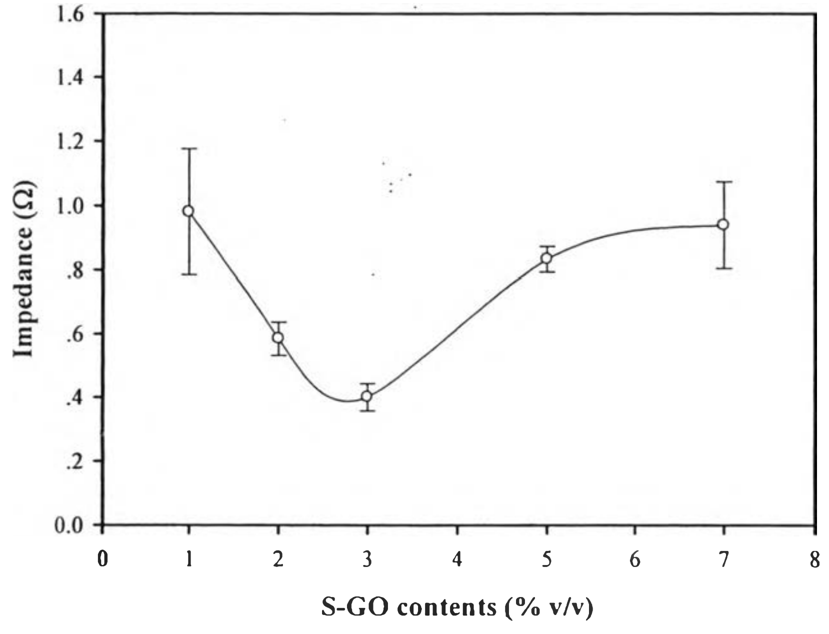

Figure F25 Impedance of the S-PSF/S-GO composite membrane with a DS of 0.72 at 27 °C under wet state.

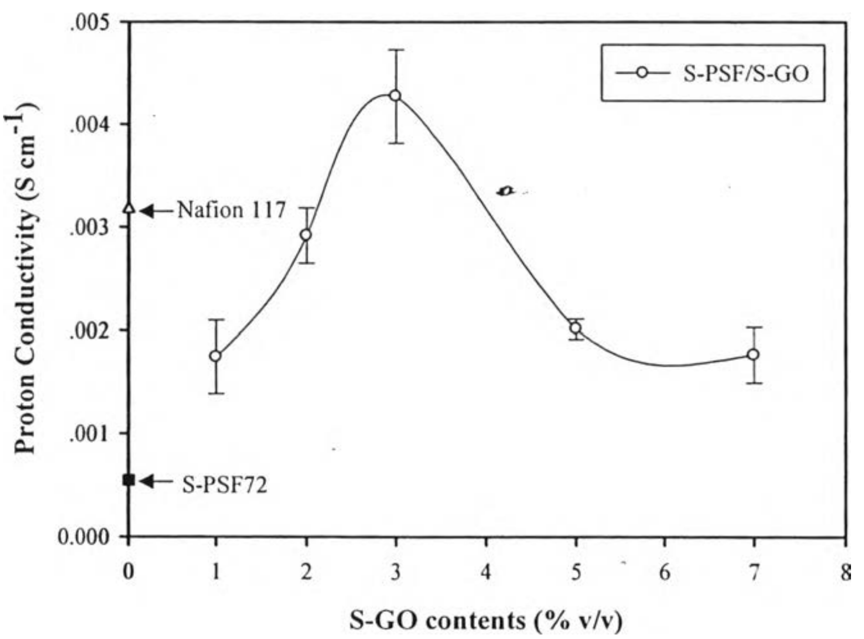

Figure F26 Proton conductivity of the S-PSF/S-GO composite membrane with a DS of 0.72 at 27 °C under wet state.

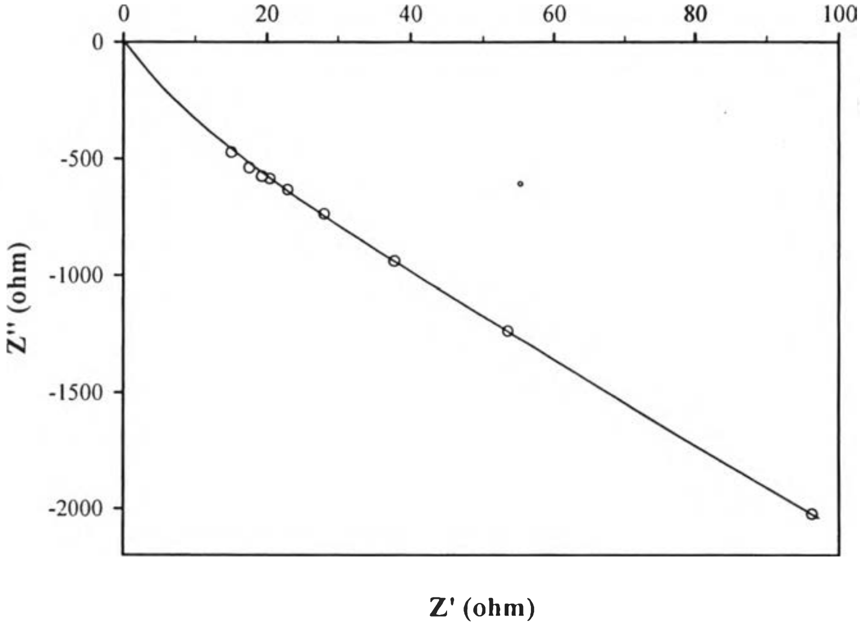

Figure F27 Enlarged Nyquist plot of the S-PSF with 3% v/v of S-GO and 12% v/v of zeolite Y at 27 °C under wet state (R = 0.41 ohm).

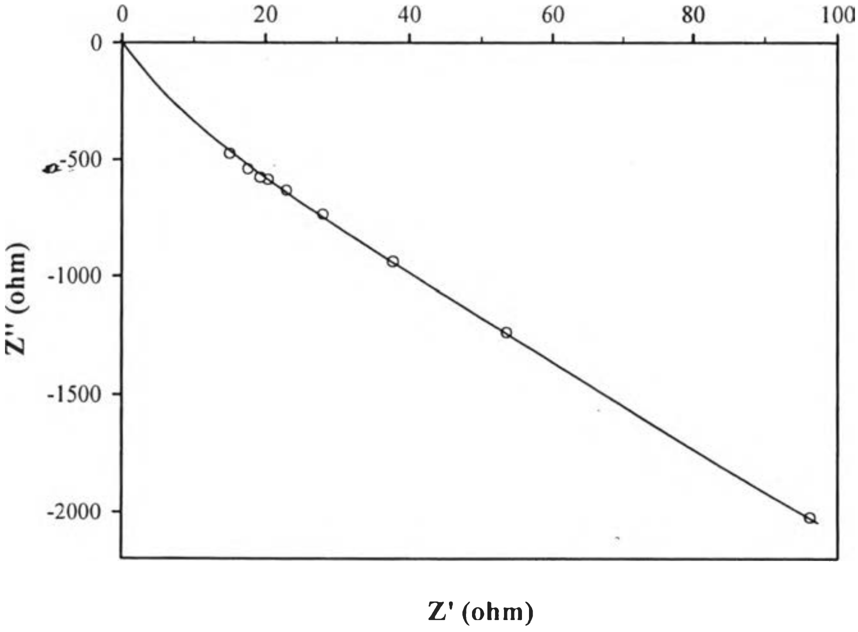

Figure F28 Enlarged Nyquist plot of the S-PSF with 3% v/v of S-GO and 12% v/v of zeolite Y at 27 °C under wet state (R = 0.41 ohm).

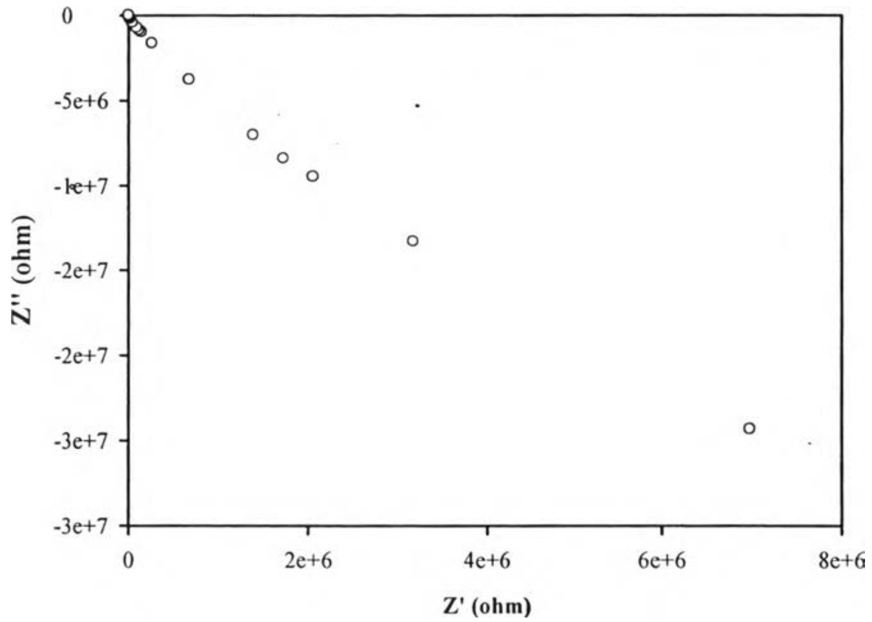

Figure F29 Nyquist plot of the S-PSF with 3% v/v of S-GO and 15% v/v of zeolite Y at 27 °C under wet state.

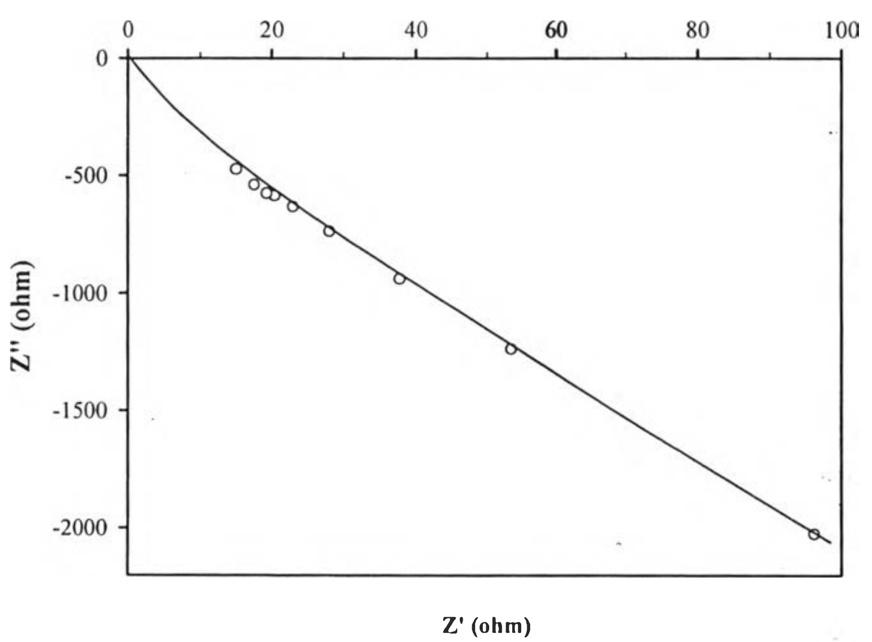

Figure F30 Enlarged Nyquist plot of the S-PSF with 3% v/v of S-GO and 15% v/v of zeolite Y at 27 °C under wet state (R = 0.53 ohm).

Table F3 Proton conductivity of the hybrid membranes with a DS of 0.72 at 27 °C under wet state

Polymer	Thickness (cm)	Contact Area (cm^2)	R (ohm)	Proton Conductivity (S/cm)
S-PSF72	0.0202 ± 0.0010	11.34	3.28± 0.25	5.46×10^{-4} ± 4.35×10^{-5}
S-PSF/15Y	0.0184± 0.0009	11.34	0.70 ± 0.08	2.33×10^{-3} ± 2.36×10^{-4}
S-PSF/3S-GO	0.0193 ± 0.0006	11.34	0.40 ± 0.04	4.27×10^{-3} ± 4.6×10^{-4}
S-PSF/3S-GO/12Y	0.0186± 0.0010	11.34	0.41 ± 0.05	4.01×10^{-3} ± 4.53×10^{-4}
S-PSF/3S-GO/15Y	0.0189 ± 0.0011	11.34	0.53 ± 0.05	3.16×10^{-3} ± 2.86×10^{-4}
Nafion 117	0.0180	11.34	5.00	2.88×10^{-4}

Appendix G Methanol Permeability

The methanol permeability shows the amount of methanol that permeates through the membrane. The permeation cell for the methanol permeability measurement consisted of chamber A and chamber B separated by a sulfonated polymer membrane. Chamber A was filled with a 250 ml 2.5 M methanol solution. Chamber B was filled with 250 ml DI water. The membrane was placed between the chamber A and chamber B. The methanol permeability was determined by the following Eq (G1):

$$P\ (cm^2/s) = \frac{k_B \times V_B \times L}{A \times (C_A - C_B)} \qquad \text{(G1)}$$

where P = the methanol permeability, C_A = the methanol concentrations in the compartment A, C_B = the methanol concentrations in the compartment B, A = the areaof a membrane , L = the thickness of a membrane, V_B = the volume of the solution in the compartment B, and k_B = the slope of the methanol concentration.

The methanol concentrations were determined by using gas chromatography (GC) with thermal conductivity detector (TCD); ethanol was used as the internal standard:

Calibration procedure

- The syringe was cleaned before sampling with DI water.
- Methanol solutions were prepared at various concentrations (0.01, 0.05, 0.1, 0.5, 1.0, 1.5, 2.0, 2.5, and 3.0 M). Methanol solution was pumped by a syringe about 0.05 ml and deposited in a bottle.
- Methanol permeability was calculated by TCD GC with a 1M 0.05ml ethanol solution as an internal standard.
- The calibration curve was established by plotting C_B with the peak ratio of MeOH/EtOH.

Measurement procedure

- The syringe was cleaned before sampling with DI water.
- Components A and B were pumped by a syringe about 0.05 ml and deposited in a bottle.
- Methanol permeability was calculated by TCD GC with 1M 0.05ml ethanol solution as an internal standard.
- The methanol concentration in component B (C_B) was determined by comparing the peak ratio of methanol/ethanol to calibration curve.

Table G1 Retention time composites

Sample	Retention Time (min)
Water	1.56
Methanol	4.30
Ethanol	12.29

Table G2 Calibration concentration of methanol

MeOH concentration (M)	Type of Media	%Area	MeOH/EtOH
3.00	Water	90.21	2.19
	Methanol	6.72	
	Ethanol	3.07	
2.00	Water	92.05	1.73
	Methanol	5.89	
	Ethanol	2.06	
1.50	Water	92.94	1.25
	Methanol	3.92	
	Ethanol	3.13	
1.00	Water	95.34	0.79
	Methanol	2.05	
	Ethanol	2.6	
0.50	Water	95.81	0.51
	Methanol	1.42	
	Ethanol	2.77	
0.10	Water	97.01	*
	Methanol		
	Ethanol	2.9	
0.05	Water	97.83	*
	Methanol		
	Ethanol	2.17	
0.01	Water	97.67	*
	Methanol		
	Ethanol	2.33	

*Methanol did not permeate across the membrane.

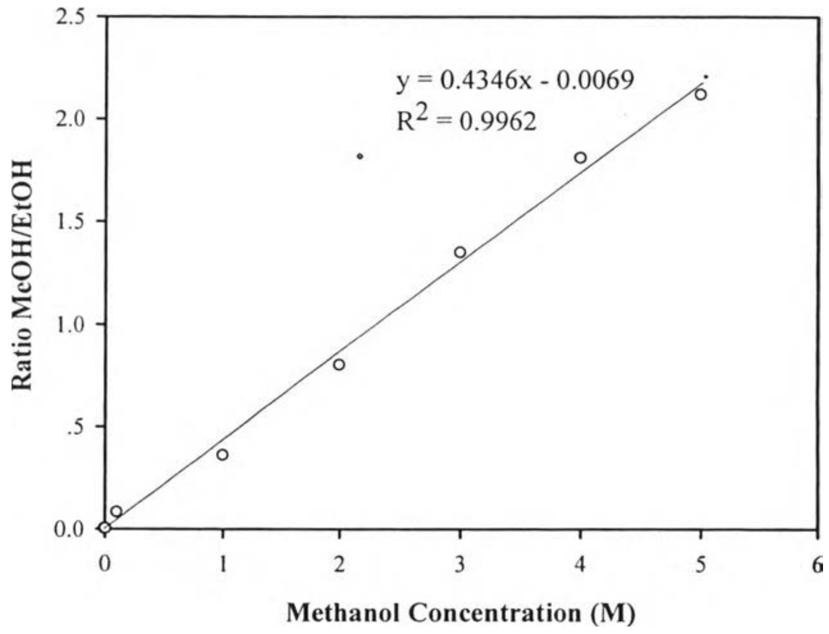

Figure G1 Calibration curve of methanol concentration versus the ratio of methanol and ethanol.

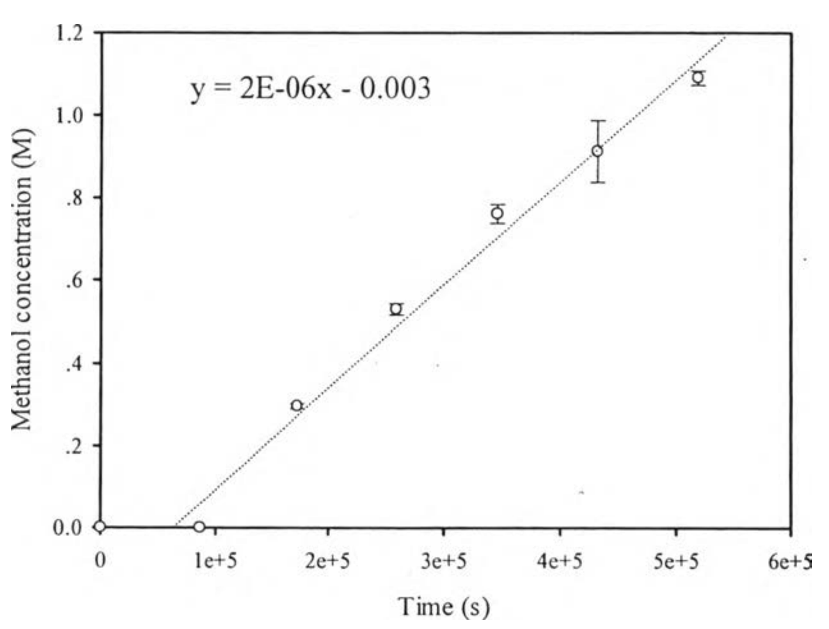

Figure G2 Methanol concentration in chamber B versus time at 70°C of Nafion 117.

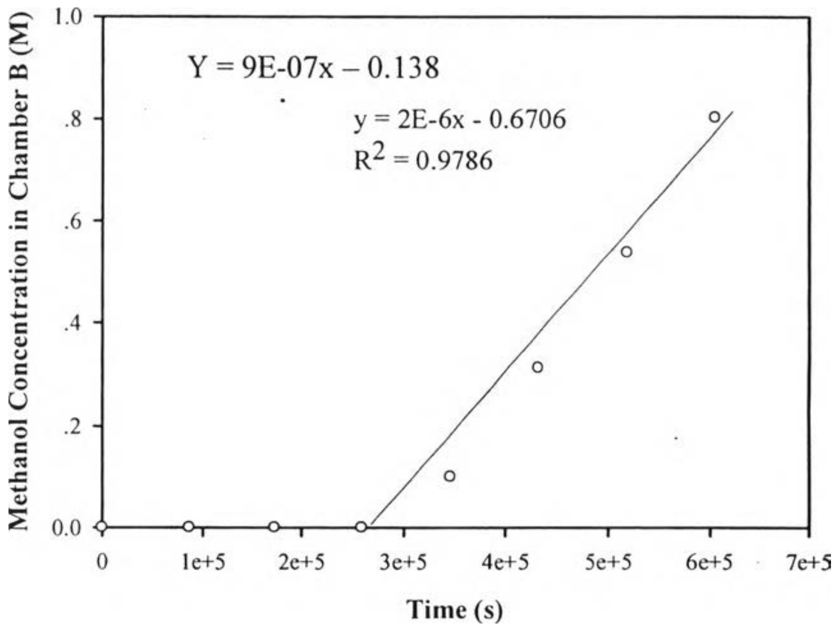

Figure G3 Methanol concentration in chamber B versus time at 70 °C of S-PSF at DS 71.55%.

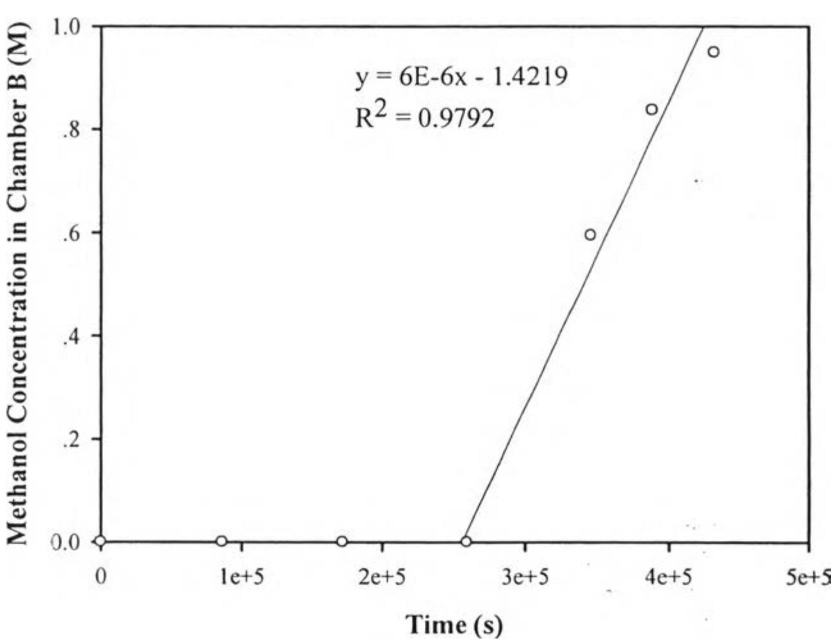

Figure G4 Methanol concentration in chamber B versus time at 70 °C of S-PSF/Zeolite Y 5 % v/v.

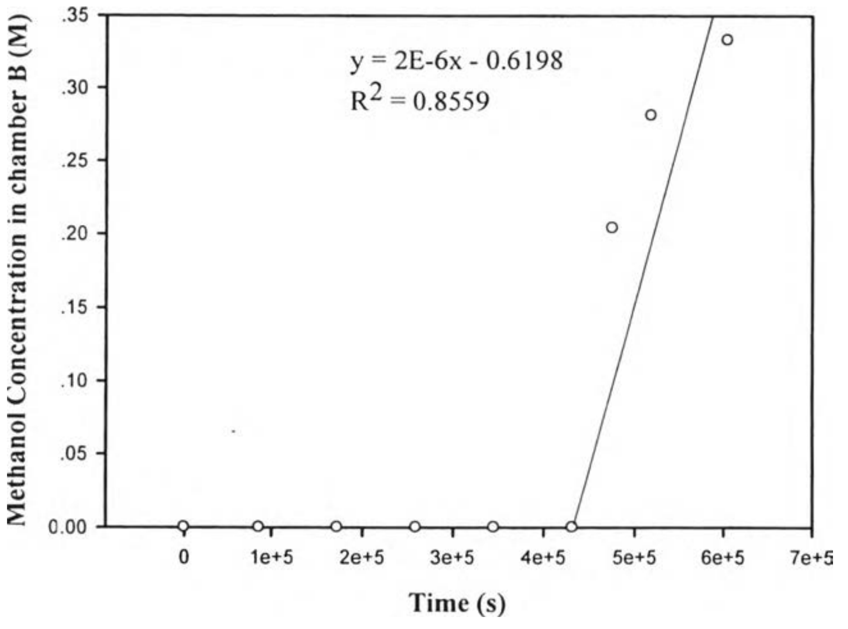

Figure G5 Methanol concentration in chamber B versus time at 70 °C of S-PSF/Zeolite Y 10 % v/v.

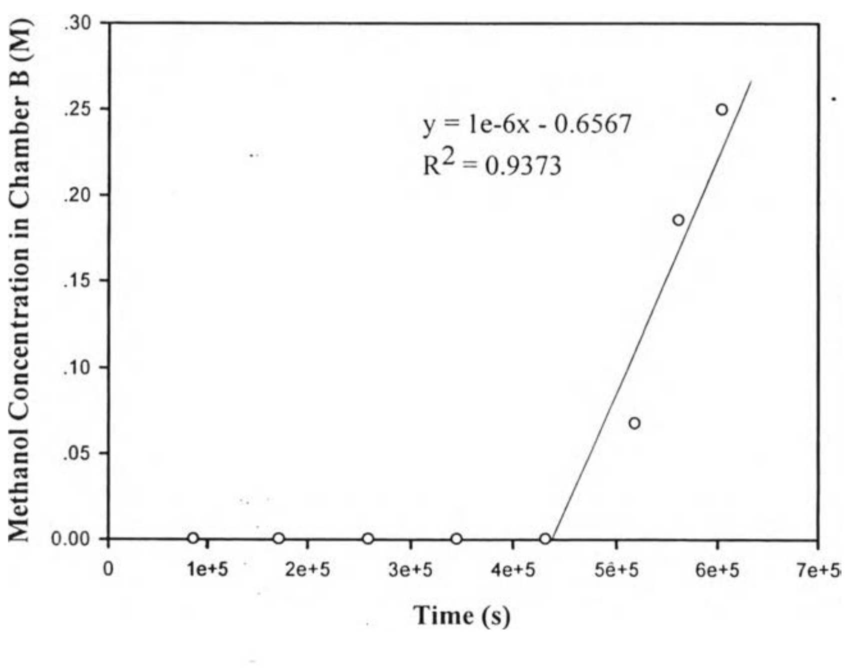

Figure G6 Methanol concentration in chamber B versus time at 70 °C of S-PSF/Zeolite Y 15 % v/v.

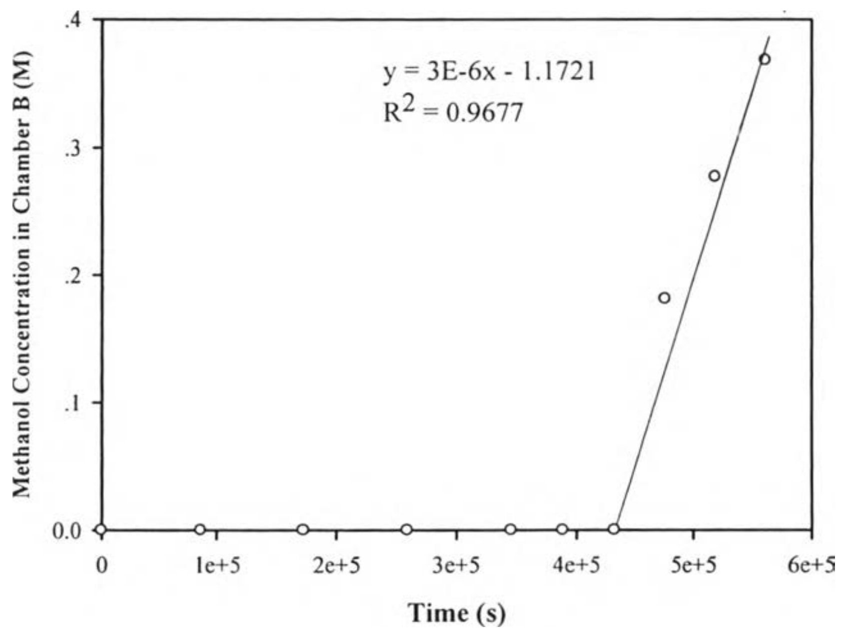

Figure G7 Methanol concentration in chamber B versus time at 70 °C of S-PSF/Zeolite Y 20 % v/v.

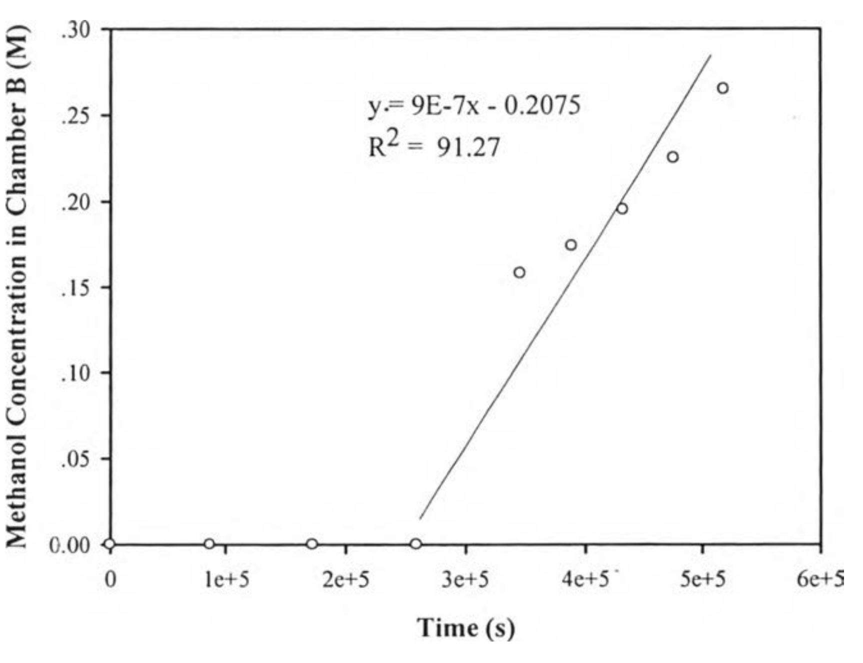

Figure G8 Methanol concentration in chamber B versus time at 70 °C of S-PSF/S-GO 1 % v/v.

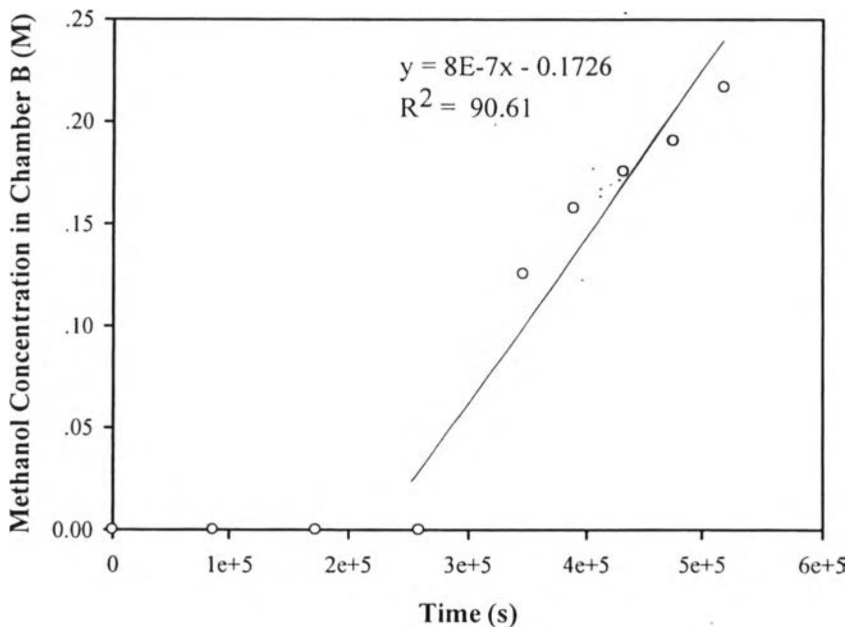

Figure G9 Methanol concentration in chamber B versus time at 70 °C of S-PSF/S-GO 2 % v/v.

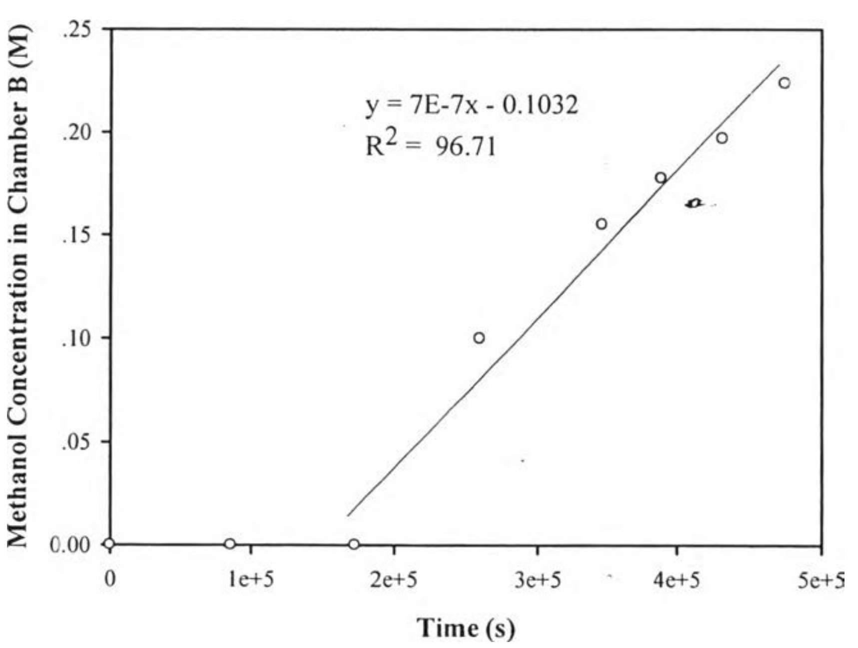

Figure G10 Methanol concentration in chamber B versus time at 70 °C of S-PSF/S-GO 3 % v/v.

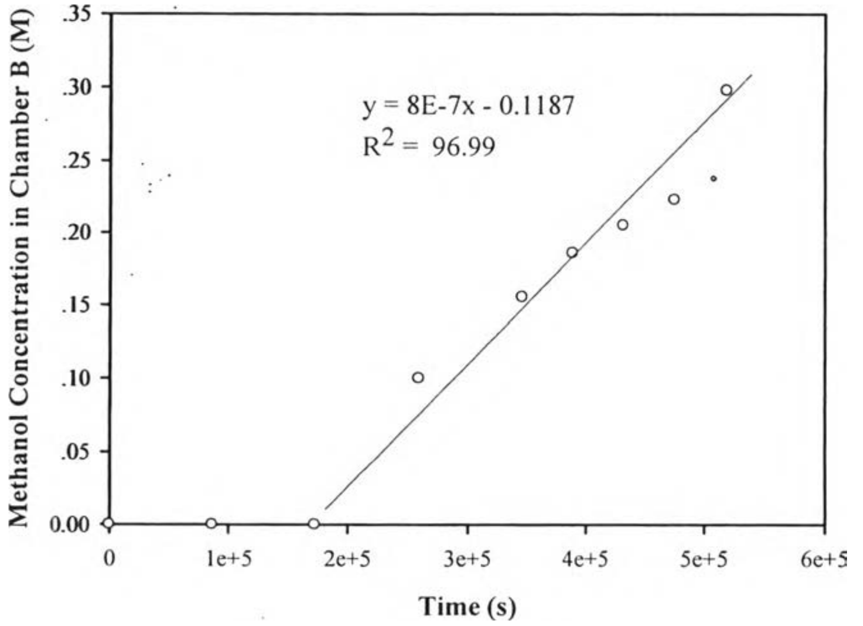

Figure G11 Methanol concentration in chamber B versus time at 70 °C of S-PSF/S-GO 5 % v/v.

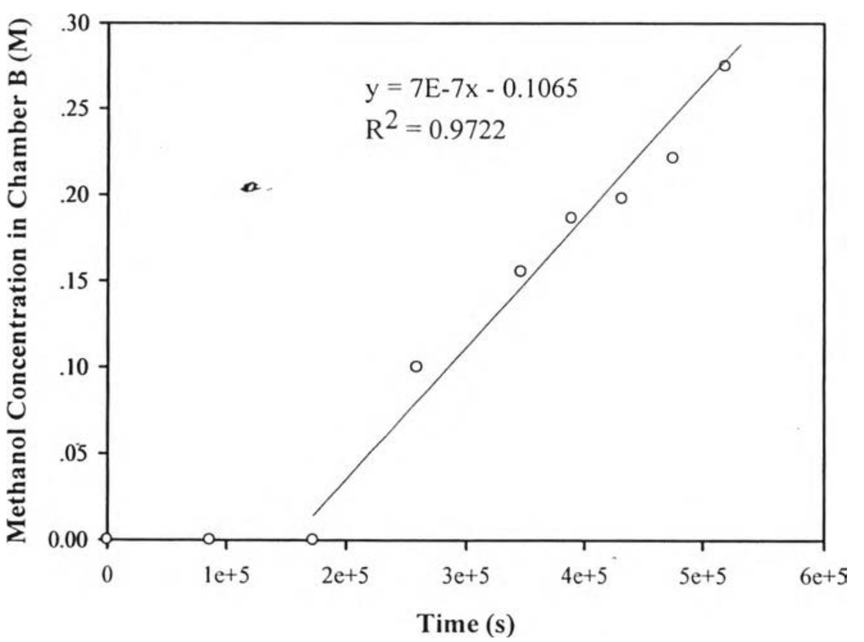

Figure G12 Methanol concentration in chamber B versus time at 70 °C of S-PSF/S-GO 7 % v/v.

Table G3 Methanol concentration in chamber A and B at 70 °C of S-PSF (DS 71.55%) and Nafion 117

Time (s)	Methanol Concentration (mol/l) in Compartment A (C_A) and Compartment B (C_B) at 70 °C			
	SPSF 71.55%		Nafion 117	
	C_A(M)	C_B(M)	C_A(M)	C_B(M)
0	2.468	0	2.028	0.000
86400	2.468	0	2.014	0.000
172800	2.338	0	1.985	0.297
259200	2.167	0	1.182	0.529
345600	2.049	0.1	1.176	0.761
432000	1.909	0.313	1.064	0.913
518400	1.761	0.537	1.033	1.025
604800	1.475	0.803	-	-

Table G4 Methanol concentration in chamber A and B at 70 °C of S-PSF/Zeolite 5 % v/v composite membrane

Time (sec)	Methanol Concentration (mol/l) in Compartment A (C_A) and Compartment B (C_B) at 70 °C	
	S-PSF/Zeolite 5 % v/v	
	C_A(M)	C_B(M)
0	2.494	0
86400	2.494	0
172800	2.494	0
259200	2.494	0
345600	2.234	0.595
388800	2.045	0.837
432000	1.844	0.949

Table G5 Methanol concentration in chamber A and B at 70 °C of S-PSF/10 %v/v Zeolite Y composite membrane

Time (sec)	Methanol Concentration (mol/l) in Compartment A (C_A) and Compartment B (C_B) at 70 °C	
	S-PSF/Zeolite 10 % v/v	
	C_A(M)	C_B(M)
0	2.473	0
86400	2.473	0
172800	2.473	0
259200	2.473	0
345600	2.147	0
432000	2.147	0
475200	2.065	0.204
518400	1.932	0.281
604800	1.717	0.333

Table G6 Methanol concentration in chamber A and B at 70 °C of S-PSF/15 %v/v Zeolite Y composite membrane

Time (sec)	Methanol Concentration (mol/l) in Compartment A (C_A) and Compartment B (C_B) at 70 °C	
	S-PSF/Zeolite 15 %v/v	
	C_A(M)	C_B(M)
0	2.812	0
86400	2.812	0
172800	2.812	0
259200	2.812	0
345600	1.049	0
432000	1.049	0.068
518400	0.756	0.185
604800	0.756	0.249

Table G7 Methanol concentration in chamber A and B at 70 °C of S-PSF/20 %v/v Zeolite Y composite membrane

Time (sec)	Methanol Concentration (mol/l) in Compartment A (C_A) and Compartment B (C_B) at 70 °C	
	S-PSF/Zeolite 20 % v/v	
	C_A(M)	C_B(M)
0	2.468	0
86400	2.468	0
172800	2.468	0
259200	2.468	0
345600	2.380	0
388800	2.812	0
432000	2.222	0
475200	2.162	0.181
518400	2.063	0.277
561600	1.951	0.368

Table G8 Methanol concentration in chamber A and B at 70 °C of S-PSF/S-GO 1% v/v composite membrane

Time (sec)	Methanol Concentration (mol/l) in Compartment A (C_A) and Compartment B (C_B) at 70 °C	
	S-PSF/S-GO 1% v/v	
	C_A(M)	C_B(M)
0	2.494	0
86400	2.494	0
172800	2.442	0
259200	2.399	0
345600	2.234	0.158
388800	2.038	0.174
432000	1.904	0.195
475200	1.858	0.225
518400	1.713	0.265

Table G9 Methanol concentration in chamber A and B at 70 °C of S-PSF/S-GO 2% v/v composite membrane

Time (sec)	Methanol Concentration (mol/l) in Compartment A (C_A) and Compartment B (C_B) at 70 °C	
	S-PSF/S-GO 2 % v/v	
	C_A(M)	C_B(M)
0	2.494	0
86400	2.494	0
172800	2.367	0
259200	2.271	0
345600	2.234	0.125
388800	2.188	0.158
432000	2.002	0.175
475200	1.937	0.190
518400	1.829	0.217

Table G10 Methanol concentration in chamber A and B at 70 °C of S-PSF/S-GO 3% v/v composite membrane

Time (sec)	Methanol Concentration (mol/l) in Compartment A (C_A) and Compartment B (C_B) at 70 °C	
	S-PSF/S-GO 3 % v/v	
	C_A(M)	C_B(M)
0	2.497	0
86400	2.497	0
172800	2.346	0
259200	2.272	0.100
345600	2.174	0.155
388800	2.031	0.178
432000	1.827	0.197
475200	1.570	0.224

Table G11 Methanol concentration in chamber A and B at 70 °C of S-PSF/S-GO 5% v/v composite membrane

Time (sec)	Methanol Concentration (mol/l) in Compartment A (C_A) and Compartment B (C_B) at 70 °C	
	S-PSF/S-GO 5 % v/v	
	C_A(M)	C_B(M)
0	2.506	0
86400	2.506	0
172800	2.348	0
259200	2.254	0.100
345600	2.146	0.155
388800	2.035	0.186
432000	1.889	0.205
475200	1.694	0.223
518400	1.607	0.298

Table G12 Methanol concentration in chamber A and B at 70 °C of S-PSF/S-GO 7% v/v composite membrane

Time (sec)	Methanol Concentration (mol/l) in Compartment A (C_A) and Compartment B (C_B) at 70 °C	
	S-PSF/S-GO 7 % v/v	
	C_A(M)	C_B(M)
0	2.504	0
86400	2.504	0
172800	2.347	0
259200	2.255	0.100
345600	2.146	0.155
388800	2.101	0.187
432000	2.011	0.198
475200	1.957	0.221
518400	1.795	0.275

Table G13 Methanol permeability (cm^2/s) of S-PSF and S-PSF/Zeolite Y composite membranes

Sample	**Membrane Thickness (cm)**	**Methanol Permeability (cm^2/s)**
Nafion 117	0.0178	3.08×10^{-5}
S-PSF72	0.0202	2.62×10^{-6}
S-PSF/Zeolite Y 5% v/v	0.0191	1.10×10^{-6}
S-PSF/Zeolite Y 10% v/v	0.0170	1.30×10^{-6}
S-PSF/Zeolite Y 15% v/v	0.0184	1.59×10^{-6}
S-PSF/Zeolite Y 20% v/v	0.0197	1.64×10^{-6}

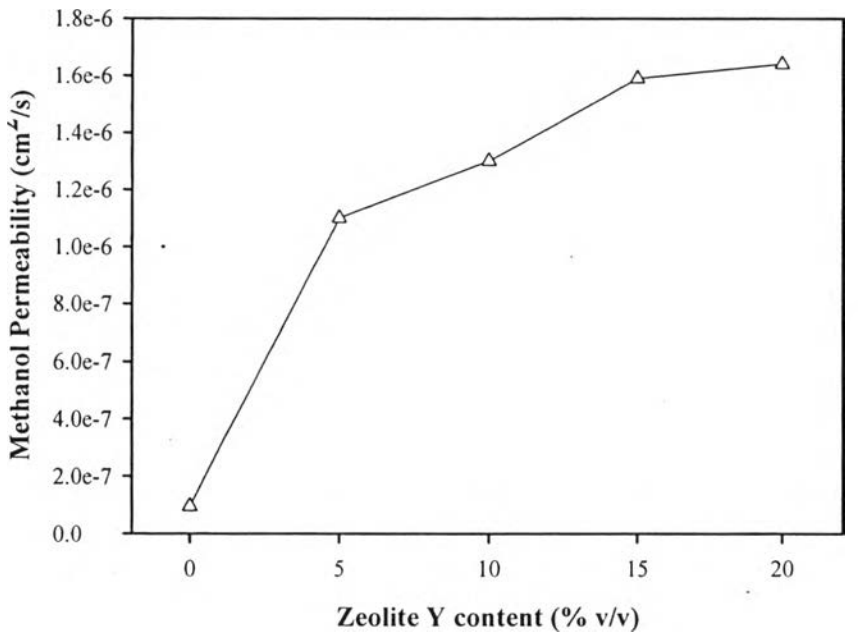

Figure G13 Methanol permeability at 70 °C of S-PSF and S-PSF/Zeolite Y composite membranes.

Table G14 Methanol permeability (cm^2/s) of S-PSF/S-GO composite membranes

Sample	Membrane Thickness (cm)	Methanol Permeability (cm^2/s)
Nafion 117	0.0178	3.08×10^{-5}
S-PSF72	0.0202	2.62×10^{-6}
S-PSF/S-GO 1% v/v	0.0191	4.23×10^{-7}
S-PSF/S-GO 2% v/v	0.0189	4.09×10^{-7}
S-PSF/S-GO 3% v/v	0.0184	3.48×10^{-7}
S-PSF/S-GO 5% v/v	0.0171	3.40×10^{-7}
S-PSF/S-GO 7% v/v	0.0171	3.44×10^{-7}

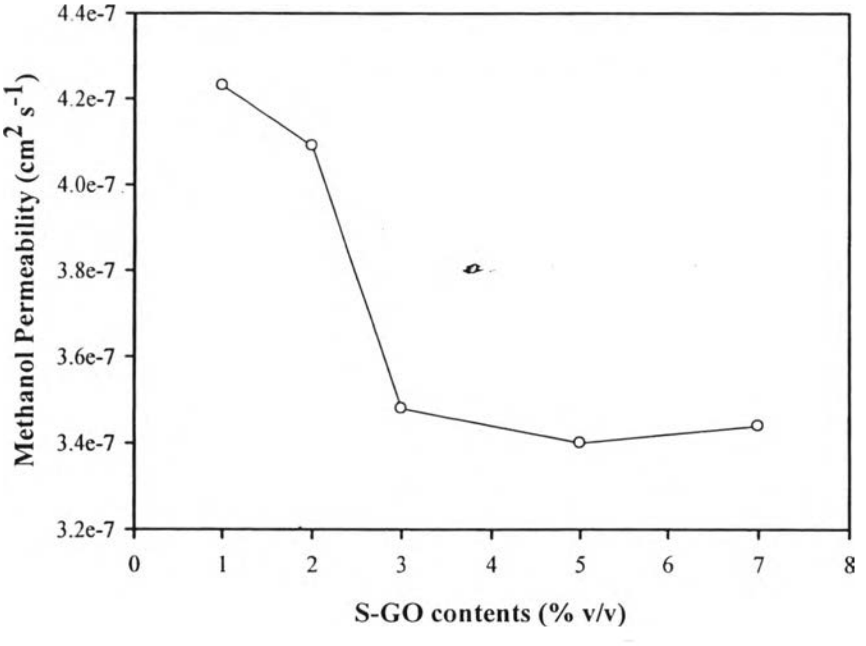

Figure G14 Methanol permeability (cm^2/s) of S-PSF/S-GO composite membranes.

Table G15 Methanol concentration in chamber A and B at 70 °C of S-PSF/3% v/v S-GO/12% v/v Zeolite Y composite membrane

Time (sec)	Methanol Concentration (mol/l) in Compartment A (C_A) and Compartment B (C_B) at 70 °C	
	S-PSF/3% v/v S-GO/12% v/v Zeolite Y	
	C_A(M)	C_B(M)
0	2.479	0
86400	2.479	0
172800	2.285	0.100
345600	2.125	0.155
432000	2.021	0.186
518400	1.958	0.365
604800	1.891	0.379

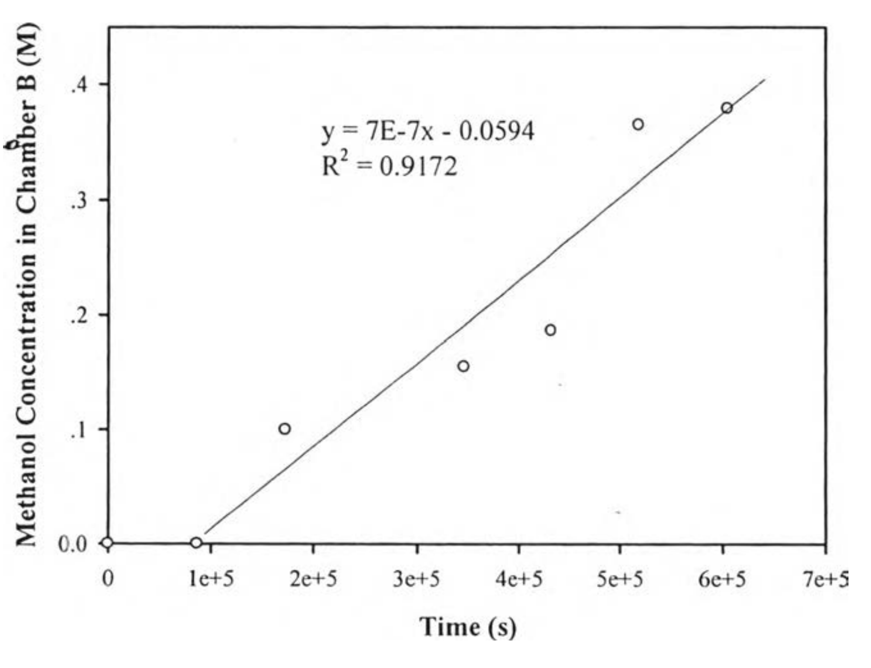

Figure G15 Methanol concentration in chamber B versus time at 70 °C of S-PSF/3% v/v S-GO/12% v/v Zeolite Y.

Table G16 Methanol concentration in chamber A and B at 70 °C of S-PSF/3% v/v S-GO/15% v/v Zeolite Y composite membrane

Time (sec)	Methanol Concentration (mol/l) in Compartment A (C_A) and Compartment B (C_B) at 70 °C	
	S-PSF/3% v/v S-GO/15% v/v Zeolite Y	
	C_A(M)	C_B(M)
0	2.453	0
86400	2.453	0
172800	2.424	0
345600	2.269	0.100
432000	2.171	0.156
518400	1.957	0.205
604800	1.717	0.239

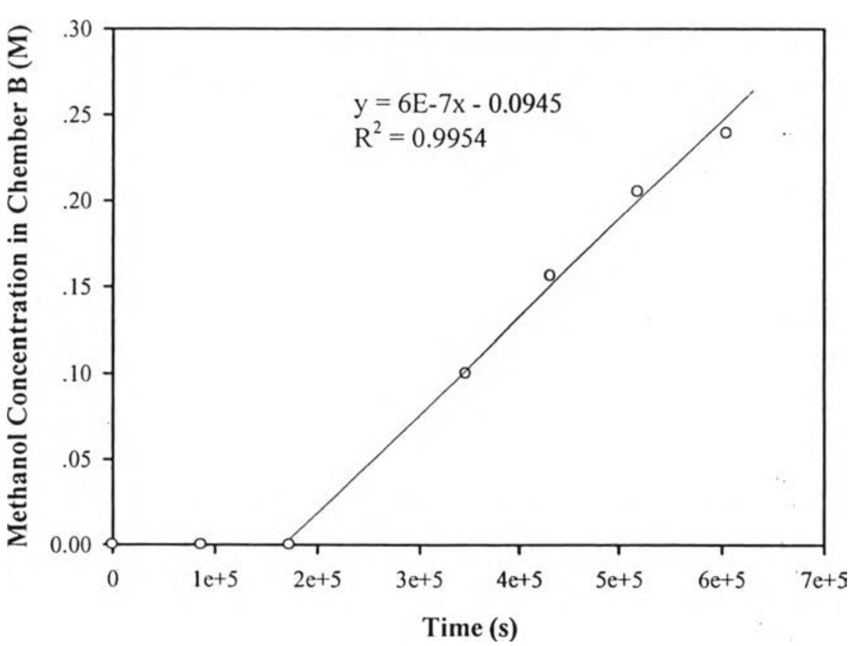

Figure G16 Methanol concentration in chamber B versus time at 70 °C of S-PSF/3% v/v S-GO/15% v/v Zeolite Y.

Table G17 Methanol permeability (cm^2/s) of the hybrid membranes

Sample	Membrane Thickness (cm)	Methanol Permeability (cm^2/s)
Nafion 117	0.0178	3.08×10^{-5}
S-PSF72	0.0202	2.62×10^{-6}
S-PSF/15Y	0.0184	1.59×10^{-6}
S-PSF/3S-GO	0.0184	3.48×10^{-7}
S-PSF/3S-GO/12Y	0.0182	3.68×10^{-7}
S-PSF/3S-GO/15Y	0.0188	3.33×10^{-7}

Appendix H Water Uptake

The membranes were immersed into DI water for 24 h at room temperature. Superabundant water was absorbed from the membrane surface with a wiping paper and the membranes were weighed (noted as W_s). The membranes were dried at 100 °C for 24 h in an oven and weighed again (noted as W_d). The percentage of water uptake was then calculated as following Eq. (H1):

$$\text{Water uptake} = \frac{(W_s - W_d)}{W_d} \times 100 \qquad \text{(H1)}$$

where W_d refers to the weight of dried polymer, and W_s is weight of swelled polymer.

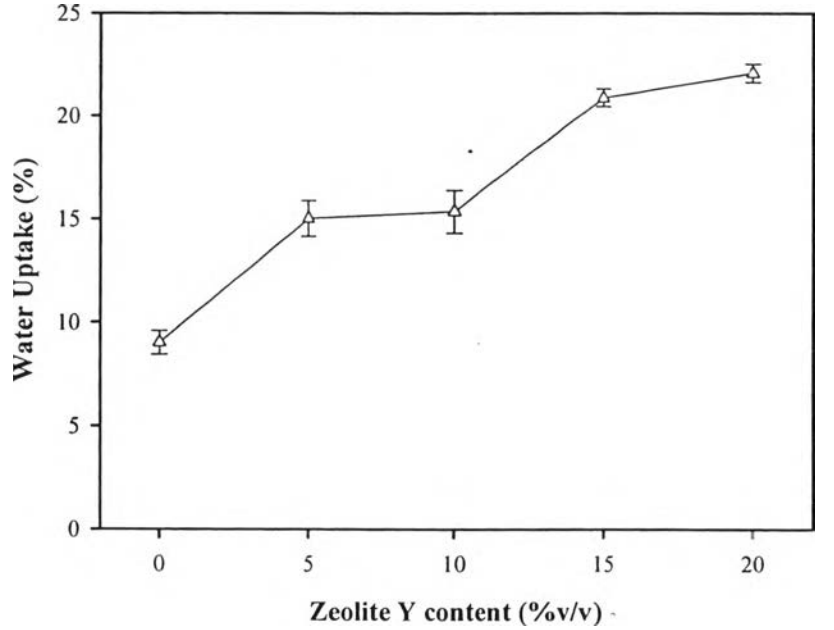

Figure H1 Water uptake (%) for S-PSF and S-PSF/Zeolite Y composite membranes.

Table H1 Water uptake of S-PSF and S-PSF/Zeolite Y composite membranes at 27 °C

Sample	Dry (g)	Wet (g)	Water Uptake (%)
S-PSF (DS = 0.72)	0.1040	0.1140	8.93
	0.1040	0.1130	8.48
	0.1030	0.1130	9.61
	Water uptake average		**9.01 ± 0.57**
S-PSF/5 %v/v Zeolite Y	0.0319	0.0370	15.99
	0.0320	0.0367	14.69
	0.0320	0.0366	14.38
	Water uptake average		**15.01 ± 0.86**
S-PSF/10 %v/v Zeolite Y	0.0375	0.0437	16.53
	0.0376	0.0432	14.89
	0.0376	0.0431	14.63
	Water uptake average		**15.35 ± 1.03**
S-PSF/15 %v/v Zeolite Y	0.0358	0.0431	20.39
	0.0357	0.0432	21.01
	0.0358	0.0434	21.23
	Water uptake average		**20.88 ± 0.43**
S-PSF/20 %v/v Zeolite Y	0.0532	0.0435	22.30
	0.0531	0.0434	22.35
	0.0530	0.0436	21.56
	Water uptake average		**22.07 ± 0.44**

Table H2 Water uptake of S-PSF/S-GO composite membranes at 27 °C

Sample	Dry (g)	Wet (g)	Water Uptake (%)
S-PSF/1% v/v S-GO	0.0352	0.0391	11.08
	0.0351	0.0388	10.54
	0.0352	0.039	10.80
	Water uptake average		**10.81 ± 0.27**
S-PSF/2% v/v S-GO	0.0361	0.0441	22.16
	0.0359	0.0440	22.56
	0.0360	0.0438	21.67
	Water uptake average		**22.13 ± 0.45**
S-PSF/3% v/v S-GO	0.0265	0.0326	23.02
	0.0266	0.0325	22.18
	0.0266	0.0324	21.80
	Water uptake average		**22.33 ± 0.62**
S-PSF/5% v/v S-GO	0.0304	0.0338	11.18
	0.0305	0.0337	10.49
	0.0305	0.0335	9.84
	Water uptake average		**10.50 ± 0.67**
S-PSF/7% v/v S-GO	0.0363	0.0377	3.86
	0.0362	0.0376	3.87
	0.0362	0.0376	3.87
	Water uptake average		**3.86 ± 0.01**

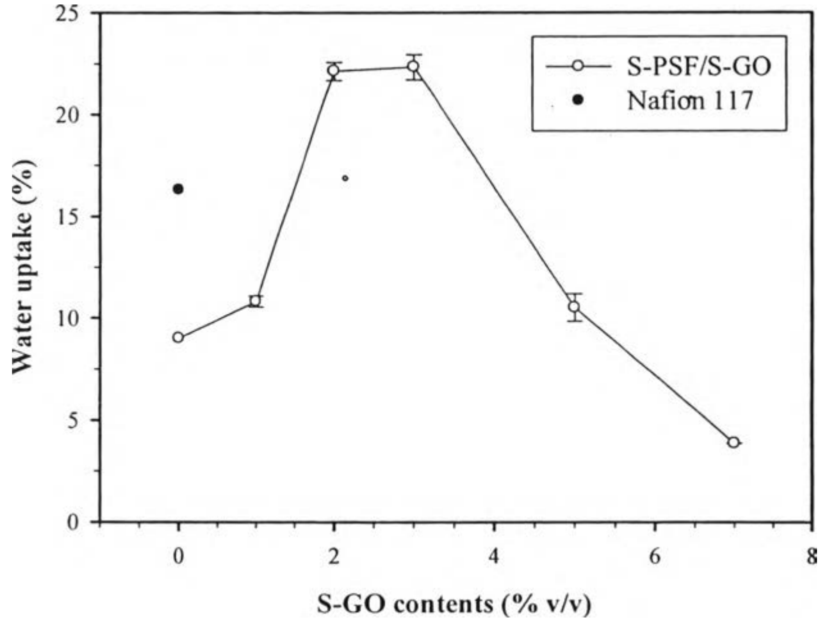

Figure H2 Water uptake (%) for S-PSF and S-PSF/S-GO composite membranes.

Table H3 Water uptake of the hybrid membranes at 27 °C

Sample	Dry (g)	Wet (g)	Water Uptake (%)
S-PSF/3S-GO/12Y	0.0348	0.0409	17.53
	0.0347	0.0408	17.58
	0.0345	0.0407	17.97
	Water uptake average		**17.69 ± 0.24**
S-PSF/3S-GO/15Y	0.0375	0.0431	14.93
	0.0376	0.0435	15.69
	0.0374	0.0430	14.97
	Water uptake average		**15.20 ± 0.43**

Appendix I Mechanical Properties

The mechanical properties: tensile strength, yield strain, and young's modulus, were recorded using a universal testing machine (Lloyd, model SMT2-500N) at room temperature with 25 $mm.min^{-1}$ speed. The membranes (thickness less than 1.0 mm) were cut into 1 cm × 5 cm. The measurements were taken at least 5 times.

Table I1 Mechanical property of PSF

Sample	Breadth (mm)	Area (mm^2)	Tensile Strength (MPa)	Yield Strain (%)	Young's Modulus (MPa)
PSF	0.37	3.72	38.6	7.3	906
PSF	0.36	3.58	41.7	7.7	993
PSF	0.39	3.92	40.5	8.6	874
PSF	0.48	4.76	37.8	8.5	813
PSF	0.34	3.36	41.1	6.6	1018

Table I2 Mechanical property of SPSF with DS of 0.72

Sample	Breadth (mm)	Area (mm^2)	Tensile Strength (MPa)	Yield Strain (%)	Young's Modulus (MPa)
SPSF72	0.48	4.77	21.8	5.5	662
SPSF72	0.39	3.91	24.7	5.9	691
SPSF72	0.28	2.83	32.2	5.8	933
SPSF72	0.31	3.11	35.2	6.5	930
SPSF72	0.22	2.16	28.2	6.9	1003

Table I3 Mechanical property of S-PSF/5%v/v Zeolite Y composite membranes

Sample	Breadth (mm)	Area (mm^2)	Tensile Strength (MPa)	Yield Strain (%)	Young's Modulus (MPa)
1	0.19	1.84	25.8	4.6	873
2	0.19	1.85	19.1	3.3	945
3	0.18	1.88	29.3	5.0	1035
4	0.18	1.92	23.1	3.6	1156
5	0.18	1.76	33.2	5.1	1047

Table I4 Mechanical property of S-PSF/10%v/v Zeolite Y composite membranes

Sample	Breadth (mm)	Area (mm^2)	Tensile Strength (MPa)	Yield Strain (%)	Young's Modulus (MPa)
1	0.19	1.93	26.4	7.0	1138
2	0.16	1.57	25.5	3.5	1303
3	0.16	1.62	24.5	3.7	1265
4	0.14	1.47	28.3	4.3	1238
5	0.14	1.34	22.7	4.2	1116

Table I5 Mechanical property of S-PSF/15%v/v Zeolite Y composite membranes

Sample	Breadth (mm)	Area (mm^2)	Tensile Strength (MPa)	Yield Strain (%)	Young's Modulus (MPa)
1	0.18	1.79	15.8	4.1	1096
2	0.17	1.68	14.0	3.2	1226
3	0.16	1.61	16.5	3.3	1268
4	0.17	1.58	15.0	3.0	1220
5	0.21	2.13	17.4	3.5	1232

Table I6 Mechanical property of S-PSF/20%v/v Zeolite Y composite membranes

Sample	Breadth (mm)	Area (mm^2)	Tensile Strength (MPa)	Yield Strain (%)	Young's Modulus (MPa)
1	0.16	1.63	13.9	2.0	3438
2	0.17	1.65	21.1	2.7	3109
3	0.17	1.72	22.3	2.7	3246
4	0.18	1.79	25.5	3.0	3047
5	0.16	1.61	24.0	2.9	3185

Table I7 Mechanical properties of S-PSF and S-PSF/Zeolite Y composite membranes

Sample	Tensile Strength (MPa)	Yield Strain (%)	Young's Modulus (MPa)
PSF	39.9 ± 1.7	7.7 ± 0.9	921 ± 85
S-PSF72	28.4 ± 5.4	6.1 ± 0.6	844 ± 156
S-PSF/5%v/v Zeolite Y	26.1 ± 5.4	4.3 ± 0.8	1011 ± 108
S-PSF/10%v/v Zeolite Y	25.5 ± 2.1	4.5 ± 1.4	1212 ± 81
S-PSF/15%v/v Zeolite Y	15.7 ± 1.3	3.4 ± 0.4	1208 ± 65
S-PSF/20%v/v Zeolite Y	21.4 ± 4.5	2.7 ± 0.4	3205 ± 150
Nafion 117	11.0 ± 0.4	24.1 ± 1.9	185 ± 10

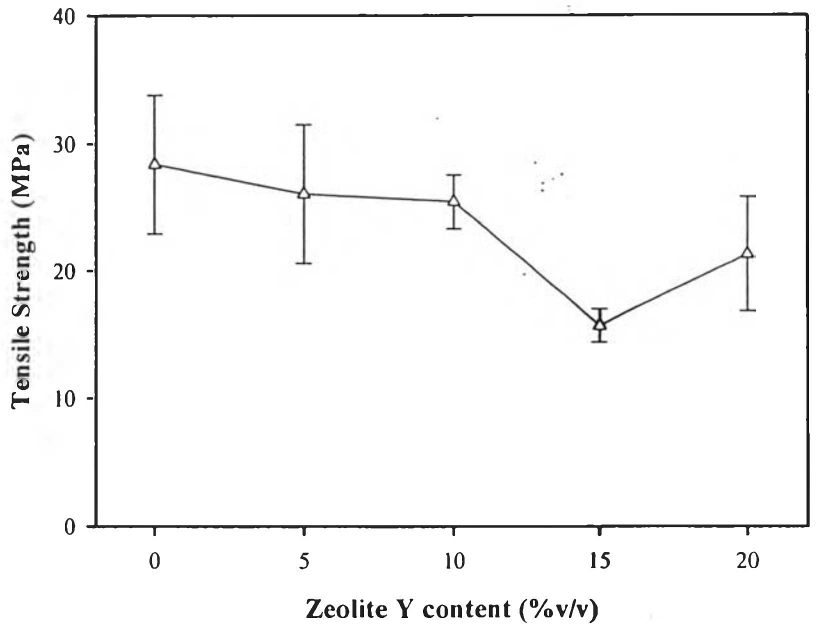

Figure I1 Tensile strength of S-PSF/zeolite Y composite membranes.

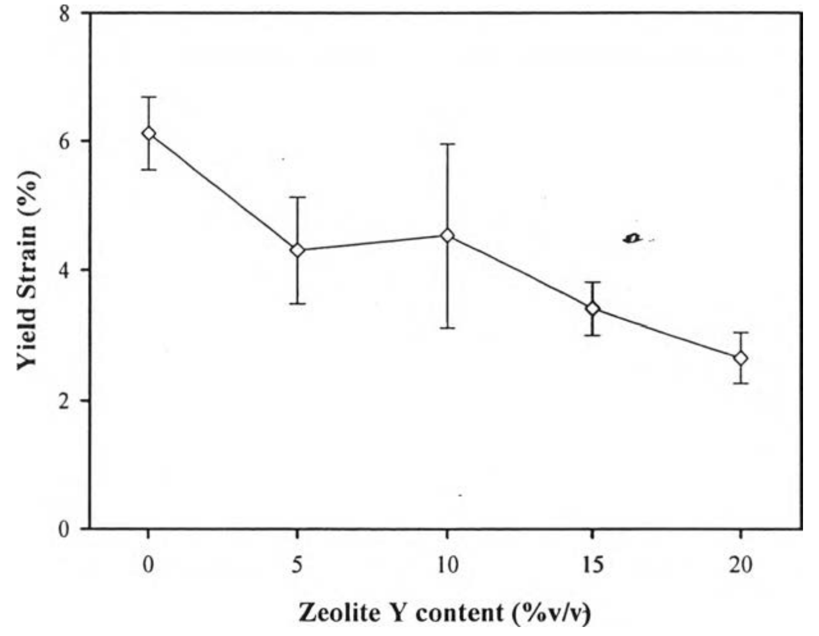

Figure I2 Yield strain of S-PSF/zeolite Y composite membranes.

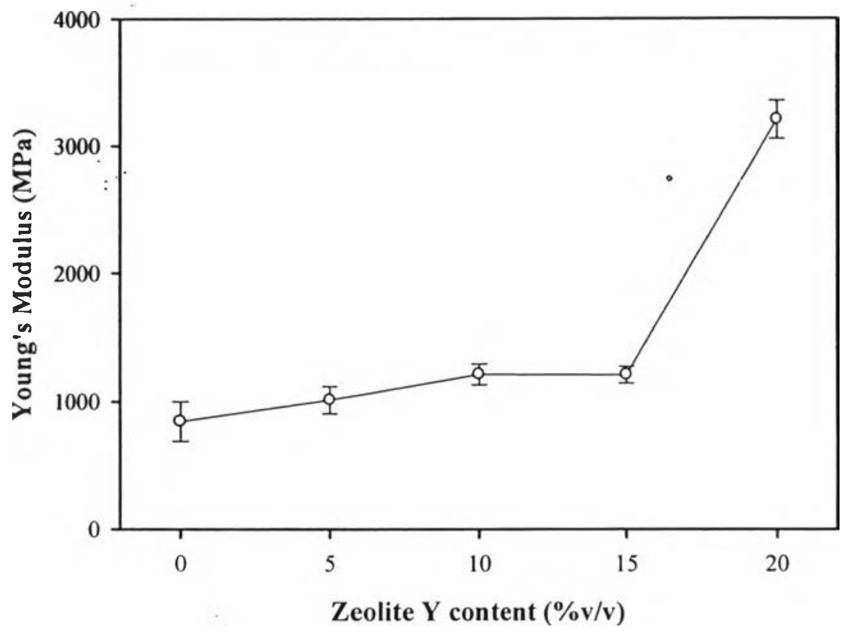

Figure I3 Young's modulus of S-PSF/zeolite Y composite membranes.

Table I8 Mechanical property of S-PSF/1%v/v S-GO composite membranes

Sample	Breadth (mm)	Area (mm^2)	Tensile Strength (MPa)	Yield Strain (%)	Young's Modulus (MPa)
1	0.211	2.11	29.57	4.88	887
2	0.182	1.82	30.25	5.79	924
3	0.213	2.13	28.17	5.75	825
4	0.196	1.96	25.72	4.82	767
5	0.209	2.09	33.35	5.55	960

Table I9 Mechanical property of S-PSF/2%v/v S-GO composite membranes

Sample	Breadth (mm)	Area (mm^2)	Tensile Strength (MPa)	Yield Strain (%)	Young's Modulus (MPa)
1	0.167	1.67	33.57	4.0	733
2	0.187	1.87	40.28	4.72	926
3	0.189	1.89	39.65	4.16	902
4	0.196	1.96	42.15	5.31	1079
5	0.201	2.01	38.04	4.05	897

Table I10 Mechanical property of S-PSF/3%v/v S-GO composite membranes

Sample	Breadth (mm)	Area (mm^2)	Tensile Strength (MPa)	Yield Strain (%)	Young's Modulus (MPa)
1	0.142	1.42	32.57	3.51	944
2	0.160	1.60	36.65	3.46	839
3	0.159	1.59	36.33	3.48	972
4	0.151	1.51	40.68	3.26	1022
5	0.163	1.63	36.04	3.32	958

Table I11 Mechanical property of S-PSF/5%v/v S-GO composite membranes

Sample	Breadth (mm)	Area (mm^2)	Tensile Strength (MPa)	Yield Strain (%)	Young's Modulus (MPa)
1	0.193	1.93	40.33	3.05	952
2	0.180	1.80	44.58	2.5	1092
3	0.176	1.76	46.18	3.01	1103
4	0.186	1.86	41.56	2.95	978
5	0.186	1.86	47.11	2.56	1122

Table I12 Mechanical property of S-PSF/5%v/v S-GO composite membranes

Sample	Breadth (mm)	Area (mm^2)	Tensile Strength (MPa)	Yield Strain (%)	Young's Modulus (MPa)
1	0.245	2.45	45.08	2.81	1100
2	0.243	2.43	49.57	2.77	1200
3	0.269	2.69	47.85	2.41	1145
4	0.235	2.35	51.23	2.63	1271
5	0.228	2.28	50.85	2.45	1217

Table I13 Mechanical properties of S-PSF and S-PSF/S-GO composite membranes

Sample	Tensile Strength (MPa)	Yield Strain (%)	Young's Modulus (MPa)
PSF	39.9 ± 1.7	7.7 ± 0.9	921 ± 85
S-PSF72	29.4 ± 2.8	6.1 ± 0.6	844 ± 156
S-PSF/1%v/v S-GO	28.6 ± 2.3	5.4 ± 0.5	873 ± 77
S-PSF/2%v/v S-GO	36.5 ± 2.9	4.4 ± 0.6	907 ± 123
S-PSF/3%v/v S-GO	40.1 ± 1.9	3.4 ± 0.1	947 ± 67
S-PSF/5%v/v S-GO	44.0 ± 2.9	2.8 ± 0.3	1050 ± 78
S-PSF/7%v/v S-GO	48.9 ± 2.5	2.6 ± 0.12	1187 ± 66

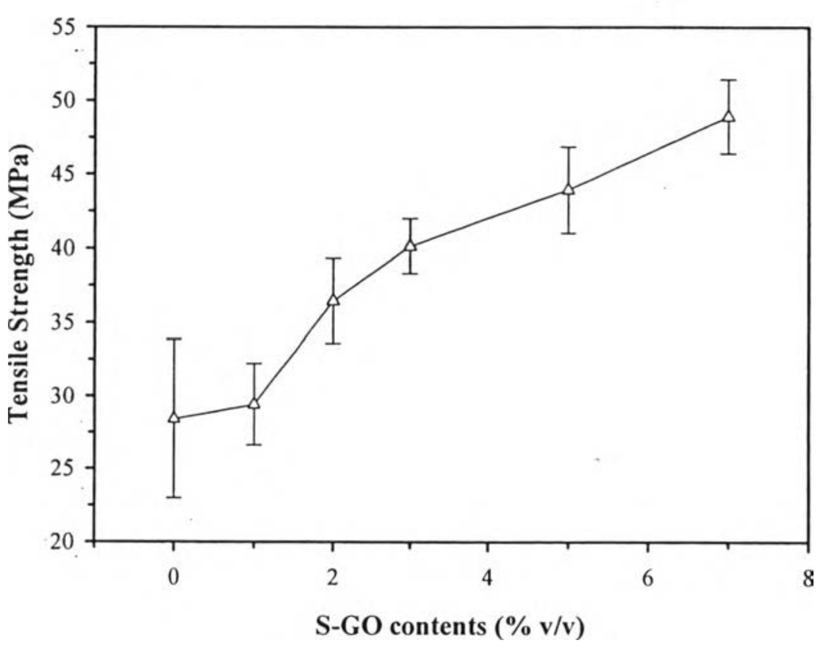

Figure I4 Tensile strength of S-PSF/S-GO composite membranes.

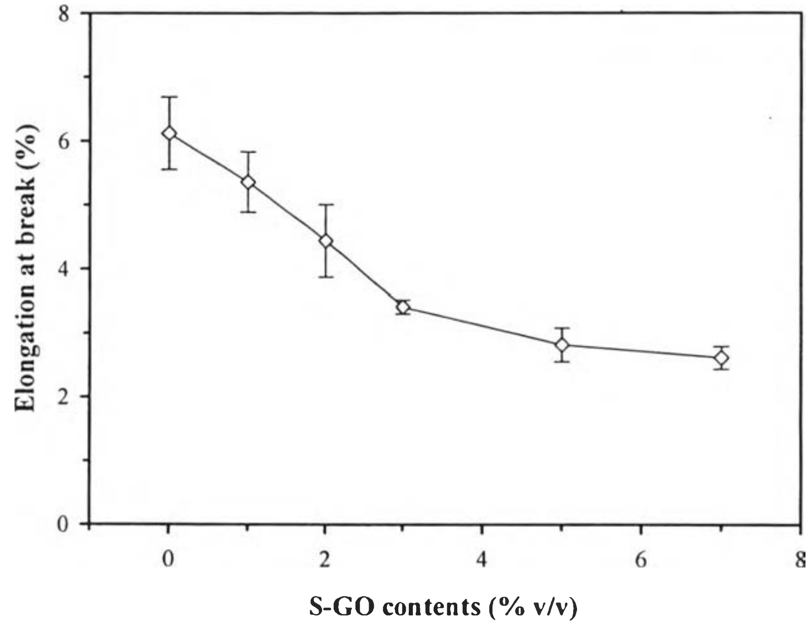

Figure I5 Yield strain of S-PSF/S-GO composite membranes.

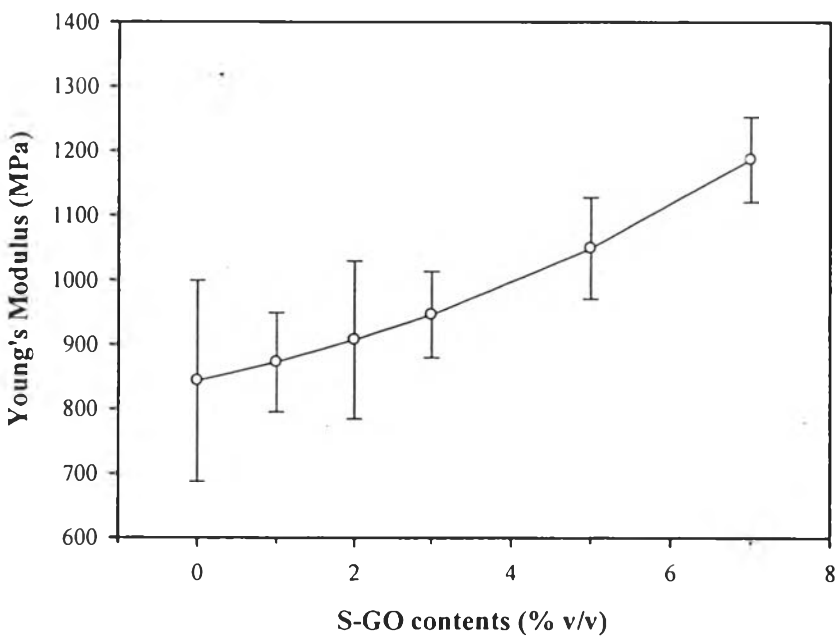

Figure I6 Young's modulus of S-PSF/S-GO composite membranes.

Table I14 Mechanical property of S-PSF/3%v/v S-GO and 12%v/v zeolite Y composite membranes

Sample	Breadth (mm)	Area (mm^2)	Tensile Strength (MPa)	Yield Strain (%)	Young's Modulus (MPa)
1	0.203	2.03	14.67	2.41	1074
2	0.206	2.06	9.68	1.23	1311
3	0.195	1.95	20.35	3.52	1280
4	0.190	1.90	13.98	2.19	1129
5	0.183	1.83	15.85	2.30	1251

Table I15 Mechanical property of S-PSF/ S-PSF/3%v/v S-GO and 15%v/v zeolite Y composite membranes

Sample	Breadth (mm)	Area (mm^2)	Tensile Strength (MPa)	Yield Strain (%)	Young's Modulus (MPa)
1	0.196	1.96	9.28	1.06	1453
2	0.215	2.15	19.14	3.04	1254
3	0.209	2.09	10.84	1.43	1429
4	0.202	2.02	12.09	1.57	1471
5	0.200	2.00	16.16	2.73	1308

Table I16 Mechanical properties of S-PSF and hybrid composite membranes

Sample	Tensile Strength (MPa)	Yield Strain (%)	Young's Modulus (MPa)
PSF	39.9 ± 1.7	7.7 ± 0.9	921 ± 85
S-PSF72	29.4 ± 2.8	6.1 ± 0.6	844 ± 156
S-PSF/15Y	15.7 ± 1.3	3.4 ± 0.4	1208 ± 65
S-PSF/3S-GO	40.1 ± 1.9	3.4 ± 0.1	947 ± 67
S-PSF/3S-GO/12Y	14.9 ± 3.8	2.3 ± 0.8	1209 ± 102
S-PSF/3S-GO/15Y	13.5 ± 4.1	2.0 ± 0.9	1383 ± 96

Appendix J X-ray Photoelectron Spectroscopy (XPS)

XPS technique was used for the determination of the surface composition of the GO and S-GO. The XPS spectra were obtained by using an incident achromatic MgKa X-ray source (1253.6 eV) operated at 14.8 kV and 20 mA for excitation and a hemisphere analyzer (Thermo VG scientific). The high-resolution XPS spectra were composite averages of 10 scans with a passing energy of 50 eV. The pressure in the analysis chamber was in the range of 10^{-8} Torr during data collection. The binding energy was adjusted to the C1s peak at 285.1 eV. Data analysis and curve de-convolution were accomplished by using the Thermo Advantage Spectra Data Processor software. The samples were dried at 100 °C for 24 h before testing.

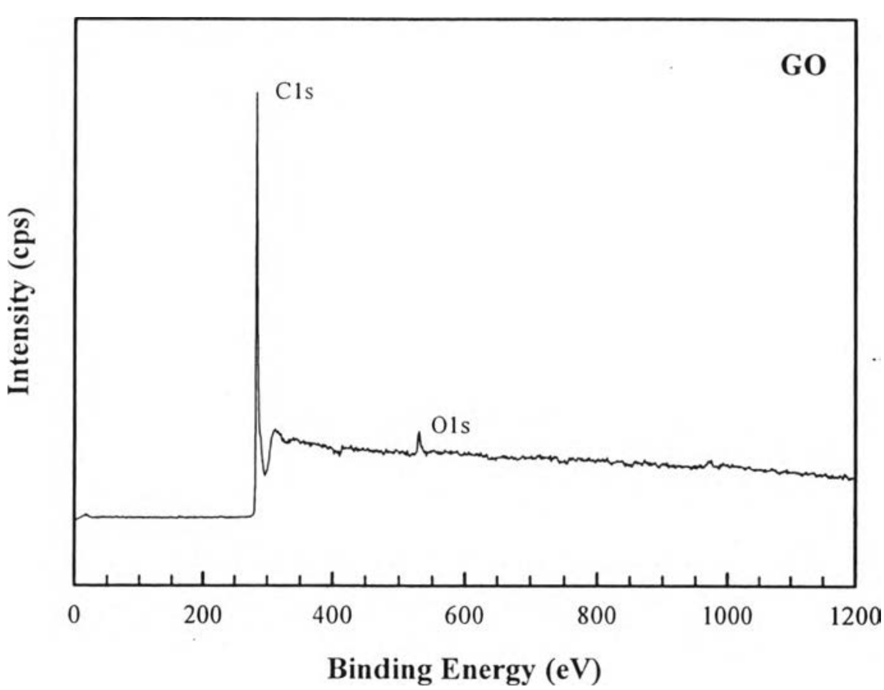

Figure J1 Wide region XPS spectra of GO.

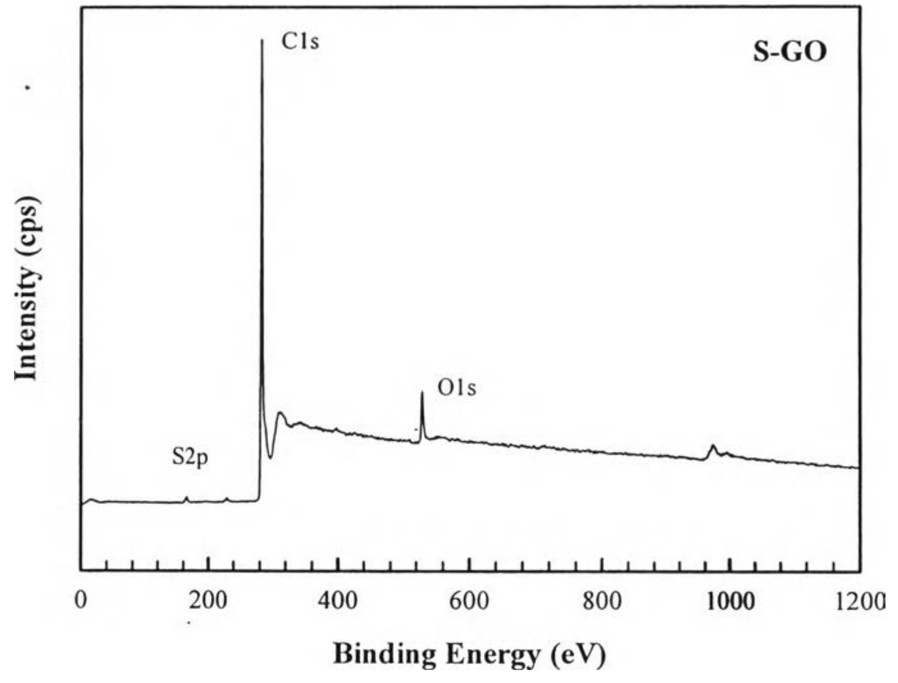

Figure J2 Wide region XPS spectra of S-GO.

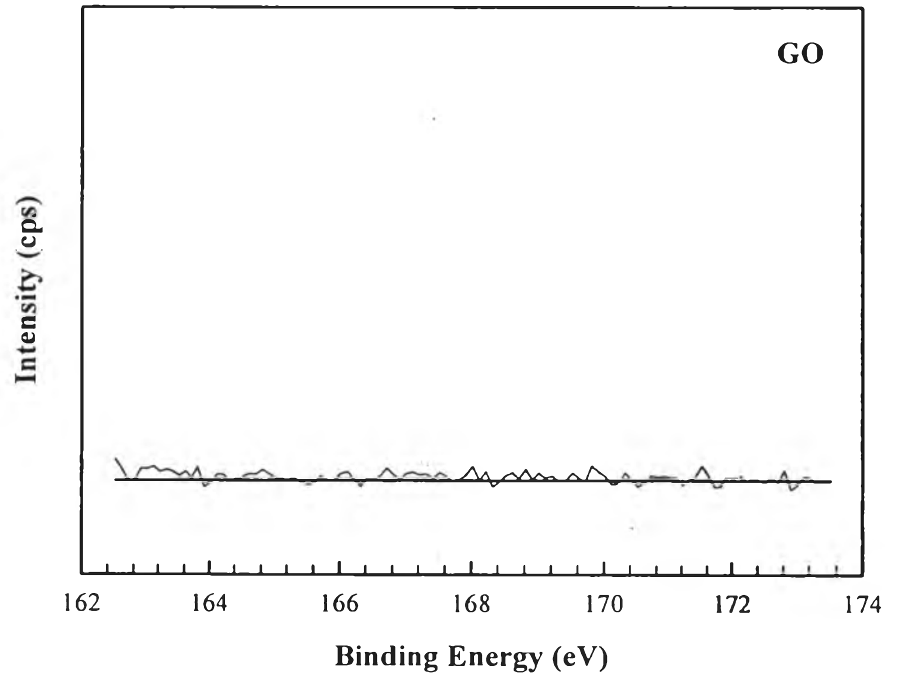

Figure J3 S2p region XPS spectra of GO.

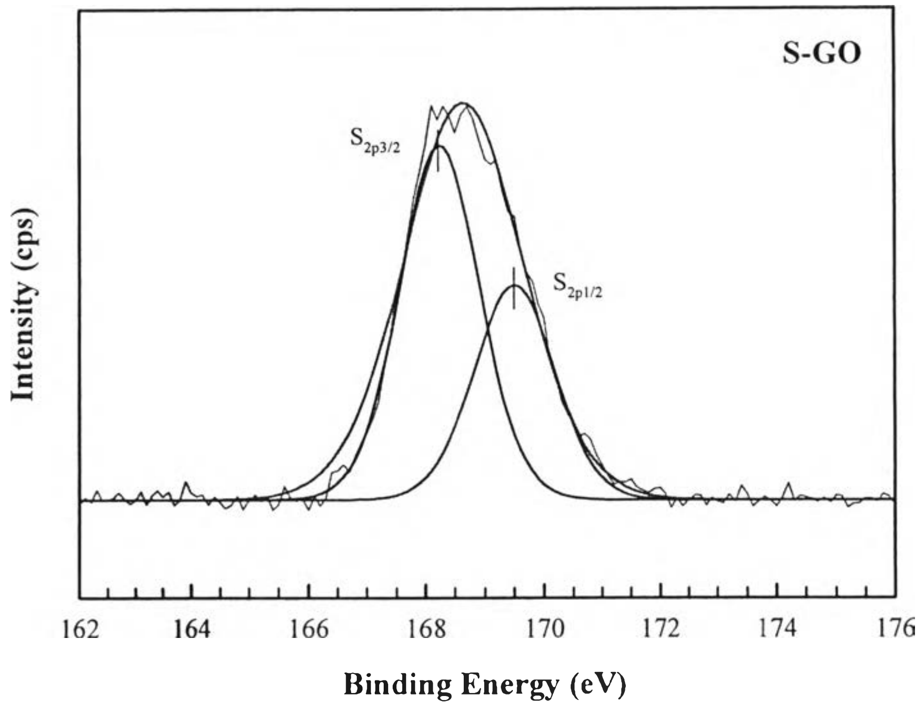

Figure J4 S2p region XPS spectra of S-GO.

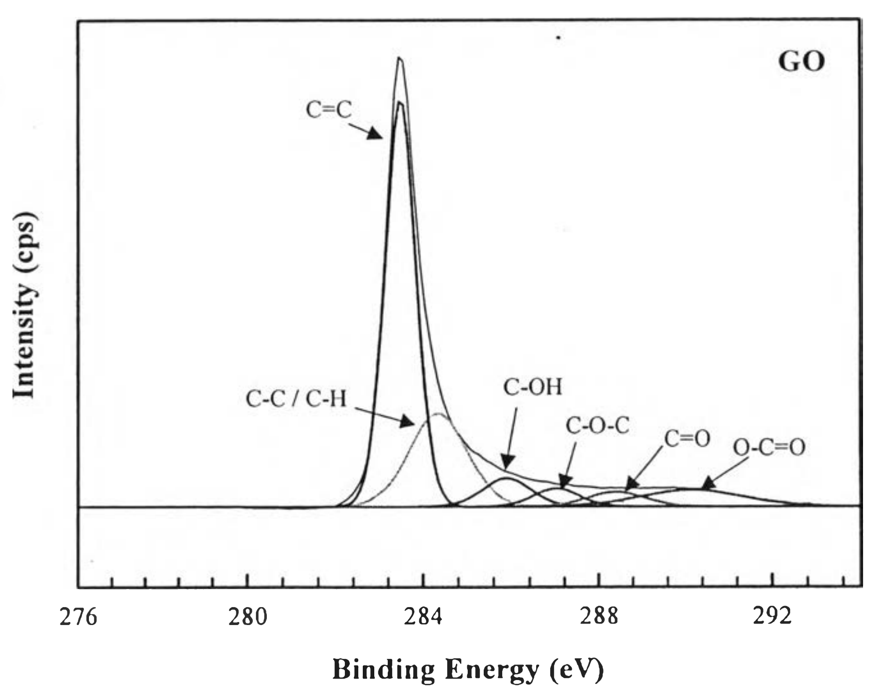

Figure J5 C1s region XPS spectra of GO

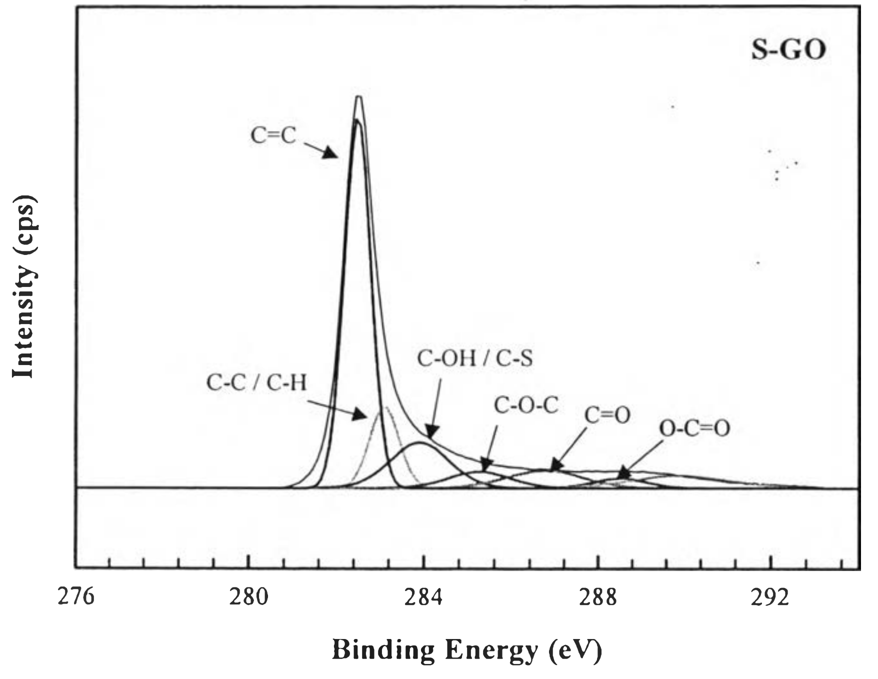

Figure J6 C1s region XPS spectra of S-GO

Table J1 Summary of S 2p and C 1s XPS spectral data

Bond	Sample	Assignment	Binding Energy (eV)	FWHM	Area
S2p	S-GO	**S(2p3/2)**	167.6	1.566	1946.3
		S(2p1/2)	168.8	1.594	1190.5
C1s	GO	**C=C**	283.5	0.815	58406.6
		C-C / C-H	284.3	1.542	25125.8
		C-OH	285.9	1.283	6529.2
		C-O-C	286.9	1.234	3986.4
		C=O	288.4	1.578	4048.9
		O-C=O	290.1	2.825	8244.1
	S-GO	**C=C**	282.5	0.712	91736.7
		C-C / C-H	283.1	0.768	22181.9
		C-OH / C-S	283.9	1.560	25063.8
		C-O-C	285.3	1.684	9684.2
		C=O	286.7	2.078	12771.4
		O-C=O	288.5	1.476	5083.0

Appendix K Scanning Electron Microscopy (SEM)

The surface morphology of GO and S-GO was investigated using a scanning electron microscope, Model S4800 (Hitachi), operated at 5kV and 15 mA. The samples were dried at 100 °C for 24 h before testing.

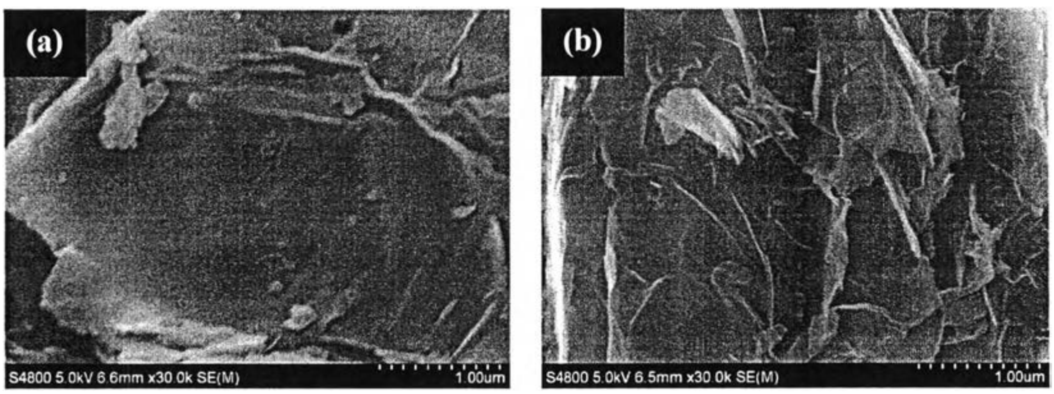

Figure K1 SEM images of the surface of: (a) GO and (b) S-GO.

CURRICULUM VITAE

Name: Mr. Phuwadon Bunlengsuwan

Date of Birth: December 5, 1990

Nationality: Thai

University Education:

2009–20012 Bachelor Degree of Petrochemical and Polymeric Materials, Faculty of Engineering and Industrial Technology, Silpakorn University, Nakornpathom, Thailand

Proceeding:

1. Bunlengsuwan, P.; Sirivat, A.; and Siemanond, K. (2015, April 21) Effect of Sulfonated Graphene Oxide on Sulfonated Polysulfone Membrane for Direct Methanol Fuel cells. Proceedings of the 6th Research Symposium on Petrochemical and Materials Technology and the 21th PPC Symposium on Petroleum, Petrochemicals, and Polymers, Bangkok, Thailand.

Presentation:

1. Bunlengsuwan, P.; Sirivat, A.; and Siemanond, K. (2015, April 21) Effect of Sulfonated Graphene Oxide on Sulfonated Polysulfone Membrane for Direct Methanol Fuel cells. Paper presented at The 6th Research Symposium on Petrochemical and Materials Technology and the 21th PPC Symposium on Petroleum, Petrochemicals, and Polymers, Bangkok, Thailand.